Dissertation zur Erlangung des Doktorgrades

der Fakultät für Chemie und Pharmazie

der Ludwig-Maximilians-Universität München

Novel nano- and microparticulate formulations for industrial preclinical research

Patrick Strack

aus Bühl (Baden), Deutschland

2021

Erklärung

Diese Dissertation wurde im Sinne von § 7 der Promotionsordnung vom 28. November 2011 von Frau Prof. Dr. Olivia Merkel betreut.

Eidesstattliche Versicherung

Diese Dissertation wurde eigenständig und ohne unerlaubte Hilfe erarbeitet.

Biberach an der Riß, den 17.03.2021

.....

Patrick Strack

Dissertation eingereicht am:	31.03.2021
1. Gutachter:	Prof. Dr. Olivia Merkel
2. Gutachter:	Prof. Dr. Wolfgang Frieß
Mündliche Prüfung am:	18.05.2021

Für meine Familie

In Liebe und Dankbarkeit

ACKNOWLEDGEMENTS

The present thesis was prepared under the supervision of Prof. Dr. Olivia Monika Merkel at the Department of Pharmacy, Pharmaceutical Technology and Biopharmaceutics at the Ludwigs-Maximilians-University München (LMU) in Munich, Germany and under the guidance of Dr. Achim Grube at the Chemistry, Manufacturing, and Control (CMC) group in the Drug Discovery Science (DDS) department at Boehringer Ingelheim Pharma GmbH & Co. KG (BI) in Biberach an der Riß, Germany.

Throughout my time at BI and the LMU I have learned a lot and I am very thankful to all the people who supported me.

First of all, I would like to express my deepest gratitude to my supervisor Professor Dr. Olivia Merkel for giving me the opportunity to work on my dissertation within her research group. I really appreciated her scientific input and support throughout all phases of this work.

This work was further supervised by Dr. Achim Grube. Thank you for giving me the opportunity to work on such interesting and innovative projects, your dedicated guidance, scientific advice, creative ideas and encouragement to work through difficult times. I am also deeply thankful for all the possibilities you offered me, including collaborations with other groups at BI, joining of several scientific conferences all over the world and allowing me the entry into the pharmaceutical industry.

I would like to thank Prof. Dr. Wolfgang Frieß for kindly agreeing on being co-referee of this thesis. I would like to extend my thanks and appreciation to Prof. Dr. Stefan Zahler, Prof. Dr. Franz Bracher, Prof. Dr. Franz Paintner, and Prof. Dr. Angelika Vollmar for kindly being members of my examination board.

Many thanks to my great office mate Dr. Anastasia Zakharyuta for her constant support during all the challenging times of this doctorate, her scientific input and countless reviewing of all my work. I learned a lot under her guidance.

This thesis would not have been possible without the support of the whole DDS CMC group. First, I would like to thank the former and current leadership team for their support: Dr. Florian Sommer, Manfred Birk, Dr. Peter Sieger, Dr. Ulrike Werthmann, Dr. Ines Trübenbach,

Dr. Joachim Schäfer and Dr. Achim Grube. The same thanks goes out to all other colleagues from our group, especially the “Wolke” team: Nicole Gröner, Diana Geiss, Bekir Karagül, Silvija Suffrian, Tanja Schwer, Amy Haasis, Conny Fuß and Steffi Schobel.

Special thanks to my colleagues who became great friends, Silvija, Tanja and Amy for all the fun we had in the lab and the great time outside the lab, during lunch, “extended” coffee breaks and of course the famous Biberacher Schützenfest. My time here would have been very boring without you.

I would moreover like to thank all students who gave me the chance to guide and teach them, Johannes Bader, Nadine Kiefer, Anna Unterholzner, Clemence Bonnefoy and Anna Ruppl. I wish you all the best for your future careers.

Many thanks are expressed to all the other colleagues at BI who supported me during my PhD thesis. Especially Dr. Kerstin Schäfer and Holger Weil from Pharmaceutical Development, Dr. Raimund Külzer, Dr. Stefan Scheuerer, Nadine Klick and Heidi Assfalg from Research PK, Dr. Martin Dass and Dagmar Rädel from NDS and Dr. Otmar Schaaf and Ida Dinold from DDS CMC BI Vienna.

A big “Thank you” goes to all the members of the AK Winter, AK Frieß and especially AK Merkel. Tobi, Rima, Gabriella, Aditi, Christoph, Domizia, Bettina, Lorenz and Natascha thank you for welcoming me so heartily to the group and creating a comfortable and funny atmosphere. All our Oktoberfest visits, Christmas parties, skiing and hiking trips were great and I wish I had the possibility to visit you more often in Munich.

Furthermore, I would like to thank the PhD community at BI. It was always amazing to meet such a diverse and interdisciplinary group of young scientist. I really appreciated the seminar series and of course, the fun time we had during Christmas market and the Schützenfest.

Above all, I would like to express my deepest gratitude and appreciation to my friends and family, who always believed in me and supported me in any imaginable way. Thank you Sarah, Nora, Micha, Bella, Flo and Rina for over 10 years of friendship and many more to come.

My deepest and immense gratitude goes to my parents, Wolfgang and Brigitte, as well as to my brother Niklas and my “little” sister Lena-Marie who gave me roots and always supported me. Thank you with all my heart for your unconditional and never-ending love!

TABLE OF CONTENTS

CHAPTER I

GENERAL INTRODUCTION AND AIM OF THE THESIS

1 General Introduction

One of the main tasks in today's drug development is to improve the pharmacokinetics and biodistribution of an active pharmaceutical ingredient (API). The overall objective hereby is to enhance the therapeutic efficacy, while simultaneously reducing toxicity of a prospective new compound. In order to achieve this altered ratio, the drug has to be protected from the environment, until exertion of its pharmacological action is required. One of the common approaches is the entrapment of an API into a biocompatible material. Hereby the drug is retained within the excipient after administration, not effecting the body. Consequently, this can facilitate the delivery and release of the drug at a specific site of action (e.g. tumor or liver targeting by nanoparticles) or after a desired time (extended release formulation).

1.1 Poly lactic-co-glycolic acid (PLGA)

Amongst all the materials available for entrapment of a compound, PLGA is amongst the most favored polymers, particularly for controlled release formulations [1]. The products of non-enzymatic hydrolysis of PLGA are lactic and glycolic acids as shown in Figure 1, which can be catabolized naturally [2].

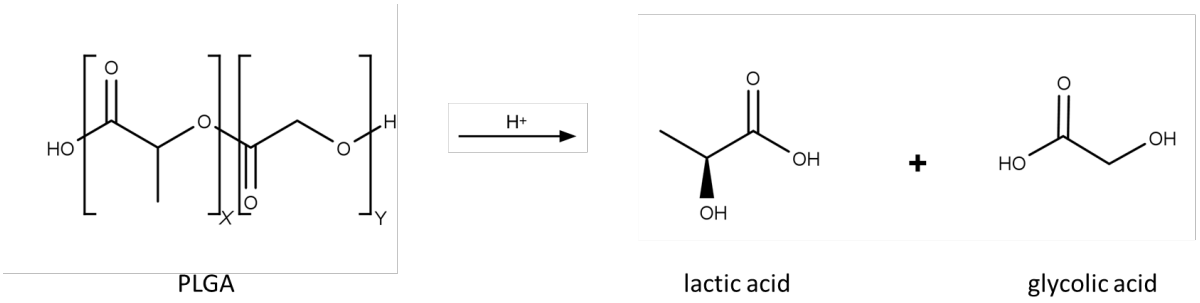

Figure 1 Illustration of the mechanism of hydrolytic degradation of PLGA.

Therefore, it can be safely applied as a parenteral formulation. Due to its superior biodegradability and biocompatibility properties, PLGA has received approval from the United States Food and Drug Administration and the European Medicine Agency [3]. A variety of structurally different compounds, ranging from small molecules [4] to nucleic acids [5] and proteins [6] can be encapsulated into PLGA-based formulations. Additionally, different types and derivatives of the polymer are commercially available [6], offering countless possibilities

of optimization. Due to these unique properties, PLGA allows the fabrication of nanoparticulate formulation e.g. for targeted drug delivery (Chapter II and III), as well as the manufacturing of extended release microparticles e.g. for pharmacokinetic profile optimization (Chapter IV).

1.2 Challenges in industrial pharmaceutical research

In industrial pharmaceutical research, there are various challenges to tackle with regard to advanced formulation development. Particularly in the early stage of preclinical research, the production costs of a newly developed compound are enormous [7]. The main factor that drives up costs is the ever-growing complexity of such molecules. Synthesis requires a great number of chemical reaction steps, each of which takes time, and many substrates have to be expensively purchased. Furthermore, an elaborate synthesis process is not yet established at this point and the compound can only be produced on a small scale with low yield. All these factors add up, putting a few grams of API in the same price range as a compact car, which becomes a problem, as formulation development can be highly compound consuming. This has to be taken into consideration for the upcoming studies, and resource efficient procedures are required.

It is additionally important for a newly developed formulation to be translatable into clinical practice. Especially from an industry perspective, investing in novel formulation approaches is only reasonable, if there is the prospect of a successful drug product. The main premise for an eventual application in humans is the physiological and toxicological safety of the product. By utilizing biocompatible polymers, such as PLGA, one requirement for this objective can be achieved. Another relevant requirement is the possibility to scale-up the manufacturing of the API loaded particles from laboratory scale to preclinical studies, as to eventually facilitate clinical trials. Therefore, manufacturing procedures have to be established, allowing scalability of the formulation.

2 Aim of the thesis

The aim of this work was the entrapment of a variety of Boehringer Ingelheim (BI) research compounds into PLGA-based nano- and microparticulate formulations. Hereby, the unique properties of the polymer are utilized, as to facilitate a controlled release of the API after a certain time or in the target tissue. The main objective herein is an improved efficacy of the developed formulation, depending on the required administration route. Special emphasis is placed on formulation development in an industrial pharmaceutical research setting, with the overall goal of clinical translation in a later phase.

2.1 Chapter II: Novel nanoparticulate formulations for tumor targeted delivery of cyclic dinucleotides

In chapter II, the development of a novel nanoparticulate formulation for a cyclic dinucleotide is described. Biodegradable polymers are used to encapsulate the immuno-oncologic compound facilitating a passive delivery into tumor tissue. Hereby, a reduced systemic toxicity and enhanced efficacy is achieved upon systemic administration.

2.2 Chapter III: Liver targeted nanoparticles for NASH treatment

The third chapter shows the manufacturing, characterization, optimization and *in vivo* proof of concept for liver-targeted nanoparticles. Optimized nanoparticulate formulations demonstrated high local concentration of a model compound in the hepatic tissue, suggesting successful targeting of the liver for NASH treatment.

2.3 Chapter IV: PLGA-based extended release formulation platform

Chapter IV describes a PLGA-based formulation platform for a variety of research compounds enabling preclinical studies, by optimizing their pharmacokinetic (PK) profile. Formulations for two model molecules with different solubilities were developed, extending mean residence time (MRT) significantly and prolonging plasma through level for a sufficient period. Based on these results, the proposed platform is successfully utilized on further BI compounds, testifying to its general applicability.

References

1. Makadia, H. K.; Siegel, S. J., Poly lactic-co-glycolic acid (PLGA) as biodegradable controlled drug delivery carrier. *Polymers* **2011,** *3* (3), 1377-1397.
2. Danhier, F.; Ansorena, E.; Silva, J. M.; Coco, R.; Le Breton, A.; Préat, V., PLGA-based nanoparticles: An overview of biomedical applications. *J. Control. Release* **2012,** *161* (2), 505-522.
3. Wang, Y., FDA's regulatory science program for generic PLA/PLGA-based drug products. *American Pharmaceutical Review* **2016,** *20*.
4. Wischke, C.; Schwendeman, S. P., Principles of encapsulating hydrophobic drugs in PLA/PLGA microparticles. *International Journal of Pharmaceutics* **2008,** *364* (2), 298-327.
5. Panyam, J.; Labhasetwar, V., Biodegradable nanoparticles for drug and gene delivery to cells and tissue. *Advanced Drug Delivery Reviews* **2003,** *55* (3), 329-347.
6. Mundargi, R. C.; Babu, V. R.; Rangaswamy, V.; Patel, P.; Aminabhavi, T. M., Nano/micro technologies for delivering macromolecular therapeutics using poly(d,l-lactide-co-glycolide) and its derivatives. *J. Control. Release* **2008,** *125* (3), 193-209.
7. DiMasi, J. A.; Grabowski, H. G.; Hansen, R. W., Innovation in the pharmaceutical industry: New estimates of R&D costs. *Journal of Health Economics* **2016,** *47*, 20-33.

CHAPTER II

NOVEL NANOPARTICULATE FORMULATIONS FOR TUMOR TARGETED DELIVERY OF CYCLIC DINUCLEOTIDES

This work was conducted in close cooperation with the Boehringer Ingelheim Research Site Vienna. The personal contribution covers manufacturing and characterization of all described nanoparticulate formulations. Cryo-TEM measurements were performed by Dr. Ingo Lieberwirth. Animal experiments (PK/PD study) were performed by Dr. Ottmar Schaaf.

1 Introduction

1.1 Nanoparticles for targeted drug delivery

Targeted drug delivery, as opposed to the traditional drug delivery methods via systemic circulation throughout the body, aims at accumulation of the substance directly in the tissue of interest [1]. This approach has many benefits; from enabling accurately localized high dosages at the sites of action, hence improving the action of active pharmaceutical ingredient, to limiting systemic drug toxicity [2]. Nanoparticle formulations are one of the plausible strategies for the drug targeting route.

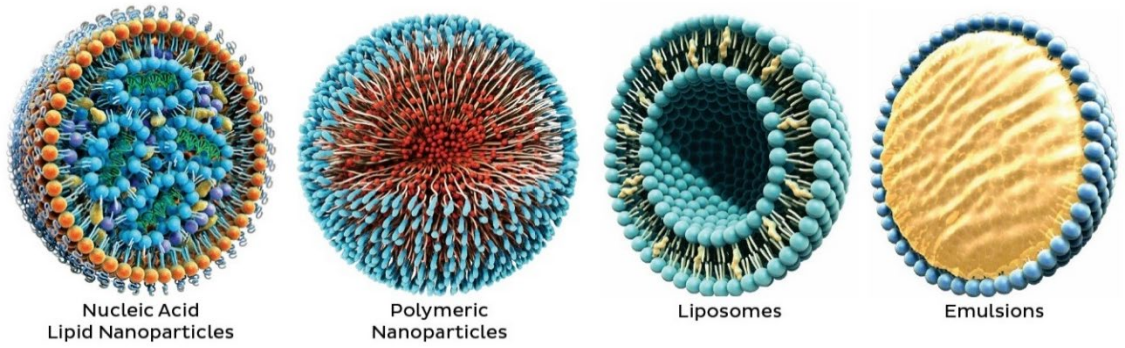

Figure 2 Illustrated image of nanoparticulate formulations (adapted from [3]).

A variety of different nanoparticulate formulations are precedent in literature as shown in Figure 2. Those formulations are mainly comprised of polymers or lipids, which are used to encapsulate a wide range of structurally different drugs, including small molecules [4], nucleic acids [5] and proteins [6]. Nanoparticulate formulations are widely explored for targeted delivery to different organs, e.g. brain [7], lung [8], liver [9], as well as tumors [10]. Additionally, these formulations can protect the drug from biodegradation or excretion and consequently increase its bioavailability [11]. Additionally, some nanoparticulate formulations enhance cellular uptake [12]. All these characteristics offer an improved targeting and distribution of the medication, especially for anti-tumor therapy. Therefore, nanoparticles have been extensively researched as drug delivery systems.

1.2 Tumor targeting

Cancer treatment is the most common application field in nanoparticular drug delivery [4, 10, 13]. In recent years, there has been enormous development in the field of nanomedicines for use in cancer therapy and many of those nanomedicines are currently being applied in clinical practice [14, 15]. The superior properties of nanoparticles in the targeted delivery field is most pronounced in the size range of approx. 20-200 nm [16]. Following intravenous administration, particles within this size range can localize in the tumor region due to the so-called enhanced permeability and retention (EPR) effect [17]. Tumor neovasculature formation, occurring as to accommodate nutrition and oxygen supply, results in poorly aligned defective endothelial cells with wide fenestrations. This leaky vasculature and insufficient lymphatic drainage of a tumor tissue increases permeability and subsequently accumulation of particles. The EPR effect does not occur in normal tissues, and therefore can be utilized as a passive tumor-targeting strategy [18].

In addition to the passive targeting properties, interaction of nanoparticle-coupled ligands specific to a receptor on the cell surface, can be used, to optimize the drug targeting further [19]. The specific binding of nanoparticles to a target cell type forms an active targeting approach, consequently increasing therapeutic efficacy (Figure 3). This approach is revisited in more detail in Chapter IV.

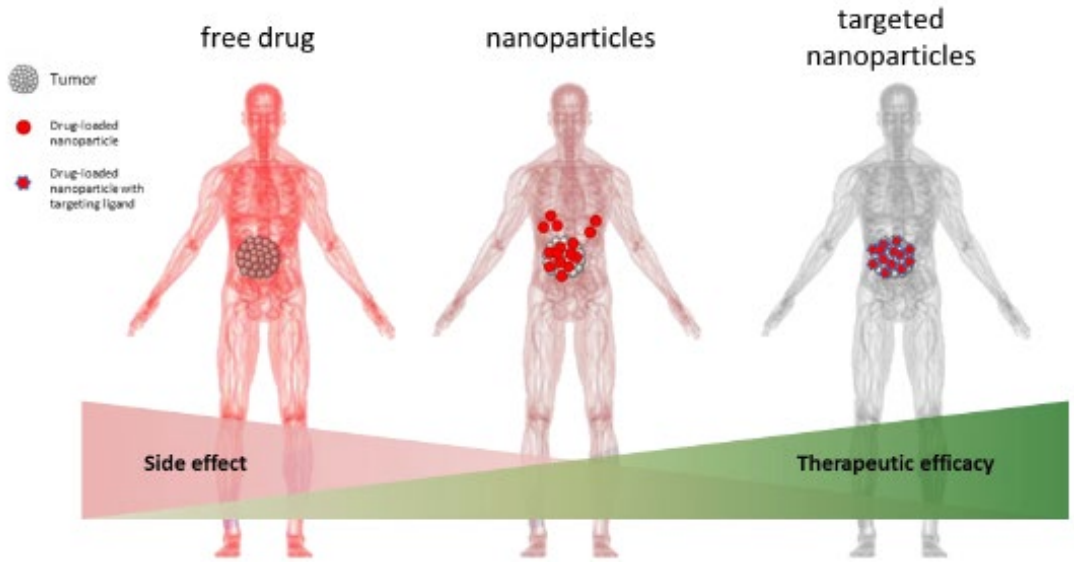

Figure 3 Benefit of targeted drug delivery utilizing nanoparticles (adapted from Wu, Liu [20]).

Although the EPR effect has been confirmed in many animal studies and is utilized in a number of commercial formulations, as well as in an extensive number of ongoing clinical trials, its benefits for clinical application are still controversially discussed [21]. Therefore, it is vital to consider the heterogeneity of EPR effect in different tumor types, in order to enable successful translation of nanoparticles into clinical practice [18].

1.3 Cancer immunotherapy

The activation of the immune system as the means to fight cancer has been the goal of scientist for decades [22-24]. In recent years, many approaches have been aimed at improving the immune system's natural ability to attack tumor cells. The biggest step forward was achieved with the development of immune checkpoint blockage, based on the inhibition of T-cell blocking proteins (e.g. PD-1). This approach has fundamentally changed the possibility to treat a diversity of advanced tumors [25, 26]. It comes as no surprise that the inhibition of negative immune regulation, was awarded with the Nobel Prize in Physiology or Medicine in 2018.

However, this novel principle for immune therapy is only effective when the tumor microenvironment is infiltrated with tumor antigen specific T-cells [27]. In contrast to these immunological "hot" tumors, "cold" tumors contain few infiltrating T cells and do not provoke a strong immune response, making them difficult to treat with such immunotherapies [28]. Therefore, turning "cold" tumors into "hot" ones is one of the most important issues for the future of immunotherapy.

1.4 STING

The stimulator of interferon genes (STING) pathway is known as a major mechanism for innate immune sensing of cancer [29]. STING is a pattern recognition receptor that detects cytosolic nucleic acids and transmits signals that activate type I interferon (IFN) responses. Tumor-derived DNA binds and activates the protein, cyclic GMP-AMP synthase, which in turn generates the cyclic dinucleotide, cGAMP, binding and activating STING (Figure 4).

This induces the downstream pathways, ultimately leading to the expression and secretion of type I IFN and other inflammatory cytokines. The secretion of type I IFN in the tumor

microenvironment leads to the induction of a T cell-dependent immune response, by activating the tumor-associated dendritic cells, presenting tumor specific antigen to cytotoxic $CD8^+$ T cells.

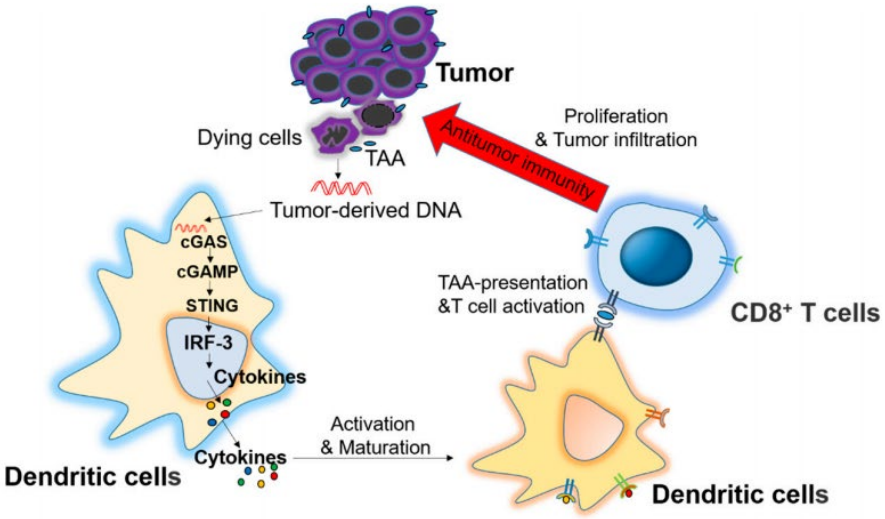

Figure 4 Role of the stimulator of interferon genes (STING) signaling pathway in antitumor immunity (adapted from [30]).

This leads to an improved priming and activation of tumor-specific cytotoxic $CD8^+$ T cells, increased $CD8^+$ T cell infiltration into the tumor, ultimately resulting in enhanced tumor cell death [31]. Thus, STING agonists can be used in patients that do not respond to a PD-1 therapy due to low tumor-infiltrating lymphocyte numbers.

1.4.1 STING Agonist (BI X)

The therapeutic modality utilized in this work is a synthetic cyclic dinucleotide (CDN) (denominated as BI X in the following text), which acts as a STING agonist consequently activating the STING pathway, leading to the immune response in the manner described above.

Although the described mode of action is very promising, the applicability and efficacy is limited by the STING agonist itself. The anionic and highly water-soluble API has a very low bioavailability and does not readily cross the cellular plasma membrane. As a result, only minor amounts of API reach the cytosol, where the targeted STING pathway is located [32]. Additionally due to the rapid clearance of the API, only negligible amounts reach the tumor tissue.

Therefore, only intratumoral administration was feasible so far, in order to achieve a sufficient API concentration in the tumor tissue and reduce severe systemic side effects. A nanoparticulate formulation for systemic administration, as to broaden the indication spectrum remains to be developed.

With this background, the novel formulation development is a resource consuming endeavor, requiring very high amounts of model API.

1.4.2 Model Compounds

Development of a novel formulation for early compounds such as synthetic CDN, is particularly challenging due to the high production costs of the compound. At this stage, an elaborate synthesis process is not yet established and the API can only be produced on a small scale with low yield. Here in particular, the preparation of enantiopure compounds can only be achieved by separation via chiral column chromatography, thereby also contributing to reduced yield and consequently high expenses. Therefore, the use of less expensive model compounds was evaluated in the initial trials within the scope of this work. Below a brief description of the compounds related to this study is included.

1.4.2.1 *Adenosine monophosphate (AMP)*

AMP (Figure 5) was selected as a model compound herein, due to its low pricing and structural similarity. The mononucleotide was considered sufficient as an initial model, despite the lack of the cyclic bond descriptive of the STING agonist, the cyclic dinucleotide.

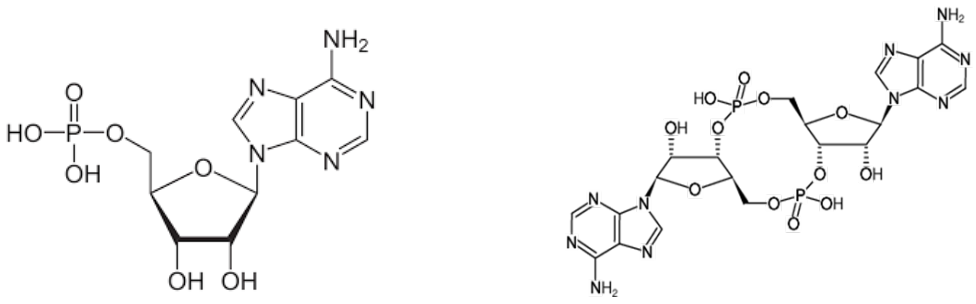

Figure 5 Structure of two model compounds, AMP (left) and c-di-AMP (right).

1.4.2.2 *Cyclic-di-adenosine monophosphate (c-di-AMP)*

C-di-AMP (Figure 5) is closely structurally related to the natural STING agonist. It consists of two guanine bases, linked by the phosphate and ribose group to form a heterocyclic

compound cycle. Only minor structural differences to the synthetic STING agonist make it a good model compound. Unfortunately, the high purchasing costs of this naturally occurring molecule limits its availability.

1.4.2.3 *BI X stereoisomer (BI Y)*

During the synthesis of the enantiopure API, the ineffective stereoisomer had to be separated from the API, utilizing chiral column chromatography. In later phase of this project, the biological inactive stereoisomer (designated herein as BI Y) could be recovered and was used as the model compound with the highest similarity to the actual API (BI X).

1.5 Chitosan

To reduce toxicity and allow a clinical translation of tumor-targeted nanoparticles, only biocompatible and biodegradable materials are considered in the selection of materials for such a formulation. One well precedent example, known to be biocompatible, minimally toxic, non-immunogenic and enzymatically biodegradable, is chitosan, which is to date a very widely used polymer for drug delivery [33-36]. Under physiological conditions, chitosan can be enzymatically degraded by lysozymes or chitinases, which are produced by the normal flora in the human digestive tract [37] and is also present in the circulation [38]. This makes chitosan widely applicable to the pharmaceutical field. Chitosan is mainly manufactured by alkaline deacetylation of chitin, primarily sourced from crustacean, insect shells and fungi [39]. It is a linear polysaccharide composed of glucosamine and N-acetyl-D-glucosamine residues (Figure 6).

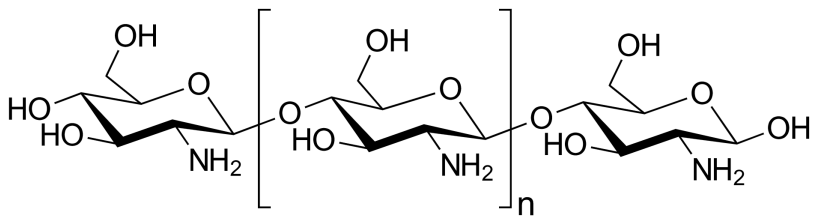

Figure 6 Structure of completely deacetylated chitosan.

Due to the abundance of the amine moieties, chitosan possesses a high positive charge density at acidic pH, allowing for complexation with anionic molecules such as small interfering RNA

(siRNA) or tripolyphosphate (TPP) [34]. The physicochemical properties of the polymer, and consequently the complexation efficiency, are strongly influenced by the degree of deacetylation and molecular weight of a chitosan. A vast variety of different quality grade chitosan is available commercially. The well-defined molecular weight and deacetylation degree is crucial for formulations involving complexation with chitosan [40]. Taken this into consideration, several studies have shown that chitosan-based nanoparticles can be utilized to deliver a variety of different APIs via various routes of administration, local [41, 42] as well as systemic [43, 44].

1.6 Microfluidic mixing

Using the routine methods to manufacture nanoparticles is very challenging and has some significant drawbacks, particularly for implementation in industrial pharmaceutical research. These techniques, such as nanoprecipitation and emulsion evaporation, often lack reproducibility and are difficult to scale. The microfluidic technique can tackle those challenges by producing nanoparticulate formulations in a well-controlled and high-throughput manner [45]. The technique involves controlled mixing of two different solutions, introduced via separate inlet microchannels, converging into one. The precision of this approach is accomplished by the homogenous and controlled mixing conditions in the mixing-chamber of the NanoAssemblr® Benchtop system. The mixing chambers are equipped with staggered herringbone mixers, allowing the required compounds to be mixed by a laminar fluid flow as shown in Figure 7 [46].

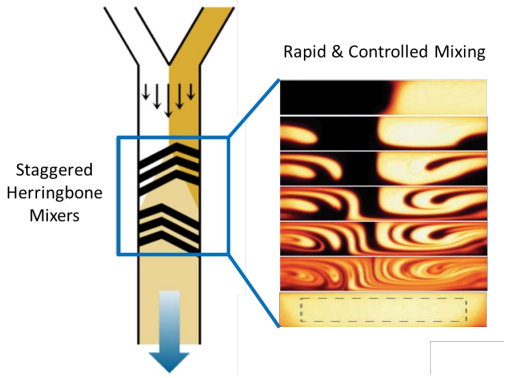

Figure 7 Graphical representation of the utilized staggered herringbone mixer in the NanoAssemblr® Benchtop system (adapted from Stroock, Dertinger et al. (2002)).

Hereby turbulent flow is avoided and replaced by diffusion, which facilitates an efficient and controllable mixing under continuous flow conditions. This leads to a very refined, highly reproducible formation of nanoparticles, as dictated by the flow parameters. In contrast to the previously mentioned bulk methods, uncontrolled nucleation and agglomeration can be avoided. The characteristics of nanoparticles produced in this manner can be readily adjusted by controlling the process parameters, such as flow ratio and flow rate [47]. The biggest advantage in case of the industrial pharmaceutical research, is the possibility to scale-up the manufacturing simply by increasing the number of mixing-chambers [48].

1.7 Aim

This chapter describes the development of a nanoparticulate formulation, as to encapsulate a highly potent CDN-type compound aiming at cancer immunotherapy. Due to the passive tumor targeting of nanoparticles, a reduced systemic toxicity and enhanced efficacy after i.v. administration is anticipated. Owing to the unique properties of the API, innovative manufacturing and screening methods had to be established, with a special focus on the challenges in industrial pharmaceutical research. In order to confirm the therapeutic concept of this novel formulation, an *in vivo* PK/PD study in tumor bearing mice was performed.

2 Material and Methods

2.1 Materials

Two novel research compounds, denominated herein as “BI X” and “BI Y” were provided by Boehringer Ingelheim Pharma GmbH & Co. KG (Biberach an der Riß, Germany). Due to intellectual properties, no further information regarding those compounds can be provided.

Poly (lactic-co-glycolic acid) (PLGA) Resomer® RG 752 H (RG752H) was obtained from Evonik Industries AG (Essen, Germany). A sample of PEGylated PLGA, EXPANSORB® DLG 50-6P (PLGA-PEG) was graciously provided by Merck KGaA (Darmstadt, Germany). Chitosan (CS) (Chitoceuticals) with different deacetylation degrees and molecular weights, namely 95/5, 95/50 and 80/5, were purchased from Heppe Medical Chitosan GmbH (Halle (Saale), Germany). Deionized distilled (DI) water was produced in-house with ultrapure water purification system by PURELAB Ultra Ionic (ELGA, High Wycombe, United Kingdom).

Acetic acid, acetonitrile (ACN), adenosine monophosphate (AMP), ammonium acetate, chitosan (low molecular weight, 50 – 190 kDa, 75 – 85 % deacetylated), cyclic-di-adenosine monophosphate (c-di-AMP), ethanol (EtOH), polyvinyl alcohol (PVA), sodium chloride (NaCl), tripolyphosphate (TPP) were obtained from Merck KGaA (Darmstadt, Germany). All solvents used were of HPLC purity grade.

2.2 Manufacturing methods

2.2.1 Double Emulsion Evaporation

API loaded nanoparticles were prepared using a double emulsion evaporation method according to the literature. Stock solutions containing 200 mg/mL AMP in DI water and 50 mg/mL PLGA 752H in DCM were prepared. The two solutions were mixed in a 1:9, 1:3 and 1:30 volume ratio (AMP:PLGA) and homogenized using a T 25 digital ULTRA-TURRAX® (IKA, Staufen, Germany) for 25 sec at 20.000 rpm. This pre-emulsion was then added in a 1:10 and 1:20 volume ratio into a 1% and 5% PVA solution. The resulting mixture was homogenized using a Model 120 Sonic Dismembrator (Thermo Fisher, Waltham, USA) for 1 min at 50 % power output. After homogenization, the resultant emulsion was stirred for 1 h to let the

organic solvent evaporate. The hardened particles were subsequently washed three times by centrifugation (14,000 rpm, 4 °C, 30 min) and redispersed in DI water. Directly after this process the nanoparticle suspension was lyophilized.

2.2.2 Ionic crosslinking method

Chitosan/TPP nanosized complexes were manufactured using the ionic crosslinking method utilizing TPP as a crosslinking agent. Chitosan was dissolved in a 1% (v/v) acetic acid solution at a concentration of 1 mg/mL. TPP was dissolved in DI water in various concentrations ranging from 2.5 to 20 mg/mL. In subsequent steps, 1 mg/ml AMP or 1 mg/mL c-di-AMP were added to 2.5 mg/mL TPP solution. Subsequently, 1 ml of the TPP solution was introduced dropwise into 3 mL of the chitosan solution. The resulting mixture was incubated under stirring for 30 min to complete crosslinking of the positively charged chitosan with the negatively charged TPP.

2.2.3 Microfluidic mixing of chitosan complexes

2.2.3.1 *Chitosan/TPP complexes*

Chitosan/TPP complexes were manufactured using the microfluidic mixer Nanoassemblr Benchtop Instrument (Precision NanoSystems, Inc., Vancouver, Canada) by mixing designated volumes of chitosan and TPP solutions. Microfluidic cartridges were pre-processed before every run, by washing both channels with DI water. Chitosan was dissolved in 1% (v/v) acetic acid solution at a concentration of 0.5 and 0.25 mg/mL. TPP was dissolved in DI water at concentrations of 0.1, 0.25, 0.5 and 1.25 mg/mL. All prepared solutions were filtered through a 0.45 µm cellulose acetate membrane (Sartorius AG, Göttingen, Germany). For manufacturing of chitosan/TPP-complexes, the chitosan solution was injected through one inlet of the microfluidic mixer, whereas TPP solution was injected through the other inlet. The complexes were prepared at TPP/chitosan solution ratio of 1:1 – 1:5 and 2:1 with a flow rate of 1 mL/min. A total volume of 1 mL of stock solution was injected through the microfluidic mixer, including an initial waste volume of 0.25 mL and a final waste volume of 0.05 mL. A graphical representation of the manufacturing process is shown in Figure 8.

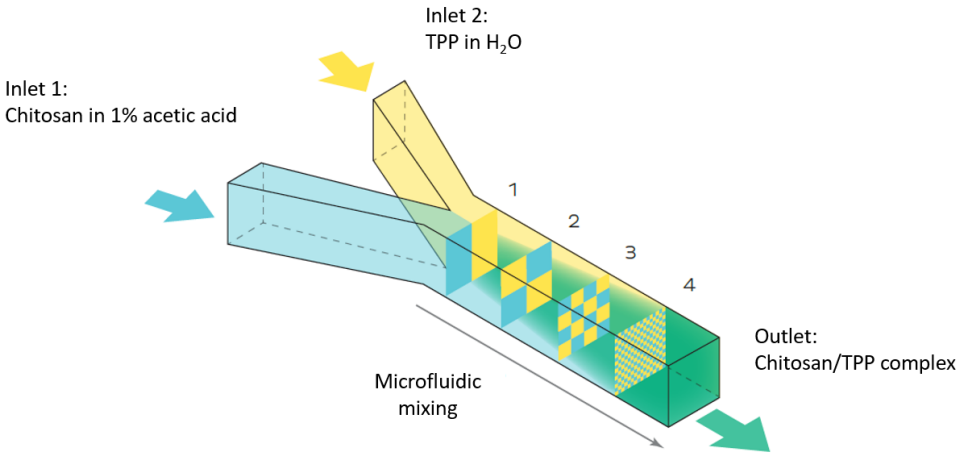

Figure 8 Graphical representation of the microfluidic mixing procedure.

2.2.3.2 *Chitosan/TPP/BI Y and Chitosan/BI Y complexes*

The chitosan/TPP/BI Y complexes were prepared as described in the previous section. Here, BI Y was added into 0.5 and 0.1 mg/mL TPP solution in concentrations of 0.625, 1.25 and 2.5 mg/mL. The resulting solution was mixed with 0.5 mg/mL chitosan at a ratio of 1:1. Additionally, stand-alone BI Y solutions at concentrations of 0.5, 1.25 and 2 mg/mL were mixed with 0.5 mg/mL chitosan solution at a ratio of 1:1, 1:2, 1:4 and 2:1.

2.2.3.3 *High-grade chitosan/BI Y and BI X complexes*

Chitosan with a molecular weight (MW) of 10 – 50 kDa, and a deacetylation degree (DD) of 95% (CS95/5) was dissolved in 1% (v/v) acetic acid solution at a concentration of 0.5 mg/mL and diluted with DI water to a concentration of 0.1 mg/mL. BI Y was dissolved in DI water at concentrations of 0.1, 0.5, 1.0 and 1.25 mg/mL. The complexes were manufactured as described previously and the filtered solutions were injected through the two inlets of the microfluidic mixer at flow ratios of 1:1 and 1:2. BI X was prepared at a concentration of 0.5 and 0.25 mg/mL and processed accordingly.

2.2.4 Cleaning

The manufactured complexes were purified by Spectra/Por™ Float-A-Lyzer™ G2 Dialysis Devices (Repligen, Waltham, USA). The dialysis devices were prepared by submerging the filter membrane in 10 % ethanol solution for 10 min and subsequently soaked in DI water for 30

minutes. Further, 1 mL of the manufactured complexes was loaded into the prepared device and kept floating in 200 mL of an acidic, neutral or alkaline media (pH 4.5, 6.8 and 10) for 2 and 20 hours. The floating media were changed after 2 and 4 hours. All manufactured precursor formulations (chitosan/API-complexes) were purified utilizing the acidic media for 20 hours.

2.2.5 PLGA-PEG coating

Microfluidic mixing was utilized in order to coat the pre-fabricated chitosan/API-complex by mixing PLGA-PEG solutions with the precursor formulation. PLGA-PEG was dissolved in acetonitrile in concentrations of 0.1, 0.25, 0.5, 1 and 2 mg/mL. The PLGA-PEG solution was injected through one inlet, whereas precursor formulation was injected through the other inlet of the microfluidic mixer at a flow ratio of 1:1 and flow rate of 1 mL/min. The resultant nanoparticulate formulations were subjected to centrifugal filtration by 100 kDa Amicon® Ultra Centrifugal Filters (Merck KGaA, Darmstadt, Germany). The samples were washed twice with DI water and centrifuged for 15 min (2,000 rpm, 4°C). Flow-through was discarded from collection tube and filtration residue was collected.

2.3 Physicochemical characterization

2.3.1 Particle size measurement

The hydrodynamic diameter and size distribution were determined in DI water by dynamic light scattering (DLS) using a NanoPartica SZ-100 (Horiba, Kyoto, Japan). All measurements were conducted at 25°C with a detection angle of 173° for 120 sec. Z-average and polydispersity index (PDI) were estimated from autocorrelation function using the cumulant analysis. For each sample, the measurement was recorded in triplicates, and the average of the measurements was calculated. All values of Z-average and PDI were expressed as the mean and standard deviation.

2.3.2 Zeta Potential

Surface charge of the nanoparticles of the nanoparticles dispersed in 1 mM NaCl solution was measured in carbon-coated microelectronics cells (Horiba, Kyoto, Japan) using the NanoPartica SZ-100 (Horiba, Kyoto, Japan). The measurements were repeated at least three

times without sample dilution. The zeta potential was calculated from electrophoretic mobility using the Helmholtz-Smoluchowski equation.

2.3.3 Determination of complexation efficiency

Chitosan-based complexes were isolated from free compound by centrifugation (30 min, 14,000 rpm, 4°C). The amount of free compound (non-complexed compound) in the clear supernatant was measured using HPLC. The complexation efficiency was calculated from the total amount of the compound introduced and the amount of free compound in the supernatant using the following equation:

Complexation efficiency: $\left(\frac{total\ amount\ of\ compound - amount\ of\ free\ compound}{total\ amount\ of\ compound}\right) \text{x } 100\%$

2.3.4 Determination of washing efficiency

Nanoparticle formulations in dialysis device were centrifuged (30 min, 14,000 rpm, 4°C) after the designated cleaning protocols and the compound amount, retained within the formulation, was determined indirectly by measuring the concentration of the free compound in the supernatant using HPLC. The washing efficiency was calculated from the amount of free compound after manufacturing and residual amount of free compound in the dialyzed sample using following equation:

Washing efficiency:

$$(1 - (initial\ free\ compound\ amount - residual\ free\ compound\ amount)) \text{ x } 100\%$$

2.3.5 Determination of drug load

The final formulation was lyophilized to determine the drug load of the nanoparticles. Subsequently, 1 mg of the lyophilized sample PLGA/API-formulation was resuspended in 0.5 mL acetonitrile and sonicated in an ultrasonication bath for 60 min, as to extract the chitosan/API complex from the nanoparticles. Then 0.5 mL 0.9% NaCl solution was added and sonicated again for 60 min to destroy the complex. The resulting mixture was centrifuged (30 min, 14000 rpm, 4°C) and the concentration in the supernatant was measured by HPLC. Drug load (DL) was calculated as shown here:

Drug load: $\left(\frac{amount\ of\ drug\ present\ in\ formulation}{total\ weight\ of\ formulation}\right) \text{ x } 100\%$

2.3.6 Determination of administered dose

An aliquot of 100 µL of the final formulation was processed as described previously. After lyophilization, acetonitrile and NaCl solution were added and after sonication and centrifugation, the supernatant was analyzed by HPLC. Based on the amount of API in the supernatant, the concentration in the final formulation was determined.

2.3.7 Cryo-transmission electron microscopy (Cryo-TEM)

All cryo-TEM measurements were performed by Dr. Ingo Lieberwirth (Max Planck Institute for Polymer Research, Mainz).

For cryo-TEM examination, the samples were vitrified using a Vitrobot (FEI) plunging device. Further, 10 µl of the sample dispersion was applied to a holey carbon coated TEM grid that has been glow discharged shortly before. After removing excess sample solution with a filter paper, the grid was immediately plunged into liquid ethane. For the subsequent examination, the specimen was transferred to a TEM (FEI Tecnai F20) keeping cryogenic conditions using a cryo-EM holder (Gatan 926).

2.3.8 Transmission electron microscopy (TEM)

All TEM measurements were performed by or with assistance from Dr. Martin Dass (Boehringer Ingelheim, Biberach and der Riß).

Negative staining TEM was applied for the evaluation of the nanoparticle morphology. Briefly, 2 µL of a water-diluted sample was placed on a carbon film coated copper grid. Excess sample solution was removed with a filter paper. The grid was stained with 10 µL of 2% phosphotungstic acid for 1 minute. The surplus staining solution was removed afterwards with a filter paper and the sample was dried at ambient environment before imaging using a LEO 912 AB (Carl Zeiss AG, Jena, Germany) operating at an acceleration voltage of 80 kV.

2.3.9 High-performance liquid chromatography (HPLC)

All HPLC measurements were performed on an Agilent 1100 Series (Agilent Technologies, Santa Clara, USA). For each HPLC run, 2 µL of sample solution was aliquoted and analyzed with a Synergi™ 4 µm Fusion-RP 80 Å, LC Column 100 x 2 mm (Phenomenex Inc., Torrance, USA), at a flow rate of 1 mL/min. A gradient method was used to elute the API, starting with 95% 20 mM filtered ammonium acetate buffer (pH 4.5). The ratio of acetonitrile was increased

progressively until the mobile phase consisted of 85% acetonitrile after 9 min. Finally, the amount of acetonitrile was increased to 95% in the last minute of the run. The overall runtime was 10 min with a retention time of 5 min for the API. *Empower 3* software (Waters, Milford, USA) was used to process and quantify sample peaks.

2.4 PK/PD

2.4.1 Animal experiments

All animal experiments were performed at BI Vienna by Otmar Schaaf.

The different formulations were administered intravenously (i.v.) to tumor bearing mice (17 – 24 g body weight, three female animals per treatment group, respectively). Blood samples were collected at specified time points via puncture of the saphenous vein using Ethylendiamintetraacetic acid (EDTA)-coated microvettes. Plasma was captured after centrifugation and immediately frozen at -20 °C until LC-MS/MS analysis. Tumor, liver and spleen were removed and homogenized in an aqueous buffer prior to protein precipitation with acetonitrile. The samples were stored at −20 °C until LC-MS/MS analysis.

Animal experiments were approved by the local animal ethics committee and were in agreement with the German Animal Welfare Act.

2.4.2 LC-MS/MS analysis

Plasma aliquots of 5 µL were supplemented with 400 nM of BI-1052 (internal standard). Plasma proteins were precipitated by the addition of 70 µL 50% acetonitrile : 50% methanol and subsequent centrifugation at 4000 rpm, 4 °C for 10 min in an Eppendorf 5810 centrifuge (Eppendorf AG, Hamburg, Germany). From the resulting supernatant 30 µL were diluted in 170 µL 0.1% formic acid in a 96-well plate (Greiner, Frickenhausen, Germany).

An API 6500 mass spectrometer (ABSciex, Darmstadt, Germany) was equipped with an Agilent 1290 LC system, a CTC autosampler and a Kinetex 30 x 2.1 mm, 2.6 µm C18 LC column (Phenomenex, Aschaffenburg, Germany). The MS conditions were set as follows: Positive mode, 400 °C source heating, curtain gas = 40, gas 1 = 50, gas 2 = 50, a capillary voltage of 5000 V. The following MS transitions were recorded: EX 7123: 473.3/256.2, DP = 81, CE = 19; internal standard: 453.0/275.0, DP = 91, CE = 29. Solvent A consisted of 0.1% aqueous formic

acid and solvent B of 0.1% formic acid in 50% acetonitrile: 50% methanol. The gradient started at 90% solvent A, which increased within 2.6 min to 5%. After 0.7 min solvent A was set to 90% for re-equilibration. The flow rate was set to 400 µL·min-1 and the injection volume was 20 µL.

3 Results and Discussion

Herein, an optimal nanoparticulate formulation was developed, in order to enable a systemic administration of the CDNs for broadening the indication spectrum and to differentiate against alternative formulations suitable only for direct administration into the tissue of interest. As described previously, nanoparticles tend to accumulate in the tumor tissue via the EPR-effect. An additional advantage resulting from such a formulation is the reduced systemic toxicity and enhanced efficacy. A number of formulation approaches were explored herein, as to obtain an optimized nanoparticulate formulation, particularly with regard to particle size, stability and drug load.

3.1 Initial trials

A major challenge in encapsulating CDNs into PLGA-based nanoparticles using the emulsion evaporation techniques is the high water solubility of the compound. Hydrophilic APIs tend to partition from the hydrophobic polymeric phase into the external aqueous phase before solidification of the particles [49]. Therefore, initial attempts were made to encapsulate the API into nanoparticles without elaborate modification.

3.1.1 Emulsion-based technique

The plain single emulsion method is a well-established method used to manufacture API-loaded PLGA-based nanoparticles. Here, polymer and API are dissolved in a water-immiscible organic solvent and subsequently emulsified in an aqueous solution containing an emulsifier [50]. By utilizing this technique, various hydrophobic APIs such as Docetaxel [51], Paclitaxel [52], Capsaicin [53] and Naproxen [54] were encapsulated in nanoparticles. Additionally, using a similar approach, API-loaded microparticles were successfully manufactured in-house as described in Chapter IV of this thesis. However, this approach was not suitable for the current project due to the low solubility of the API in an organic solvent.

For those hydrophilic compounds, the double emulsification is considered to be a practical approach to manufacture API-loaded particles. However, this approach is utilized predominantly in preparation of microparticles as described in literature [55-58].

Due to the limited availability of BI X, AMP was used in these initial experiments as a model drug.

After manufacturing and washing of nanoparticles as described in Material and Methods section, the final formulation was analyzed for drug loading as shown in Table 1.

Table 1 Formulation parameters and characterization of AMP loaded nanoparticles prepared by emulsion evaporation method.

Formulation parameters			Characterization		
AMP : PLGA ratio	**Pre-Emulsion : PVA solution ratio**	**Concentration PVA [mg/mL]**	**Drug load [%]**	**Z-average [nm]**	**PDI**
1:9	1:10	0.1	0.10 ± 0.02	-	-
1:9	1:10	0.5	0.32 ± 0.05	-	-
1:9	1:20	0.1	0.16 ± 0.03	-	-
1:3	1:10	0.1	0.94 ± 0.15	187.6 ± 19.9	0.227 ± 0.046
1:30	1:10	0.1	0.19 ± 0.03	-	-

As expected for water-soluble compounds, all manufactured formulations showed a drug loading of <1%. Only by using a high ratio of AMP, a drug load close to 1% was achieved. Additionally, with these parameters a suitable Z-Average < 200 nm and PDI < 0.3 was accomplished. In literature, compounds with a similar water-solubility like propranolol [59], midazolam [60] and doxorubicin [61] were also encapsulated into nanoparticles utilizing the double emulsion technique. In these studies, a similar size distribution between 116 and 261 nm was generated and a maximum drug load of 1.5% was achieved.

However, for all manufactured formulations a comparably high amount of AMP (> 30 mg) was necessary. This would by far exceed the amount of the actual API available at this stage of preclinical research. Therefore, additional techniques had to be applied to enhance the drug load and therefore reducing the required amount of API.

3.1.1.1 *Counter-ion approach*

For a successful formulation, it is vital to retain the API in the nanoparticle during manufacturing. By utilizing the ionic properties of the compound, API retention may be achieved by incorporation of a counterion terminated hydrophobic molecule. Hereby, an ionic pair is formed, resulting in an overall more hydrophobic complex, consequently enhancing the retention time of the API in the particle. This has been documented previously by Ashton, Song [62] who used organic acid counterions to decrease the API release rate from PLA-PEG nanoparticles for basic APIs. Similar results were achieved in-house, as described in Chapter IV. Here, lauric acid was incorporated into PLGA-based microparticles, as to form an ionic pair with trimethoprim. Hereby, the enhanced drug load suggested an effective retention in the particle during manufacturing [63].

Based on these findings, a similar approach was contemplated for the CDNs. Since the API exhibits only anionic properties, cationic molecules may be utilized to form the desired ion-pair. In an initial attempt, aliphatic amines were evaluated for their efficacy as a counter ion. These attempts resulted in formation of large agglomerates. Since, most aliphatic amines have critical toxicological properties [64] and therefore this approach was not optimized further.

3.1.2 Chitosan based formulation development

Excipients posing less toxicological concern were considered for further manufacturing procedures. Therefore, the use of different cationic polymers for this purpose was investigated. By the beginning of this thesis work, the combination of a cationic polymer with an anionic CDN was not precedent in the literature. However, another structurally closely related compound has been intensively investigated with cationic polymers, namely small interfering RNA (siRNA).

SiRNAs share some similarities with CDNs. Both compounds are negatively charged, they are based on nucleotides and their target of interest is located in the cytosol [65]. Therefore, delivery techniques utilized for siRNA also represent promising approaches for CDN.

Lipid-based and polymer-based nanoparticles are the most common non-viral delivery systems for this type of API [66-68]. While liposomes and solid lipid nanoparticles have more precedence in the literature and commercialized products, this work was focused on

manufacturing of polymer-based nanoparticles, which also hold much promise as delivery vehicles.

Polyethylenimine (PEI) is a commonly used polymer for *in vivo* siRNA delivery [69, 70]. Nevertheless, the lack of non-biodegradability of this polymer is a limiting factor, especially for a later clinical translation, which was one of the aims of this work. Despite the fact that the level of toxicity decreases with MW lowering also risks [71], another well-known cationic polymer was used in this study, namely chitosan.

As described previously, chitosan offers many advantages such as biodegradability and nontoxicity. Chitosan-based nanosized complexes containing siRNA are already well described in literature [72-75]. These polyplexes can be prepared by applying ionic crosslinking method using TPP as a crosslinking agent. By dropwise addition of TPP to a chitosan solution, nanosized complexes can be formed through ionic interaction [76]. Due to the similarity between siRNA and CDN it was suspected, that exchanging siRNA for CDN could also allow the manufacturing of CDN containing complexes.

In addition to the co-complexation of siRNA, some selected small molecules such as methotrexate [77], tacrin [78] and dazomet [79], as well as proteins [80] were also encapsulated into chitosan-TPP nanoparticles.

3.1.3 Nano-precipitation approach

In a preliminary approach, as a proof of concept study, placebo complexes containing only chitosan and TPP were manufactured. Hereby, the Ionic crosslinking method, as described previously, was utilized. Since concentration of TPP is reported to determine the particle size distribution of the nanoparticles [78], various concentrations of TPP were tested.

Table 2 Formulation parameters and characterization of chitosan-based nanosized complexes manufactured by nanoprecipitation method.

Formulation parameters			Characterization		
Concentration TPP [mg/mL]	**Concentration AMP [mg/mL]**	**Concentration c-di-AMP [mg/mL]**	**Z-average [nm]**	**PDI**	**Complex. efficiency [%]**
2.5	-	-	184.6 ± 9.8	0.27 ± 0.04	
5	-	-	N.D. --> Agglomerates		
10	-	-	N.D. --> Agglomerates		
20	-	-	N.D. --> Agglomerates		
2.5	1	-	174.3 ± 6.4	0.31 ± 0.07	4.1
2.5	-	1	N.D. --> Agglomerates		24.8

As shown on Table 2, a specific concentration of TPP was necessary to form the desired complex. Here, nanoparticles with a Z-Average of 184.6 and a PDI of 0.27 were successfully manufactured by using a TPP concentration of 2.5 mg/mL. Higher concentrations of TPP lead to visible agglomeration. These findings vary from the results described in literature [78, 79], where no agglomeration was observed for similar parameters.

This effect may be attributed to the undefined deacetylation degree (DD) and broad range in molecular weight (MW) of the commercially available chitosan. The applied batch might have

had a lower DD or lower MW than indicated, and a higher amount of TPP may have led to agglomeration due to the potentially excessive concentration of crosslinking agent.

Despite the successful manufacturing of a nanosized complex formulation, the described issue had to be addressed. It was assumed that a higher-grade chitosan form with a better defined DD and MW would reduce manufacturing variability. Due to delivery difficulties, a more defined polymer was not available at this point of study and this issue was addressed later.

Addition of AMP and c-di-AMP

As next step, AMP was added to the formulation described above, which achieved the most optimal nanoparticle formulation. Hereby, a similar size distribution was generated and approximately 4 % of AMP was retained in the nanosized complex.

Due to the successful complexation of AMP, a model compound structurally closer to the actual API was used, namely c-di-AMP. However, due to the high purchasing costs only a limited amount of experiments were conducted.

With one of the parameters shown in Table 2, a very high complexation efficiency of 24% was measured. However, after addition of c-di-AMP, fast agglomeration was observed and no nanosized particles were detectable. This strengthens the assumption, that a high amount of the actual API can be complexed by chitosan. Further optimization efforts were needed to prevent agglomeration and achieve stable nanosized particles.

However, by applying the described method, a relatively high compound amount was needed to form the complex, which can easily exceed available amounts of actual API. Due to the high costs and limited availability of the actual API, only a very limited amount of tests to manufacture and optimize the formulation can be conducted. Additionally, similar to the double emulsion evaporation method, an upscaling optimization may be challenging due to different mixing conditions for producing higher quantities. The manual dropwise addition is not very accurate due to different mixing and dispensing conditions, which may lead to insufficient reproducibility. Therefore, to achieve precise control of the nanoparticle properties, a scalable procedure is necessary.

3.2 Microfluidic Mixing approach – development of precursor formulation

Microfluidic mixing method was implemented to manufacture the chitosan-based formulation reproducibly. Microfluidic mixing methods applied to chitosan-based formulations using similar mixing devices are already described in the literature [81-84]. Due to the differences between the various devices, the described methods could not be transferred directly to the available microfluidic device. Therefore, preliminary tests were conducted to manufacture nanosized chitosan/TPP complexes. With the experience gained from the previous method, it was obvious that successfully manufacturing nanosized complexes highly depends on the right concentration of cationic polymer and anionic crosslinking agent. Similar to the ionic gelation method performed previously, various concentrations and ratios of chitosan and TPP were tested in the first step.

3.2.1 Chitosan/TPP complex

As shown in Figure 9, increasing the concentration of TPP (0.1 mg/mL to 1.25 mg/mL), while keeping the concentration of chitosan constant (0.5 mg/mL), increased the Z-average of the nanoparticles. At very high TPP concentration of 1.25 mg/mL, large particle sizes and PDI of > 1.0 were observed, which is a clear sign for emerging agglomerates. At lower concentrations of TPP tested, nanosized particles were obtained with a Z-average between 126.7 and 317.5 nm. At low TPP concentration of 0.1 mg/mL, the amount of the crosslinking agent was not sufficient to form the nanosized complex. Consequently, no signal was detected during DLS measurements, pointing at no particle formation. Furthermore, lower chitosan concentrations lead to clearly visible agglomerates. This might be caused by the excessive TPP concentration compared to the amount of chitosan present. Similar results were reported by Hassani, Laouini [78] and Li and Huang [85] who also observed that TPP concentration is an essential parameter for the formation of nanoparticles, as it effects their crosslinking efficiency.

In addition to the TPP concentration, by adjusting the chitosan-TPP ratio, the particle size and PDI was further refined to achieve the desired Z-Average between 100 and 150 nm.

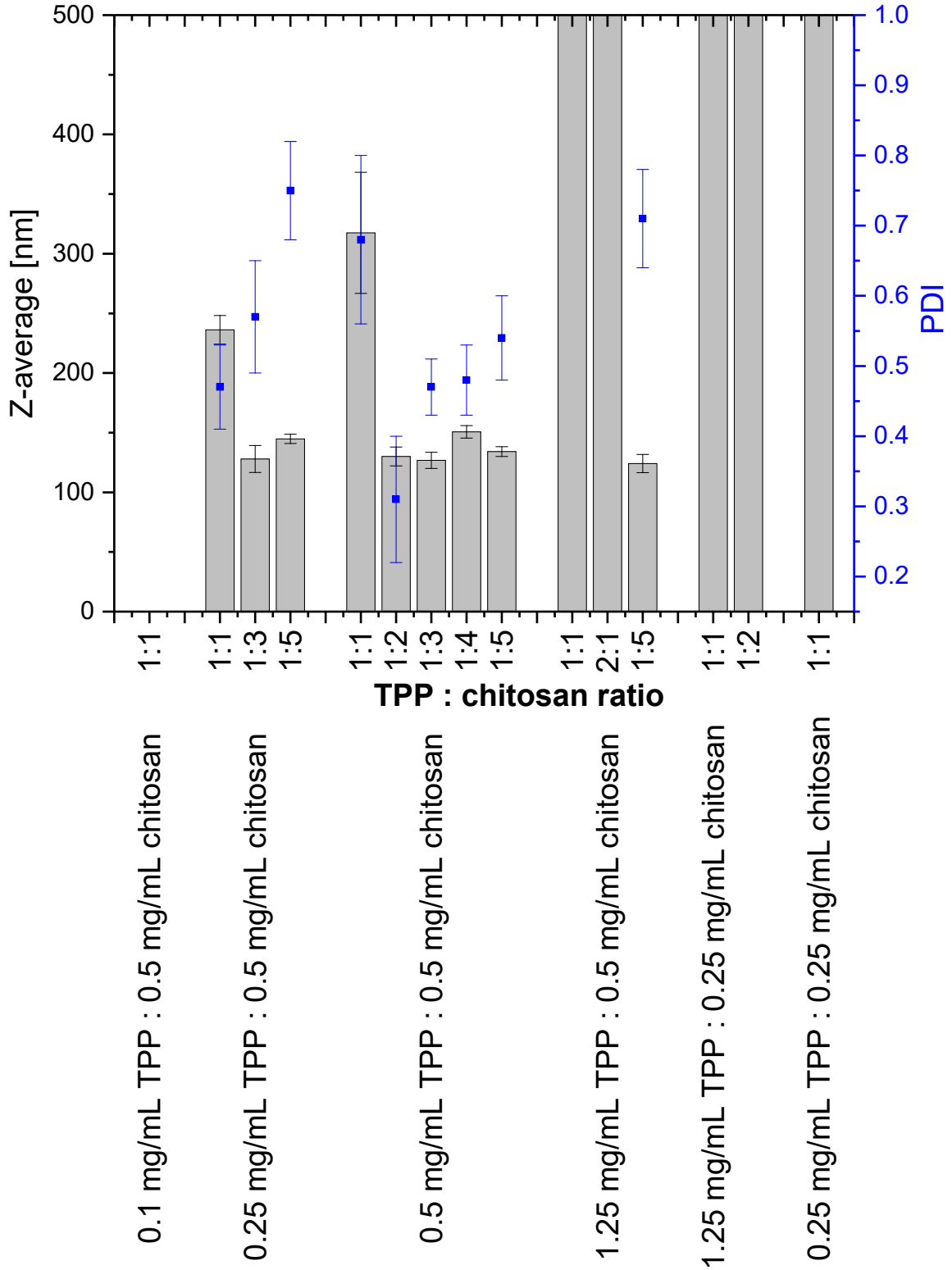

Figure 9 Z-average and PDI of chitosan/TPP complexes manufactured by microfluidic mixing with variation of ratio and concentration of chitosan and TPP.

As a result, it was successfully demonstrated in this preliminary experiment that manufacturing of a nanosized chitosan-TPP complex can be transferred to the more reproducible and better scalable microfluidic mixing method. This study forms a good reference point for future optimization. Emerging agglomerates can be attributed to an excessive concentration of crosslinker, whereas no detection of nanosized complexes in DLS was an indicator for insufficient crosslinking.

Since the placebo complexes were successfully manufactured, the model compound was added in the next step. As shown in Figure 9, optimized nanosized complexes with a Z-average of 130 nm and a PDI of 0.31 were achieved using a concentration of 0.5 mg/mL TPP and chitosan with a flow ratio of 1:2. Since a suitable size distribution was achieved, the parameters of this formulation were used as starting point for the following trials.

3.2.1.1 *Addition of BI Y*

Since the actual API was not available in a sufficient amount, the stereoisomer of the API (BI Y) was utilized for the following approaches.

BI Y was added to the TPP solution in concentrations of 0.625, 1.25 and 2.5 mg/mL.

As shown in Figure 10, introduction of the CDN, instead of c-di-AMP, led to increased particle size and PDI in all manufactured formulations. This may be caused by an additional negatively charged functional group contributing to crosslinking. This could have a similar effect as the excessive amount of TPP described earlier. A similar effect was observed previously, during the addition of c-di-AMP.

Therefore, the concentration of the crosslinking agent TPP was reduced to 0.1 mg/mL in a second step and nanosized complexes with a Z-average between approx. 200 and 300 nm were generated. Nevertheless, even with a minimal amount of TPP an increase in particle size compared to the formulation without the CDN was clearly visible.

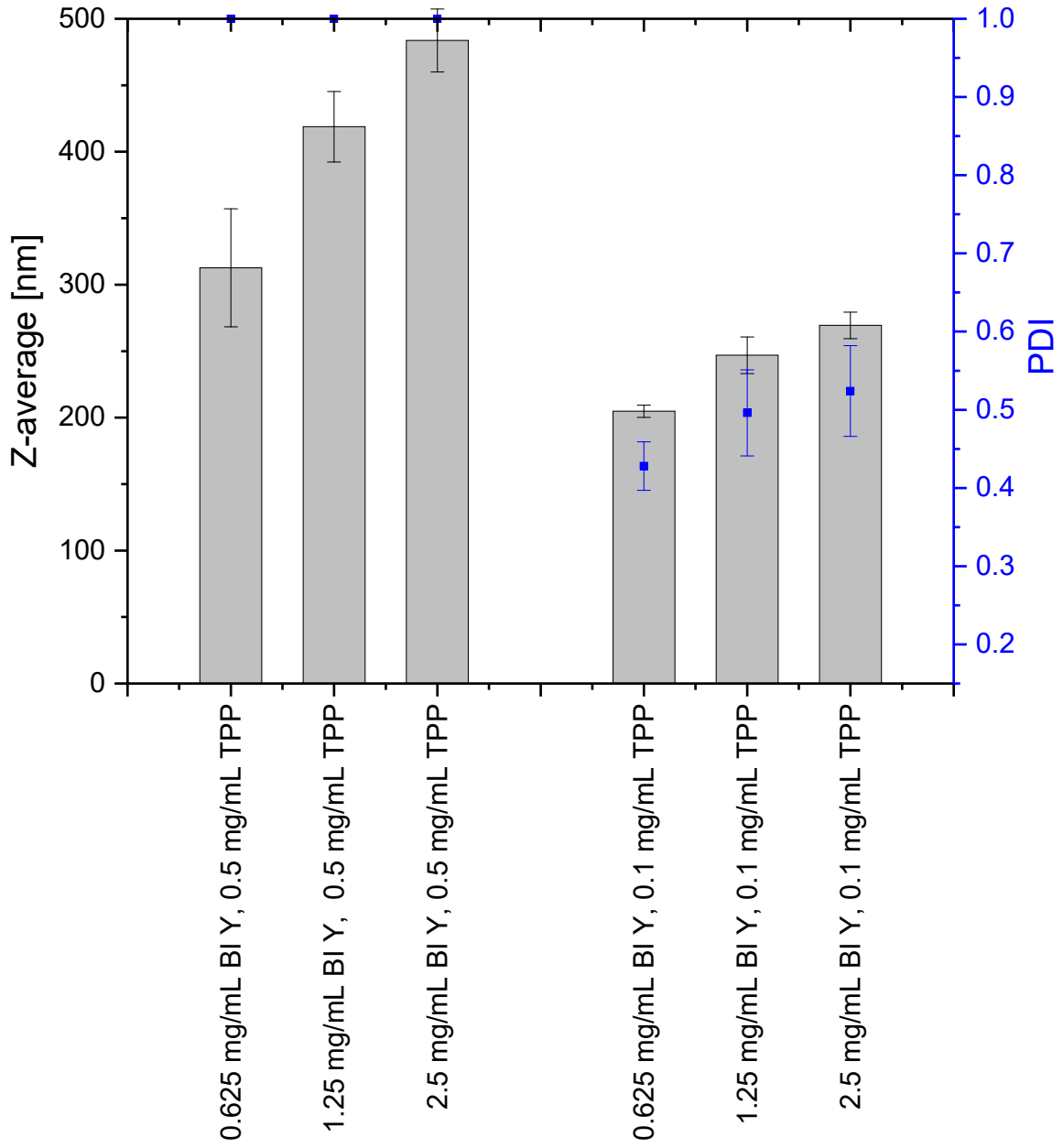

Figure 10 Z-average and PDI of chitosan/TPP complexes after addition of BI Y with variation of TPP and BI Y concentration.

The nanoparticles with a suitable size distribution were further characterized with regard to their complexation efficiency. Hereby, a very high complexation efficiency between 20 and 35 % was achieved as shown in Table 3.

Table 3 Formulation parameters and characterization of chitosan/TPP complexes after addition of BI Y.

Formulation parameters		Characterization		
Concentration TPP [mg/mL]	**Concentration BI Y [mg/mL]**	**Z-average [nm]**	**PDI**	**Complexation efficiency [%]**
0.1	0.625	204.8 ± 4.6	0.42 ± 0.03	20.0 ± 4.4
0.1	1.25	246.9 ± 13.8	0.46 ± 0.06	34.4 ± 9.7
0.1	2.5	269.4 ± 10.0	0.52 ± 0.06	35.4 ± 4.9

These results confirm the assumption that CDN can act as a crosslinking agent on its own, without the addition of TPP. This would offer some advantages for future formulations. Excluding TPP would simplify the manufacturing process, since an influential parameter would be removed and further improve complexation efficiency of the CDN in the complex.

Therefore, nanosized complexes were manufactured without addition of TPP in the next step.

3.2.2 Chitosan/CDN (BIY) complex

Since no comparable formulation using only a small molecule CDN as crosslinker is described in literature, only the experience gained from in-house previous studies could be used as a starting point for this approach. One indication for the right concentration and ratio between chitosan and STING agonist might be the N/P ratio, as it is well described for siRNA formulations [86]. Since N/P ratio is defined as the ratio between chitosan nitrogen (N) per nucleic acid phosphate (P), it may be transferred to CDN. However, since the chitosan used had no clearly defined DD or MW, as mentioned previously, the nitrogen amount of chitosan could not be determined. Therefore, the optimal manufacturing parameters, including concentration and ratio of chitosan and the STING agonist, had to be determined experimentally. A further difficulty was the limited availability of the CDN, and experiments with a minimal API consumption had to be performed.

To overcome these difficulties, a two-step screening method was established. In a first step the available parameters (chitosan and CDN concentrations, chitosan : TPP ratio) were altered until a suitable size distribution was achieved (Figure 11). In the second step, complexes with adequate sizes between 100 and 200 nm and minimal PDI were manufactured in a larger scale for further characterization with regard to zeta-potential and complexation efficiency (Table 4).

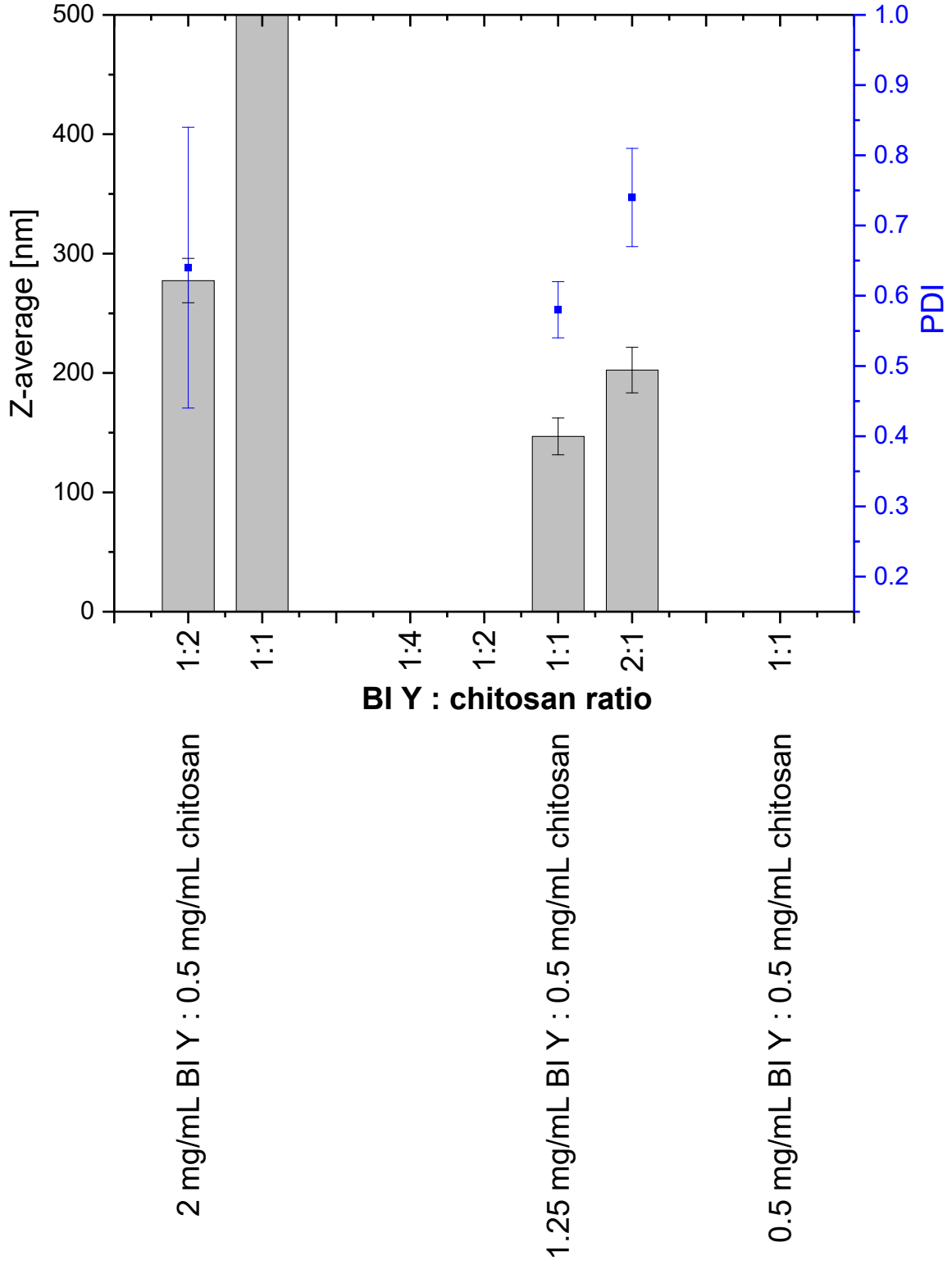

Figure 11 Z-average and PDI of chitosan/BI Y complexes manufactured by microfluidic mixing with a variable amount of BI Y and different ratios of BI Y and chitosan.

In the first screening step, it was shown that concentration of 2 mg/mL CDN was too high, since particle size > 200 nm and agglomeration were observed. Reducing the amount of BI Y to 1.25 mg/mL and applying the BI Y : chitosan ratio of 1:1 or 1:2 led to a suitable Z-average. Further reduction of the of BI Y concentration does not provide sufficient crosslinking agent to form the nanosized complex, resulting in no particles detected.

A similar phenomenon had been observed with the TPP formulation, where increasing concentration of the crosslinking agent lead to increase in the particle size.

According to the proposed two-step screening, Zeta-potential and complexation efficiency of the nanoparticulate formulations with a suitable Z-average were measured as shown in Table 4.

Table 4 Formulation parameters and further characterization of chitosan/BI Y complexes with different ratios of BI Y and chitosan.

Formulation parameters		Characterization			
Concentration BI Y [mg/mL]	**BI Y : chitosan ratio**	**Z-average [nm]**	**PDI**	**Zeta-potential [mV]**	**Complexation Efficiency [%]**
1.25	1:1	146.9 ± 15.1	0.58 ± 0.04	22.3 ± 1.0	28.3 ± 1.5
1.25	2:1	202.4 ± 19.4	0.74 ± 0.07	8.9 ± 1.4	32.1 ± 0.3

Hereby, zeta potential was reduced from 22.3 mV to 8.9 mV at higher ratio of BI Y. This effect might be caused by the higher concentration of the STING agonist, which contributes higher amount of negatively charged ions reacting with the positively charged amino groups. Therefore, the positive surface charge of the complex decreases. A similar effect was observed when TPP was used as a crosslinker, as described by Hassani, Laouini [78].

The decreased zeta potential can also explain the higher complexation efficiency of 32.1 % for this formulation, since more of the CDN is crosslinked in the chitosan complex. However, De Smedt, Demeester [87] reported, that polyplexes with a neutral surface charge are more likely

to agglomerate due to the lack of interparticular repulsive force. It was assumed, that a similar phenomenon is expected for the manufactured complexes, explaining the larger PDI observed.

Therefore, the nanoparticles with a slightly lower complexation efficiency of 28.3 % were used for the following studies, since the high zeta-potential indicated a more stable formulation. Additionally, by applying the described parameters (0.5 mg/mL chitosan, 1.25 mg/mL BI Y, BI Y : chitosan 1:1 ratio) a suitable Z-average of 147 nm was achieved. However, the high PDI indicates polydisperse size distribution. It was presumed that the used low quality chitosan stock caused the increased PDI, due to its broad range in MW. In a later step, this was optimized by utilizing high quality grade chitosan.

It was demonstrated that the STING agonist BI Y can act as a crosslinking agent to form nanosized complexes. In Figure 12, the hypothesized mechanism of the crosslinking is demonstrated. For this purpose, due to intellectual properties of BI Y, c-di-AMP is depicted as substitute for the utilized CDN. Similar to TPP, the negatively charged CDN has the ability to interact with the positive charged chitosan resulting in the formation of a nanosized complex.

To the best of our knowledge, those are the first nanoparticles manufactured only utilizing chitosan and CDN. Although some other ionic crosslinkers for chitosan nanoparticles are described in literature, such as dextran sulfate and poly-D-glutamic acid [75] this is the first time that a CDN and the actual API was shown to act as a stand-alone crosslinking agent to form nanoparticles with chitosan.

This modified approach offers some significant advantages for further optimization. As already confirmed, a much higher amount of the CDN was complexed in the nanoparticulate formulation. Additionally by excluding TPP, an influential parameter was removed, simplifying the manufacturing procedure.

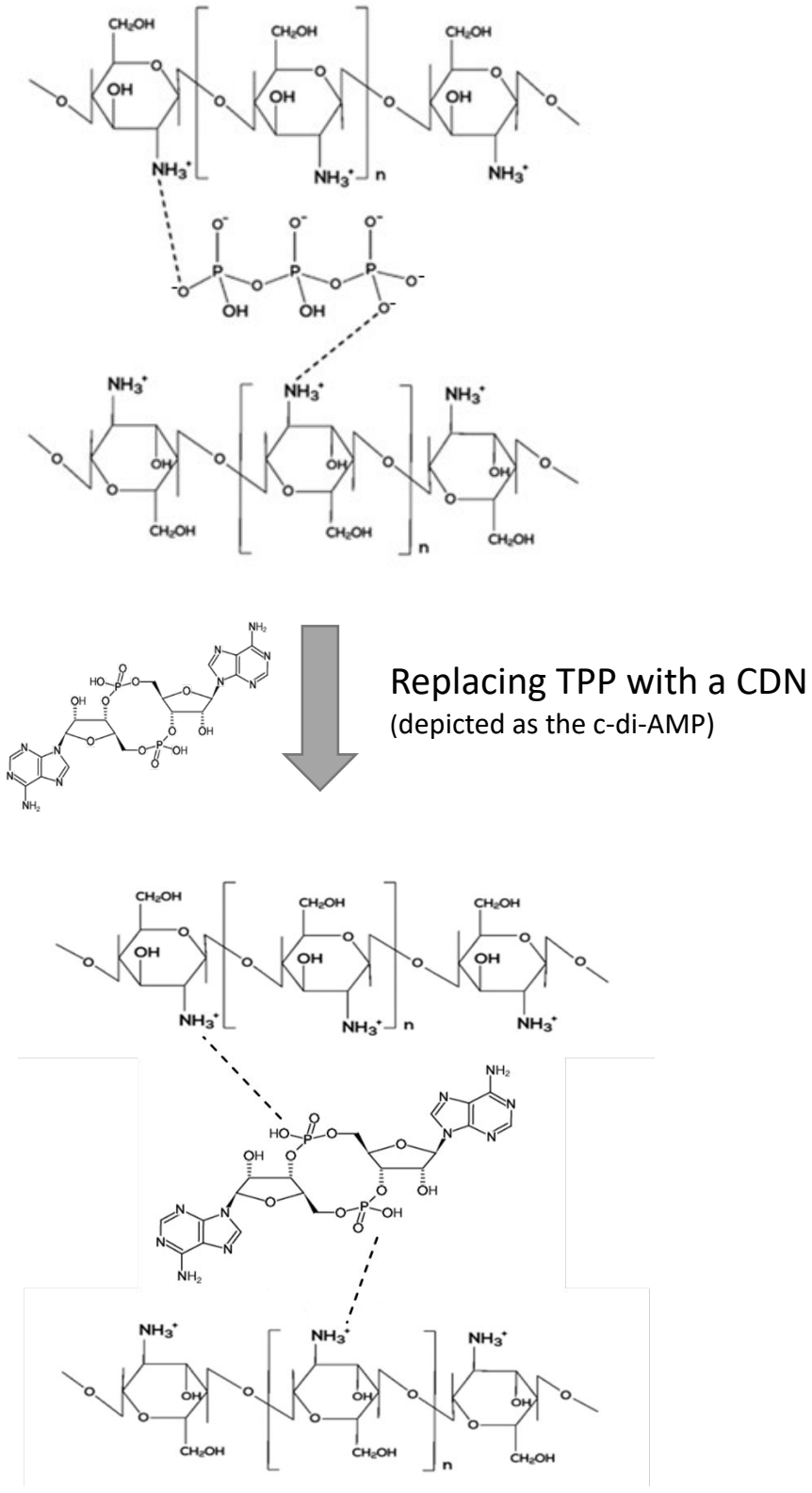

Figure 12. Representation of possible crosslinking reaction of anionic CDN (here depicted as c-di-AMP) with cationic chitosan.

Alongside the successfully manufactured nanoparticles, the proposed two-step screening method was established. This methodology has provided a minimal consumption of API, while screening for nanosized complexes with a high complexation efficiency, suitable Z-average and zeta potential. Therefore, the described method was used for future approaches as well.

3.2.2.1 *Variation of Flow Rate*

Another parameter, which is reported to have an influence on the particle forming, is the total flow rate (TFR), defining the flow rate within the microfluidic system, upon mixing of the two input solutions. For PLGA-based nanoparticles Garg, Thomas [88] reported a decrease in size from 150 to 120 nm by speeding up the TFR from 2 to 12 mL/min.

To examine if these observations can also be applied to chitosan-based complexes, different TFR ranging from 1 mL/min to 12 mL/min were applied during manufacturing.

The effect observed for PLGA particles was not confirmed with the chitosan formulation (results not shown). Here the Z-average was constantly approximately 140 nm. Thus, for following approaches, the TFR was kept at 1 mL/min. For a later upscaling, a higher TFR might be favorable due to the larger throughput.

3.2.3 Formulation post-processing

For later administration, the residual, uncomplexed API is highly undesirable, since it may cause severe side effects and has to be removed from the formulation.

For cleaning and purification of nanoparticulate formulations, in principle, two methods are described in the literature, namely centrifugation and dialysis [89]. Since centrifugation based methods would offer many advantages (fast and easy to apply), this technique was tested first. However, basic centrifugation, as well as centrifugal filtration method, caused visible agglomerates, which could not be dispersed afterwards. The agglomeration may be effected by the high centrifugal forces during centrifugation.

With dialysis remaining as a cleaning method, various dialysis techniques were tested to assess applicability.

Different commercially available dialysis devices were evaluated. “SnakeSkin Dialysis Tubing” was already tested during a previous in-house project, but was abandoned due to a user-

unfriendly set-up. “Slide-A-Lyzer™ MINI Dialysis Devices” were also not considered due to the small maximal volume. Hence, “FLOAT-A-Lyzer Dialysis Device” was used, due to the large range of sample volumes (0.5 – 10 mL) and convenient applicability.

In order to guaranty the optimal washing efficiency, different pore sizes, cleaning buffers, and duration of cleaning were evaluated.

Due to the original purpose of the dialysis set-up (protein purification), the pore size is stated in molecular weight (kilodaltons, kDa). It is described in literature [90] that globular proteins with a mass around 100 kDa (Catalase, Phosphofructokinase) correspond to sizes smaller than 20 nm. Thus, it was assumed that a pore size of 100 kDa would retain nanoparticles with sizes larger than 100 nm. Additionally, since the MW of the CDN is far below 100 kDa, the API could pass the dialysis membrane. Therefore, the pore size of 100 kDa was used for the following approaches.

In order to evaluate a suitable washing solution conditions, acidic, neutral and alkaline pH media were tested. Here, only with an acidic pH of 4.5, the complex remained stable. A pH value of 6.8 led to particle growth (344.1 nm) and in alkaline pH, agglomerates were detected (Table 5). This can be explained with a reduced degree of amine protonation at the particle surface with increasing pH value. Hereby the electrostatic repulsion between the complexes might be reduced, increasing the probability of agglomeration [91].

Table 5 Cleaning parameters and characterization of post-processed formulation chitosan/BI Y formulation.

Cleaning parameters			Characterization		
Pore size [kDa]	**Wash solution pH**	**Duration [h]**	**Z-average [nm]**	**PDI**	**Washing Efficiency [%]**
100	4.5	0	146.9 ± 15.1	0.58 ± 0.04	0.0
100	4.5	2	-	-	62.5
100	4.5	20	140.5 ± 8.1	0.34 ± 0.04	97.8
100	6.8	0	146.9 ± 15.1	0.58 ± 0.04	
100	6.8	20	344.1 ± 26.5	> 1	
100	10	0	146.9 ± 15.1	0.58 ± 0.04	
100	10	20	N.D. --> Agglomeration		

Since washing solution with a pH-value of 4.5 yielded a stable formulation, washing efficiency after 2 and 20 h points was determined. As shown on Table 5, after 2 hours 62.5 % of the API, not bound to the complex, was removed. After 20 hours, nearly 98 % of the free API was extracted, leaving only a negligible amount of API residue in the supernatant of the formulation.

An additional advantage of cleaning the formulation was the reduction of the PDI. Probably not only CDN, but also a fraction of free chitosan and particles smaller than 100 kDa passed the pores of the dialysis membrane.

As a result, 20 h washing duration in a pH 4.5 buffer with 100 kDa pore size was standardly used for cleaning and purification of all following nanosized complexes.

3.2.4 Alternative chitosan grade – final precursor formulation

At his point of the project, the higher grade, well-characterized chitosan was available and thus consequently implemented into the manufacturing procedure. It is described in the literature, that chitosan DD and MW has a major influence on complex formation. For siRNA previous studies showed, that different MW chitosan forms differently sized complexes [92] and that effectively mean particle size increases with increasing MW [93]. Additionally, according to the literature only chitosan polymers 5 – 10 times larger than siRNA can form stable nanosized complexes [40] and the optimal range of chitosan MW should be between 65 – 170 kDa [94]. Since CDN are significantly smaller than siRNA, it was assumed, that low MW chitosan could also be successfully utilized.

Deacetylation degree determines the positive charge of chitosan due to a higher amount of available primary amines. This leads to an increased binding capacity and consequently complexing efficiency of negatively charged molecules, siRNA, as well as CDN [95, 96]. It was also reported that a DD of > 80% is necessary to achieve stable particles [33].

As already mentioned, those results were mostly evaluated using siRNA, and had to be confirmed experimentally for the CDN. Therefore, chitosan with a DD of 95% and 80% as well as MWs of 10 – 50 kDa and 80 – 200 kDa were assessed.

3.2.4.1 *High quality grade chitosan/TPP complex*

Since the manufacturing procedure using microfluidic mixing was already established at this point, a fast optimization of nanosized complexes with the new polymers was anticipated. Regardless, due to the limited availability of the API, preliminary approaches were performed using TPP.

Hereby, a smaller Z-Average of 100 – 170 nm was achieved, using chitosan with a MW of 10 – 50 kDa, as compared to a MW of 80 – 200 kDa, where all complexes were above 200 nm in size. Additionally, with a low DD of 80 %, less TPP was needed to build the complex compared to 95% deacetylation degree. It was assumed, that these results can be transferred to the complexation efficiency of the CDN. Therefore, the 10 – 50 kDa, 95% DD chitosan (subsequently named CS95/5) was selected for future approaches, since a suitable Z-average and optimal complexation efficiency can be achieved with this polymer.

3.2.4.2 *CS95/5 + BI Y*

Similar to previous approaches, the optimal concentration and ratio of STING agonist in order to generate an optimal nanosized complex were determined. Due to the experience gathered from the preliminary studies, only few trials had to be conducted to achieve a suitable formulation, by using the established screening method.

Applying the same parameters as with the low-grade chitosan (0.5 mg/ml chitosan, 1.25 mg/mL BI Y and a flow ratio of 1:1) did not generate nanosized particles (Figure 13). This might be caused by the higher deacetylation degree, as a result of which more crosslinking agent was necessary to engage the increased number of primary amines. Therefore, the flow ratio was changed to increase the BI Y relative content, leading to successful complexation. However, to reduce the API consumption, a lower chitosan concentration was also tested. Not surprisingly, optimization was achieved while decreasing the absolute amount of CS95/5, as to avoid agglomerate formation. Therefore, the amount of BI Y was reduced gradually, until a suitable size distribution was reached.

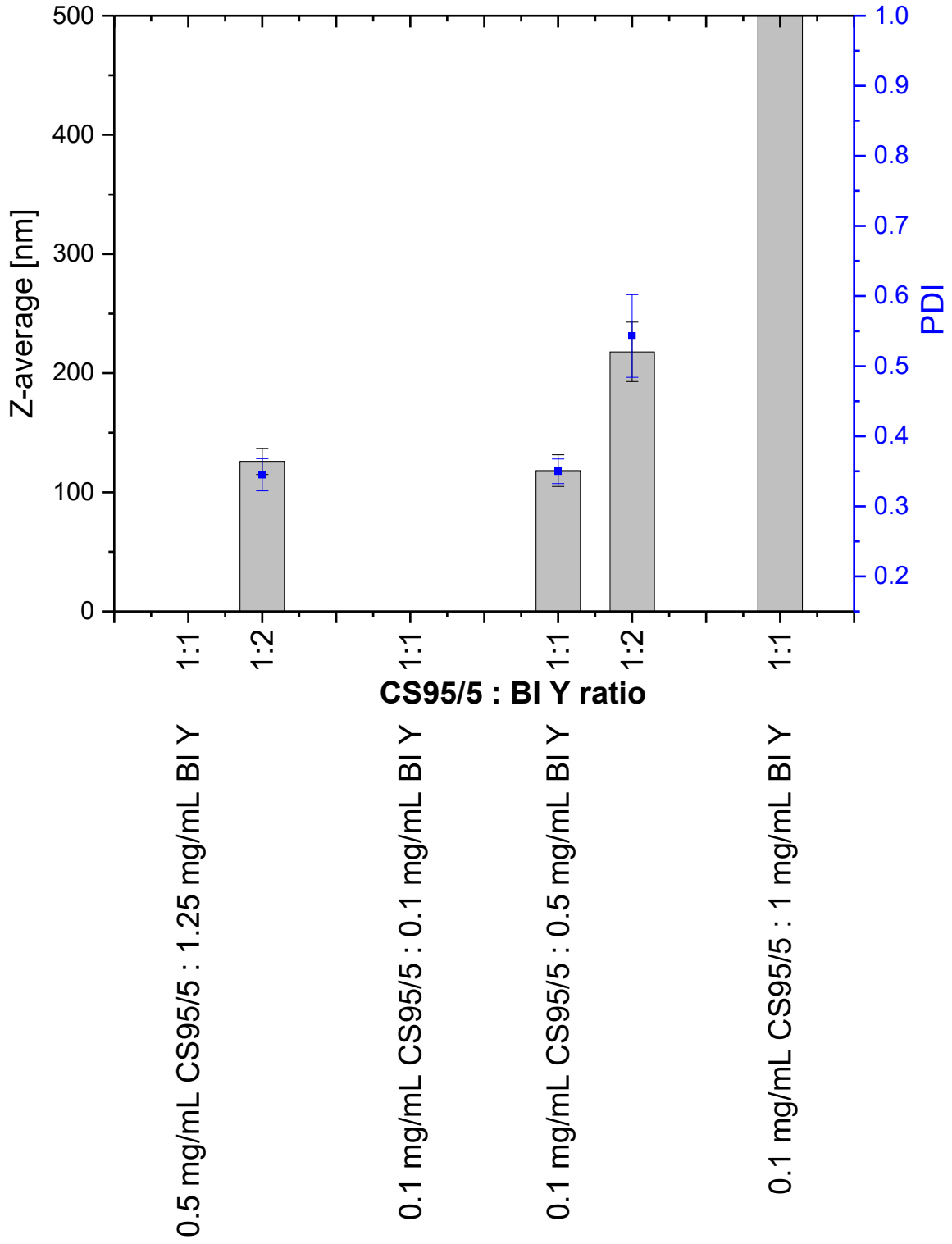

Figure 13 Z-average and PDI of high-grade chitosan CS95/5-BI Y complexes manufactured by microfluidic mixing with a variable amount of BI Y and different ratios of BI Y and CS95/5.

Thereby, nanosized complexes with a Z-Average of 118.2 and a PDI of 0.35 were manufactured by using 0.1 mg/ml CS95/5, 0.5 mg/mL BI Y and a flow ratio of 1:1. Additionally, by using the

higher-grade chitosan, a higher complexation efficiency was achieved. This comes as no surprise, since a high amount of negatively charged API can be complexed by the increased amount of primary amines. The abundance of primary amines contributes to the high Zeta-potential of 36.5 mV detected (Table 6).

Table 6 Formulation parameters and further characterization of CS95/5-BI Y complex.

Formulation parameters			Characterization			
Conc. CS95/5 [mg/mL]	**Conc. BI Y [mg/mL]**	**CS95/5 : BI Y ratio**	**Z-average [nm]**	**PDI**	**Zeta-potential [mV]**	**Complex. Efficiency [%]**
0.1	0.5	1:1	118.2 ± 13.3	0.35 ± 0.02	36.5 ± 2.4	64.3 ± 5.1

3.2.4.3 *CS95/5 + BI X – final precursor formulation*

The successful complexation of the model compound had provided a plausible precedent for the trials with the actual intended API, BI X. It was expected, that using the stereoisomer would have only a minor impact on the complex formation and the established parameters could be directly transferred, reducing consumption of the actual API.

However, by applying the same parameters, agglomeration of the complex was observed. This may be explained by steric effects of the two compounds, hindering the ionic interaction between the anionic moieties and the free amino groups. Additionally the actual API BI X was highly purified whereas BI Y was a lower grade synthesis product, which may contain unspecified residues.

Due to the stated reasons, it was suspected that using a lower concentration of BI X would prevent agglomeration and concentration was reduced to 0.25 mg/mL.

With this established parameter, shown in Figure 14, the definitive BI X containing chitosan-based, nanosized complex was successfully manufactured.

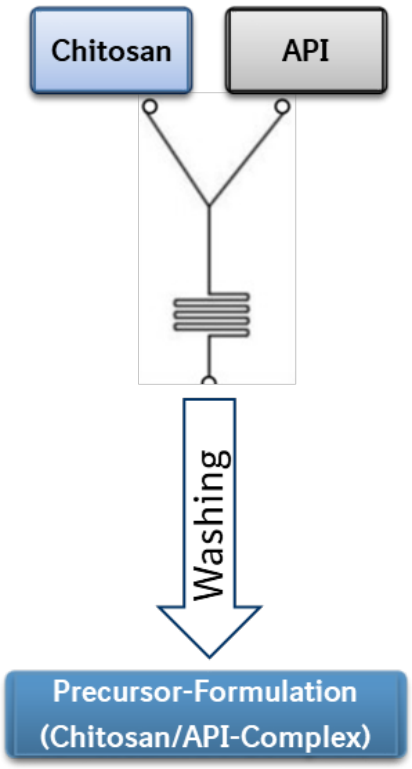

Manufacturing			
Conc. CS95/5 [mg/mL]	**Conc. BI X [mg/mL]**	**CS95/5 : BI X ratio**	**Flow rate [mL/min]**
0.1	0.25	1:1	1

Washing			
Dialysis device	**Pore size**	**Cleaning solution**	**Cleaning duration**
Float-A-Lyzer	100 kDa	pH 4.5	20 h

Figure 14 Overview of manufacturing and cleaning procedure for final CS95/5-BI X precursor formulation.

Table 7 Characterization of final CS95/5-BI X precursor formulation.

Characterization			
Z-average [nm]	**PDI**	**Zeta-potential [mV]**	**Complexation efficiency [%]**
94.7 ± 5.0	0.38 ± 0.07	26.9 ± 3.1	70.9 ± 3.1

Hereby, a Z-average of 94.7 with a PDI of 0.38 was achieved. Additionally, the reduced STING agonist concentration aided the complexation efficiency further to 70.9% (Table 7). As mentioned previously, the higher complexation efficiency might be explained with reduced steric hindrance of the API. Due to the now higher amount of complexed primary amines, less positive charged chitosan on the particle surface is available, which is also reflected by the reduced zeta-potential of 26.9 mV.

Since this is the first report of a chitosan/CDN-complex, those results were compared with chitosan/siRNA formulations available from the literature.

With regard to particles size distribution, all described siRNA polyplexes have a higher Z-average mostly ranging from 130 to 300 nm [74, 97, 98]. Even particle sizes up to 500 nm are described [75, 94]. The higher size distribution might be explained with the much higher MW of the siRNA compared to CDN, contributing to an increased particle size. For Zeta-potential, similar results - between 20 and 30 mV - are described in literature [74, 97, 98]. Due to the very low amount of siRNA utilized for polyplex formulations, entrapment efficiency is much higher and can reach up to 99% [75, 98].

3.2.4.4 *Further characterization of the optimized precursor formulation*

To acquire a better understanding of the manufactured chitosan/CDN-complex, additional characterization methods were applied.

To confirm that cleaning of the complex is successful with the actual compound, the API residue in the final, washed formulation was measured. Hereby, a washing efficiency of 92.6% was observed. The reduced efficiency (compared to the previous 98.4 %), might be explained with the now nearly doubled complexation efficiency. Thus, a higher cleaning duration might be necessary for a complete removal. However, <10% API residue was considered to be sufficient for consequent steps and no further cleaning was included.

Another important parameter for nanoparticulate formulations is the morphological appearance, as assessed by electron microscopy. Basic TEM was not sufficient to visualize the complex, due to agglomeration occurring during sample preparation. Therefore, a cryo-TEM method was applied, which freezes the sample before measurement, consequently preserving the structure of the complex. In Figure 15, cryo-TEM images show spherical structures (red circles) with a size diameter between 100 and 200 nm. These findings, demonstrating spherical particles, nicely confirming the particle size analysis of the same formulation.

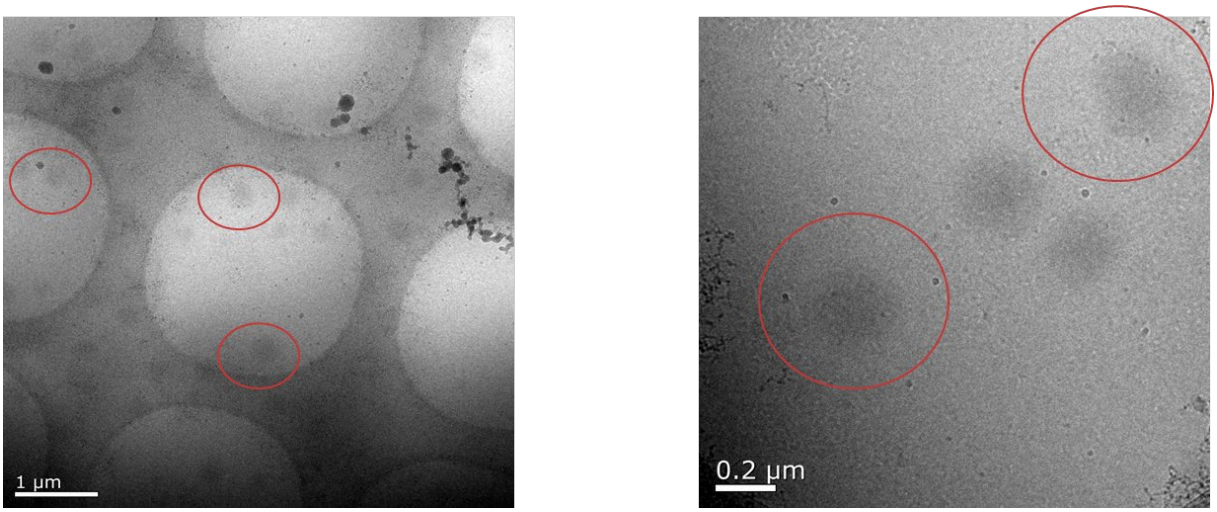

Figure 15 Cryo-TEM pictures of CS95/5-BI X precursor formulation (red circles) on punched grids.

A few other publications providing TEM images of chitosan-based particles [73, 74], further confirm the results obtained herein, demonstrating spherical structures with a similar particle size.

3.2.5 Evaluation of the precursor formulation

In this first part, the BI X/chitosan-complex formulation was successfully manufactured, hereafter referred to as the precursor formulation. As shown in Figure 16, the negatively charged API forms a nanosized complex with the cationic polymer. The desired size range in combination with a suitable Zeta-potential and high complexation efficiency was achieved.

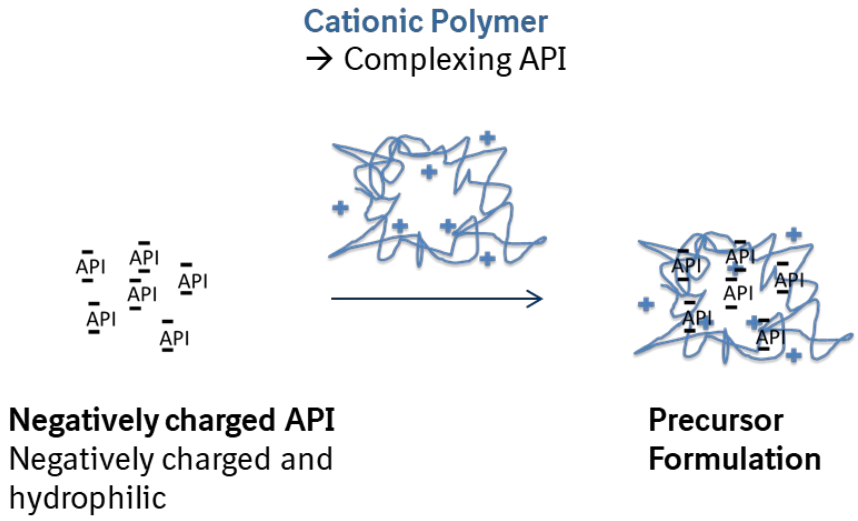

Figure 16 Graphical representation of the formation of the chitosan/BI X nanosized complex.

This formulation offers some advantages with regard to an improved delivery of the API. Especially after an intratumoral administration, there may be an enhanced efficacy due to the positive zeta-potential of the formulation. The positive charge can lead to an enhanced cell uptake of the formulation, compared to the free compound with low cell permeability [99]. Therefore, a decreased dose might be sufficient to achieve the desired effect, consequently minimizing side effects of this highly potent API.

While no experiments were conducted to show a cellular uptake of the precursor formulation, vast data exist in the literature demonstrating cell internalization of chitosan-based nanosized complexes. Nucleic acids [75, 94, 100, 101], as well as small molecules [77] and fluorescein-labeled chitosan-nanoparticles [102] were evidentially internalized into the cell. Therefore, it can be safely assumed, that the manufactured BI X/chitosan-complex may also show an enhanced cell uptake.

A similar approach to improve the delivery of a STING agonist was performed by Wilson, Sen [103]. They utilized a different cationic, biodegradable polymer (poly(beta-amino ester)), to complex the CDN. This formulation improved the ability to activate the innate immune system biomarker IRF3 *in vitro* at >100 fold compared to stand alone CDNs. Additionally, after intratumoral administration of the nanoparticles, an order of magnitude reduction in the necessary dose was shown to be sufficient in order to eliminate poorly immunogenic melanoma tumors.

As a result, these reports strongly suggest the applicability of the proposed BI X/chitosan nanoparticles for intratumoral application. Owing to the presumed enhanced cellular uptake of the formulation, the required effective dose might be reduced, consequently enhancing efficacy of the API.

3.3 Modification for intravenous administration – PLGA-PEG coated complex

In contrast with the discussion on intratumoral administration, the main purpose of this work was to enable an i.v. administration of the formulation. First, intratumoral administration is not feasible for many cancer types, especially in case of advanced, metastatic disease. Thus, i.v. administration might broaden the indication spectrum. Additionally, a formulation for i.v. administration would form an alternative to the existing formulations for direct administration to the tumor tissue.

However, the described CDN/chitosan-complex is not suitable for this route of administration. After injection into the blood, molecules such as albumin, fibrinogen, glycosaminoglycan and even chloride ions can compete with the CDN for binding with the complex. This can result in an early release of the API from the nanoparticle, before the tumor tissue is reached [104, 105]. Additionally, interaction with these serum constituents can cause aggregate formation potentially leading to embolism and eventual blockage of blood flow in the affected vessel [106].

As for most nanoparticulate formulations, opsonization also occurs in case of chitosan-based complex. Here, nanoparticles' circulation in the blood is recognized by opsonins (complement system compounds, antibodies etc.) and are adsorbed on the particle surface. This leads to phagocytosis in the mononuclear phagocyte system, subsequently eliminating the nanoparticles from the blood stream [107].

As a preventive measure, PEGylation is one of the most common approaches to "mask" nanoparticulate formulations from the immune system. Bulky hydrophilic PEG-chains on the particle surface sterically preclude an interaction between blood components and neighboring nanoparticles [107]. In doing so, not only opsonization, but also agglomeration can be prevented [108, 109].

Thus, PEGylated chitosan is widely applied for siRNA-loaded nanoparticulate formulations to enhance stability in human plasma [98, 109, 110]. Furthermore, *in vivo* studies by Mao, Roy [111] showed a reduced clearance of PEGylated chitosan-based nanoparticles after i.v. administration.

Based on these findings, it was initially planned to utilize PEGylated chitosan for the CDN formulation as well. Due to the successfully established manufacturing and screening method, a fast and resource-efficient implementation of the new polymer was expected.

Unfortunately, PEGylated chitosan was not commercially available and synthesis of such polymer was not feasible in the brief period given.

Therefore, an alternative approach was utilized to PEGylate the CDN/chitosan-complex.

3.3.1 Biodegradable PLGA-PEG Coating

Due to its biodegradability, PLGA is an ideal polymer for targeting the tumor tissue via EPR-effect, where it can release its payload. Numerous publications describe several techniques for the encapsulation of different APIs into PL(G)A-PEG-based nanoparticles [51, 62, 111-118].

Pre-formed cationic polymer complexes were encapsulated into microsized PLGA-particles, including PEI-based [119-122], as well as chitosan-based precursors [123]. In addition, PLGA nanoparticles containing PEI/oligonucleotide-complexes [124, 125] are described in literature. Furthermore, Stigliano, Aryal [126] successfully encapsulated siRNA/chitosan complexes into PLGA-based nanoparticles.

However, the mentioned formulations were manufactured by the emulsion evaporation method. As mentioned previously, this technique was not suitable, due to the high compound consumption and lack of scalability for this method. Therefore, a microfluidic mixing approach was developed to manufacture CS/API-loaded PLGA-based nanoparticles.

As described by Rezvantalab and Keshavarz Moraveji [45], PLGA-PEG copolymers assemble into nanoparticles in the aqueous phase. Therefore, it was rationalized, that microfluidic mixing results in controlled precipitation of PLGA-PEG in the aqueous phase, hypothetically coating the precursor as demonstrated graphically in Figure 17.

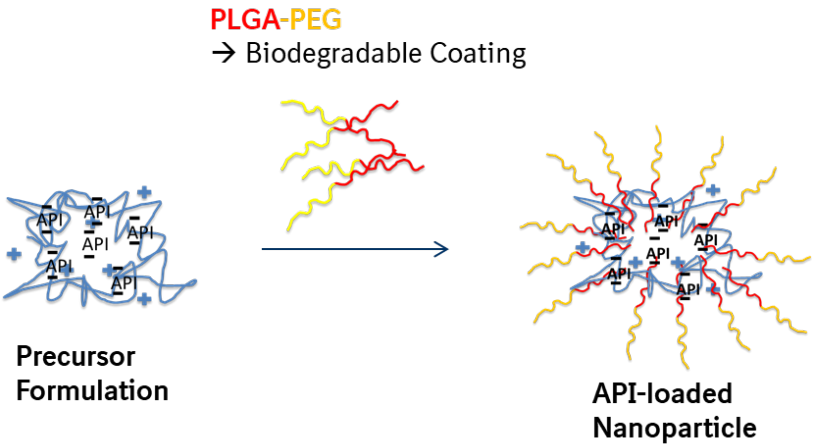

Figure 17 Graphical representation of biodegradable coating by PLGA-PEG.

3.3.2 PLGA-PEG/CS955-BIX

Owing to limited API availability and a tight timeline due to upcoming *in vivo* experiments, only a small number of parameters were tested. Since the precursor formulation was already established, different concentrations of PLGA-PEG, ranging from 0.1 to 2 mg/mL were evaluated.

After manufacturing, the PEGylated nanoparticulate formulation had to be washed for purification and solvent removal. For this purpose, similar cleaning techniques as described previously were utilized. However, in contrast to the precursor formulation, the formulation was stable enough to allow for centrifugation filtration. Presumably, the PLGA-PEG coating is also stabilizing the formulation due to steric shielding effect of PEG-chains on the particle surface [108, 109]. Since this method proved to be the easiest and fastest way for purification of nanoparticles, the Amicon® Ultra Centrifugal Filters were used.

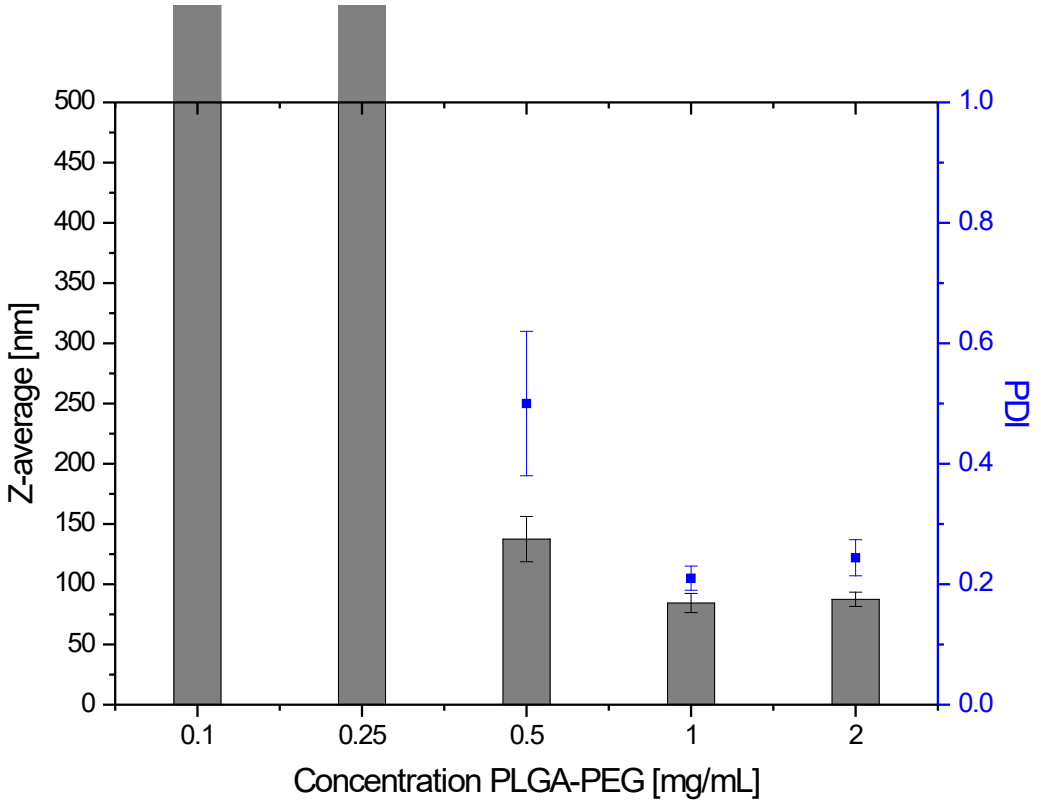

Figure 18 Influence of PLGA-PEG concentration on Z-Average and PDI of nanoparticulate formulation.

As shown in Figure 18, PLGA-PEG concentration was an important factor in order in achieving a stable formulation. A PLGA-PEG concentration below 0.5 mg/mL led to agglomeration and was not sufficient to encapsulate the precursor formulation. Starting from 1 mg/mL PLGA-PEG, nanoparticles with a suitable Z-average between 80 and 90 nm and a PDI of about 0.2 were obtained.

In the next step, the API-loaded nanoparticles were produced as described in Figure 19 in a larger batch, as to allow for further characterization for a subsequent *in vivo* PK/PD study.

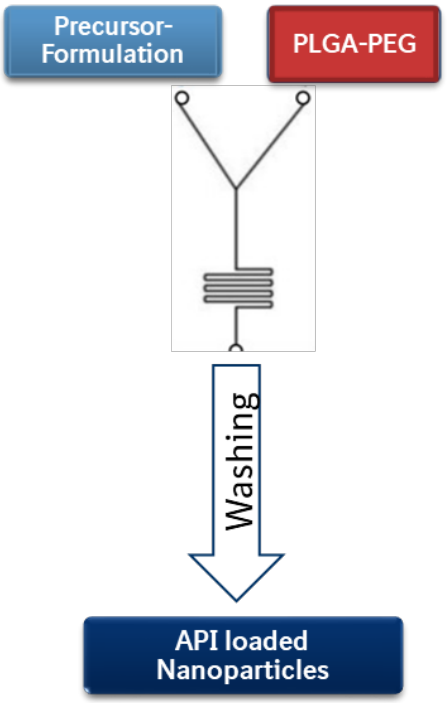

Manufacturing		
Conc. PLGA-PEG [mg/mL]	**Precursor Formulation: PLGA-PEG ratio**	**Flow rate [mL/min]**
2	1:1	1

Cleaning			
Centrifugal device	**Pore size**	**Cleaning solution**	**Centrifugal passages**
Amicon® Ultra	100 kDa	pH 4.5	3 x

Figure 19 Overview of manufacturing and cleaning procedure for API-loaded nanoparticles.

3.3.2.1 *Further Characterization*

Similar to the precursor formulation, morphological appearance of the PEGylated formulation was analyzed. In this case, due to the more stable nanoparticles, visualization was possible with standard TEM (Figure 20). The presented nanoparticles are clearly visible, and show monodisperse spherical structures with no sign of agglomeration.

However, the particle diameter appears to be smaller than the Z-average obtained from DLS measurement. This might be caused to a certain extent by the sample preparation procedure, which caused shrinking of the air-dried particles. Additionally, this type of correlation is common, while comparing microscopical data, since DLS determines the hydrodynamic radius of a particle and weighs the size distribution differently, overrating larger particles due to the stronger scattered light intensity. Therefore, larger particles are given more weight and the Z-average appears to be larger than the particles observed via TEM. A similar effect was reported for siRNA/chitosan loaded PLGA-nanoparticle, where scanning electron microscope (SEM) exhibits a size diameter of approx. 100 nm in contrast to 160 nm measured by DLS [126].

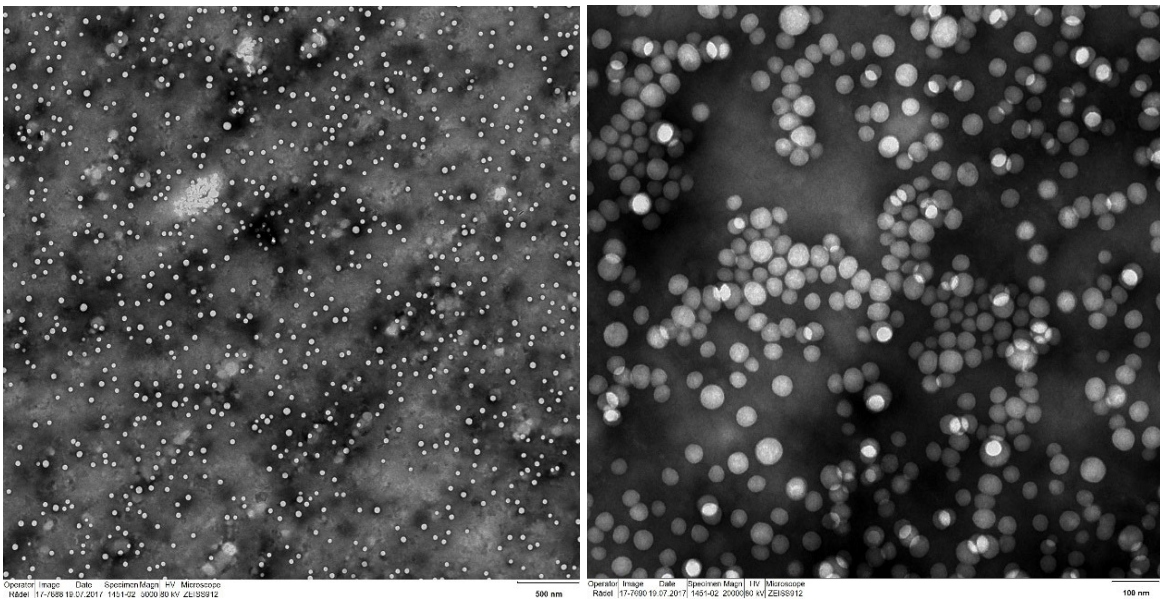

Figure 20 TEM pictures of API-loaded nanoparticles.

For *in vivo* study the determination of the actual drug load of the formulation batch to be administered, the exact drug load had to be detected. Only if the actual amount of API is known, the correct dose can be administered. Therefore, the drug load of the freeze-dried nanoparticles was quantified and determined as 6.1%. However, since no nanosized particles were detectable after freeze-drying, it was assumed that by utilizing the standard lyophilization method, the nanoparticles were destroyed. Therefore, the desired dose could not be prepared by resuspending the dried nanoparticles and an indirect method to quantify the concentration of the administered formulation was applied.

A small aliquot of the final formulation was quantified for its API content (after complete release from the nanoparticles). Hereby, the concentration of the formulation was determined, which allowed administration of a known dose.

In previous studies, it was noticed, that addition of NaCl induces the partition of the CDN from the nanoparticle. Although this effect is necessary for the effectiveness of the formulation (release of the API in the tumor tissue), a premature release before administration would reduce efficacy and might cause side effects. Therefore, mannitol, instead of the commonly used NaCl, was added to provide an isotonic medium.

The following *in vivo* experiments were conducted at the Boehringer Ingelheim site in Vienna. Therefore, the formulations had to be send over night to this location. Despite the fact that

the formulation was shown to be stable for 7 days at 4° C, signs of agglomerations were observed after arrival in Vienna, as a result of transportation. Therefore, the formulation was centrifuged to remove the agglomerates and administered at a reduced dose of 0.59 mg/kg, as detected using the same method.

3.4 PK/PD

In order to determine the impact of the nanoparticulate formulation, a proof of concept study in tumor bearing mice was performed. For this purpose, in a PK experiment, the API concentration in tumor, liver plasma and spleen was measured at three different time points. For a PD experiment, the IFN-β response in tumor and plasma were determined. Additionally, to rule out the placebo effect on PD biomarker response, a vehicle control formulation was used. These chitosan placebo nanoparticles were manufactured in the same way as the API loaded particles, but BI X was exchanged with TPP. Hereby, a similar Z-average of 83 nm and PDI of 0.23 was achieved, demonstrating that the produced chitosan placebo nanoparticles have comparable properties and can be utilized as a vehicle control formulation.

The results were compared with pure API dissolved in 0.9% NaCl solution as a compound control formulation, which was administered in an efficacious dose of 2.5 mg/kg as i.v. bolus injection. As described previously, the chitosan/PLGA-PEG formulation was administered with a drug dose of 0.59 mg/kg. It was assumed, that due to passive targeting of the nanoparticles the reduced concentration is sufficient to show efficacy.

3.4.1 *In vivo* PK study

In Figure 21, the dose normalized PK profiles of the two BI X formulations after i.v. administration in tumor tissue (A), liver tissue (B), spleen tissue (C) and plasma (D) are shown.

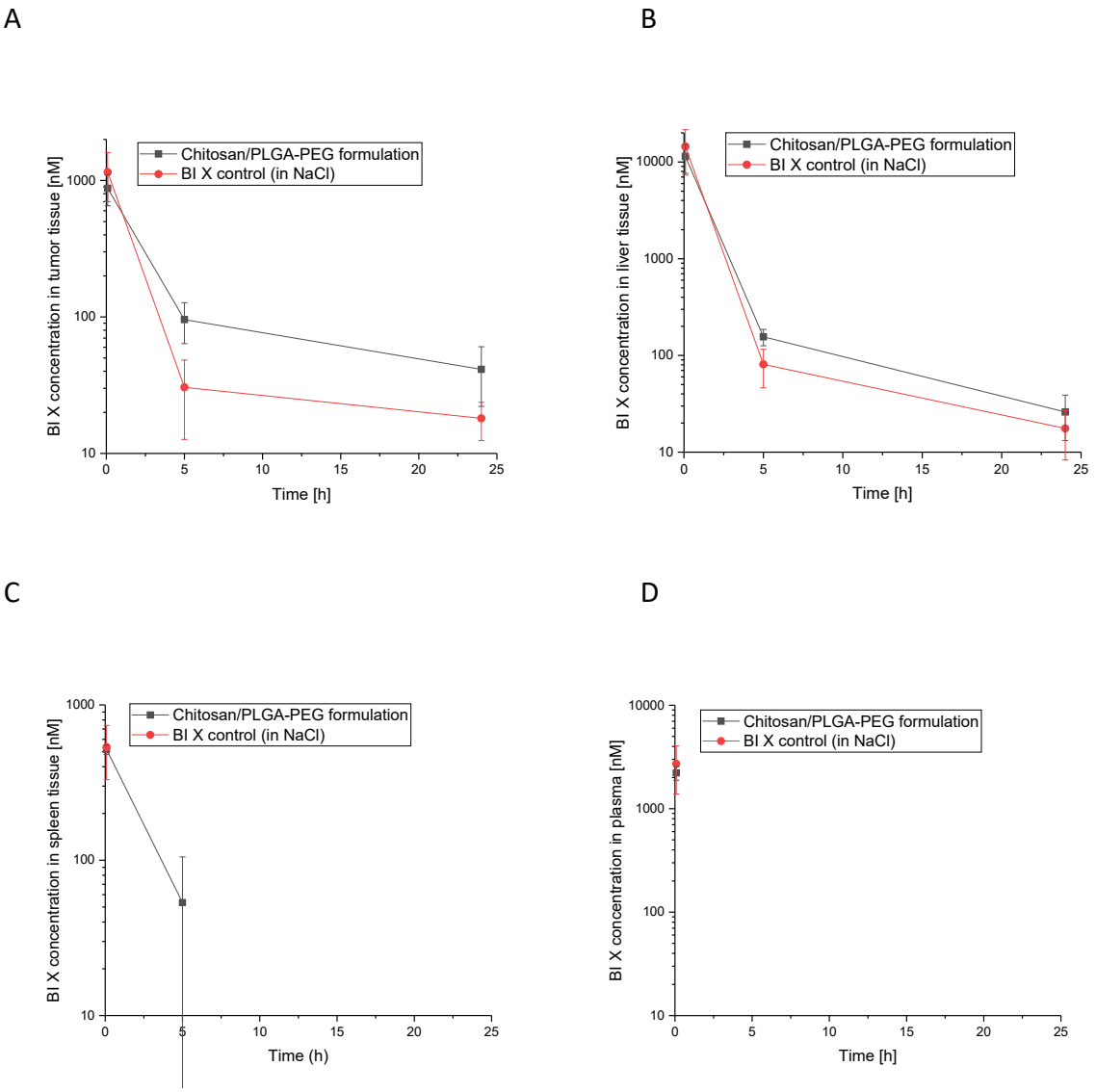

Figure 21 Dose normalized PK profile of BI X control and chitosan/PLGA PEG formulation in tumor tissue (A), liver tissue (B), spleen tissue (C) and plasma (D).

Directly after administration, the amount of API In the tumor tissue from the chitosan/PLGA-PEG and control formulation were in a similar range (Figure 21 A). However, after 5 and 24 hours, higher amounts of API from chitosan/PLGA-PEG formulation were detected in the tumor tissue, as compared to the BI X control. This result may be attributed to the EPR-effect of the nanoparticulate formulation, which leads to an enhanced accumulation of the API in the tumor tissue after administration as nanoparticles [17].

Similar effects have been reported in literature, where the highest accumulation of API in the tumor tissue after i.v. injection of nanoparticulate formulations was measured after 4 and 24 hours as well [127, 128].

It is also described in the literature, that nanoparticulate formulations tend to accumulate in liver and spleen tissue [129]. Therefore, those organs were analyzed for their API concentration. An overall higher concentration as compared to the tumor tissue of the API was detected in the liver tissue, for both the formulation and control (Figure 21 B). Analogue to the API concentration in the tumor tissue, a similar accumulation of both formulations directly after administration was observed. This was followed by a slightly increased amount of API detectable in the liver tissue from the chitosan/PLGA-PEG nanoparticles after 5 and 24 hours, which could be a result of longer circulation times of the chitosan formulation.

Accumulation of nanoparticles was also observed in the spleen (Figure 21 C). Here 5 hours after administration, only API from the chitosan/PLGA-PEG formulation was detectable in a limited amount of the tissue samples, as opposed to the BI X control, which was detectable in none of the tissue samples. These results were expected, due to accumulation of nanoparticles in those organs, as described previously [129].

A fast plasma clearance was observed with both formulations as shown in Figure 21 D. BI X from both formulations were detected in the plasma only directly after administration. At the next time point (5 h), the concentration was decreased below detection limit.

These findings contradict the literature data, where most PEGylated PLGA-based nanoparticles show an increased plasma half-life [51, 130, 131]. Since the second time point of the sample collection (5 hours after administration) may have been chosen too late, the exact plasma half-life could not be detected. In the elapsed time, the nanoparticles presumably accumulated in the previously mentioned organs and the tumor. Further pharmacokinetic analysis was not possible with the results obtained.

3.4.2 *In vivo* PD study

To assess the efficacy of the passively targeted nanoparticle formulation, IFN-β concentration in the tumor was detected. The secretion of Type I IFN (IFN-β) is induced by the activated innate immune system and can therefore be utilized as a biomarker.

In Figure 22 A, the IFN-β concentrations in the tumor tissue is shown. An increased amount of INF-β was detected 5 hours after administration for control and chitosan/PLGA-PEG formulation, whereas no INF- β was detected in the placebo formulation. The almost twice as

strong IFN- β response of the control formulation might be explained with the higher dose administered.

A

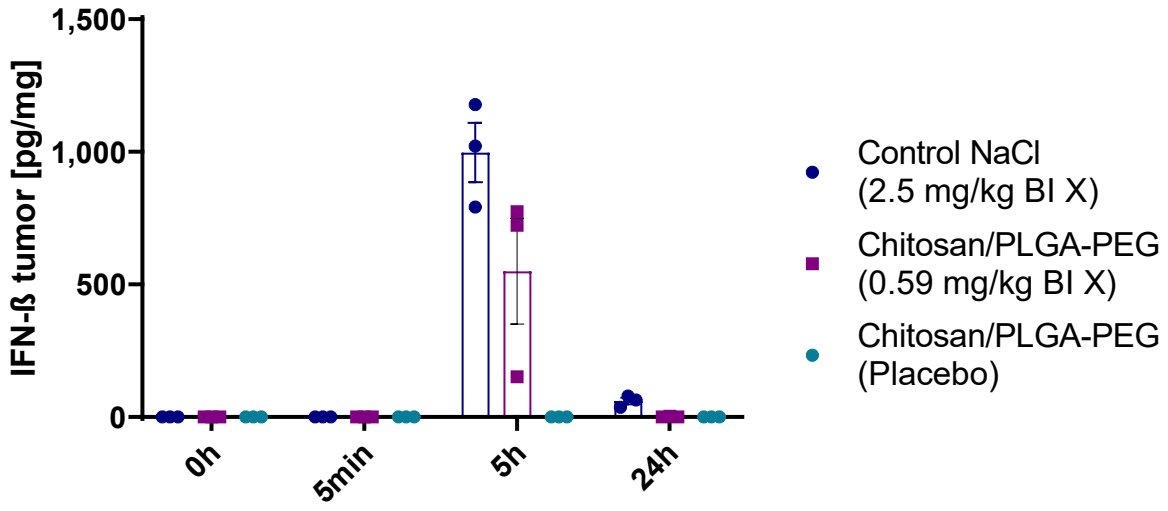

B

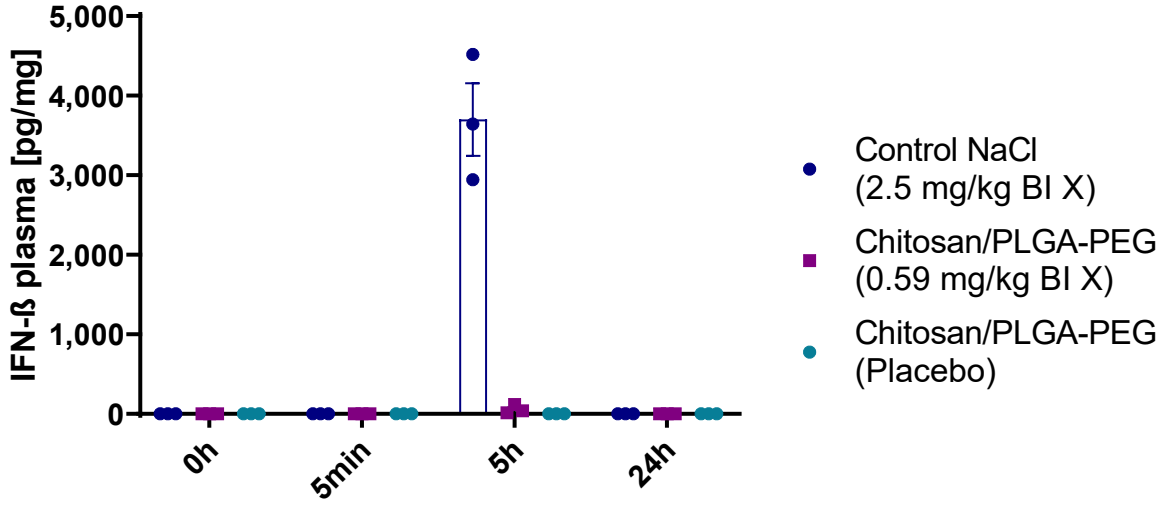

Figure 22 INF-β response in tumor tissue (A) and plasma (B) after administration of BI X control, BI X loaded chitosan/PLGA-PEG nanoparticles and placebo chitosan/PLGA-PEG nanoparticles.

This increase in INF-β and subsequently secretion of pro-inflammatory cytokines is highly desired in the tumor tissue in order to trigger a potent anti-tumor response. The secretion of these interferons in the tumor microenvironment activates tumor-associated activated

dendritic cells, presenting tumor specific antigen to cytotoxic CD8+ T cells. The increased $CD8^+$ T cell infiltration into the tumor ultimately leads to the killing of tumor cells, as described previously [31].

However, an excessive systemic cytokine release in the plasma sample, leads to severe side effects such as the cytokine release syndrome. Therefore, only a minimal amount of INF-β should be detectable in the plasma to guarantee a safe treatment.

This minimal increase of INF-β in plasma was achieved with the proposed chitosan/PLGA-PEG formulation. Here only a negligible systemic interferon release was measured in the plasma sample with the nanoparticulate formulation (Figure 22 B). In contrast, free API from the control formulation leads to a very high systemic cytokine response.

Therefore, it can be reasonably assumed, that the CDN, entrapped in the chitosan/PLGA-PEG nanoparticles, are released only after delivery to the tumor tissue not effecting the rest of the body.

Additionally, a placebo effect - induced by the immune-modulating properties of chitosan [132] - on PD biomarker response was ruled out, as demonstrated by administration of a vehicle control formulation. With those chitosan placebo nanoparticles, where BI X was exchanged with TPP, an IFN-β response was not detectable in tumor or plasma.

Consequently, these results strongly suggest an activation of the STING pathway in the tumor tissue without systemic activation after administration of the chitosan/PLGA-PEG formulation. Hereby, the severe side effects of this highly portent immune-oncologic API may be reduced, allowing for an i.v. administration, as to broaden the indication spectrum and differentiate against alternative intratumorally administered formulations.

An increasing amount of literature has been arising, describing nanoparticulate formulations for the tumor targeted delivery of STING agonists lately. Especially lipid-based nanoparticles, loaded with a STING agonist, enhancing immune activation for cancer immunotherapy [133, 134] are precedent.

Recently, Shae, Becker [135] proposed a polymer-based tumor targeted formulation as well. They encapsulated 2,3'-cGAMP, a natural STING agonist, into endosomolytic polymersomes. Hereby, the authors showed an enhanced STING pathway stimulation in the tumor tissue after

intratumoral as well as after intravenous administration. In subsequent studies, they further demonstrated inhibition of tumor growth and increased rates of long-term survival after administration of the nanoparticulate formulation (intratumoral and intravenous).

Based on the outcome of these studies, it leads to reason, that the developed formulation may not only activate the immune system response in the tumor tissue, but also could inhibit tumor growth, therefore improving the clinical outcome of the immunotherapy.

4 Summary and Outlook

In this chapter, the entrapment of CDN into biodegradable polymers for subsequent i.v. administration in a tumor-bearing mice model is described (Figure 23).

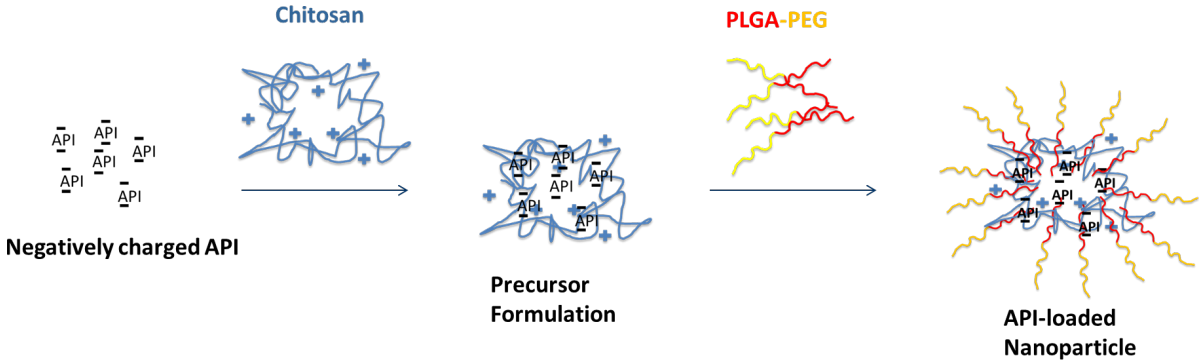

Figure 23 Graphical representation of the formulation development for novel CDN-loaded nanoparticles.

In initial attempts, various well-documented manufacturing methods were assessed, but proven insufficient. Therefore, the novel microfluidic mixing method was implemented and further optimized, yielding CDN-loaded, chitosan-based complexes with suitable properties for an intratumoral treatment. Additional modification of this precursor formulation, namely PLGA-PEG coating, facilitated a targeted delivery of these nanoparticles into tumor tissue upon i.v. administration. An increased accumulation of the API in the tumor tissue and tumor-only biomarker response, strongly suggest efficacy of the developed formulation.

However, additional *in vivo* studies have to be conducted, in order to confirm the potential of the formulation with regard to tumor growth inhibition. The consequent next step as to provide evidence of the therapeutic effect is performed by measurement of the tumor sizes. A decrease in tumor growth rate or even apoptosis of the tumor tissue, and therefore improved a survival rate, would further substantiate efficacy of this formulation.

Prior to those advanced *in vivo* studies, it might be equally important, to fully understand the fate of the nanoparticles in the body. Although the free API was detected in the tumor tissue, it is beneficial to know if the API-loaded nanoparticles are also internalized into the tumor cells prior to API release. For this purpose, cell-based uptake assays using a fluorescently-labeled PLGA can be performed.

Apart from the described in-depth characterization of the used formulation, it would appear of benefit to further optimize the current nanoparticulate formulation process. Particularly vital is the implementation of a freeze-drying step for the final formulation, as to enhance the storage stability. In chapter III, a lyophilization method was developed successfully, which might also be applicable for this formulation.

Additionally, a reduction of steps in the manufacturing process would also be beneficial. One possibility to achieve this might be the use of a PEGylated chitosan, which would enable a one-step manufacturing, rendering the PLGA-PEG reaction step redundant.

5 References

1. Allen, T. M.; Cullis, P. R., Drug Delivery Systems: Entering the Mainstream. *Science* **2004,** *303* (5665), 1818-1822.
2. Hans, M. L.; Lowman, A. M., Biodegradable nanoparticles for drug delivery and targeting. *Current Opinion in Solid State and Materials Science* **2002,** *6* (4), 319-327.
3. Perrie, Y.; Ramsay, E., Nanomedicines: Exploring the past, present and future. *Drug Discovery World* **2017,** *18*, 17-22.
4. Peer, D.; Karp, J. M.; Hong, S.; Farokhzad, O. C.; Margalit, R.; Langer, R., Nanocarriers as an emerging platform for cancer therapy. *Nat Nanotechnol* **2007,** *2* (12), 751-760.
5. Panyam, J.; Labhasetwar, V., Biodegradable nanoparticles for drug and gene delivery to cells and tissue. *Advanced Drug Delivery Reviews* **2003,** *55* (3), 329-347.
6. Cao, S.-J.; Xu, S.; Wang, H.-M.; Ling, Y.; Dong, J.; Xia, R.-D.; Sun, X.-H., Nanoparticles: Oral Delivery for Protein and Peptide Drugs. *AAPS PharmSciTech* **2019,** *20* (5), 190-190.
7. Olivier, J. C., Drug transport to brain with targeted nanoparticles. *NeuroRx* **2005,** *2* (1), 108-119.
8. Lee, H. Y.; Mohammed, K. A.; Nasreen, N., Nanoparticle-based targeted gene therapy for lung cancer. *American Journal of Cancer Research* **2016,** *6* (5), 1118-1134.
9. Teng, W.; Zhao, L.; Yang, S.; Zhang, C.; Liu, M.; Luo, J.; Jin, J.; Zhang, M.; Bao, C.; Li, D.; Xiong, W.; Li, Y.; Ren, F., The hepatic-targeted, resveratrol loaded nanoparticles for relief of high fat diet-induced nonalcoholic fatty liver disease. *J. Control. Release* **2019,** *307*, 139-149.
10. Ferrari, M., Cancer nanotechnology: Opportunities and challenges. *Nature Reviews Cancer* **2005,** *5* (3), 161-171.
11. Wang, S.; Su, R.; Nie, S.; Sun, M.; Zhang, J.; Wu, D.; Moustaid-Moussa, N., Application of nanotechnology in improving bioavailability and bioactivity of diet-derived phytochemicals. *J Nutr Biochem* **2014,** *25* (4), 363-376.
12. Peng, S.; Wang, Y.; Li, N.; Li, C., Enhanced cellular uptake and tumor penetration of nanoparticles by imprinting the “hidden” part of membrane receptors for targeted drug delivery. *Chemical Communications* **2017,** *53* (81), 11114-11117.
13. Shi, J.; Kantoff, P. W.; Wooster, R.; Farokhzad, O. C., Cancer nanomedicine: Progress, challenges and opportunities. *Nature Reviews Cancer* **2017,** *17* (1), 20-37.
14. Anselmo, A. C.; Mitragotri, S., Nanoparticles in the clinic: An update. *Bioeng Transl Med* **2019,** *4* (3), e10143-e10143.
15. Anselmo, A. C.; Mitragotri, S., Nanoparticles in the clinic. *Bioeng Transl Med* **2016,** *1* (1), 10-29.
16. Tang, L.; Yang, X.; Yin, Q.; Cai, K.; Wang, H.; Chaudhury, I.; Yao, C.; Zhou, Q.; Kwon, M.; Hartman, J. A.; Dobrucki, I. T.; Dobrucki, L. W.; Borst, L. B.; Lezmi, S.; Helferich, W. G.; Ferguson, A. L.; Fan, T. M.; Cheng, J., Investigating the optimal size of anticancer nanomedicine. *Proc Natl Acad Sci U S A* **2014,** *111* (43), 15344-15349.
17. Greish, K., Enhanced permeability and retention (EPR) effect for anticancer nanomedicine drug targeting. *Methods Mol Biol* **2010,** *624*, 25-37.
18. Golombek, S. K.; May, J.-N.; Theek, B.; Appold, L.; Drude, N.; Kiessling, F.; Lammers, T., Tumor targeting via EPR: Strategies to enhance patient responses. *Advanced drug delivery reviews* **2018,** *130*, 17-38.

19. Bi, Y.; Hao, F.; Yan, G.; Teng, L.; Lee, R. J.; Xie, J., Actively Targeted Nanoparticles for Drug Delivery to Tumor. *Curr Drug Metab* **2016,** *17* (8), 763-782.
20. Wu, C.-H.; Liu, I. J.; Lu, R.-M.; Wu, H.-C., Advancement and applications of peptide phage display technology in biomedical science. *Journal of Biomedical Science* **2016,** *23*, 8.
21. Wilhelm, S.; Tavares, A. J.; Dai, Q.; Ohta, S.; Audet, J.; Dvorak, H. F.; Chan, W. C. W., Analysis of nanoparticle delivery to tumours. *Nature Reviews Materials* **2016,** *1* (5), 16014.
22. Li, C.-Y.; Huang, Q.; Kung, H.-F., Cytokine and immuno-gene therapy for solid tumors. *Cellular & molecular immunology* **2005,** *2* (2), 81-91.
23. Herr, H. W.; Morales, A., History of bacillus Calmette-Guerin and bladder cancer: an immunotherapy success story. *The Journal of urology* **2008,** *179* (1), 53-56.
24. Ehrlich, P., *Ueber den jetzigen Stand der Karzinomforschung*. 1908.
25. Pardoll, D. M., The blockade of immune checkpoints in cancer immunotherapy. *Nature Reviews Cancer* **2012,** *12* (4), 252-264.
26. Ribas, A.; Wolchok, J. D., Cancer immunotherapy using checkpoint blockade. *Science* **2018,** *359* (6382), 1350-1355.
27. Binnewies, M.; Roberts, E. W.; Kersten, K.; Chan, V.; Fearon, D. F.; Merad, M.; Coussens, L. M.; Gabrilovich, D. I.; Ostrand-Rosenberg, S.; Hedrick, C. C.; Vonderheide, R. H.; Pittet, M. J.; Jain, R. K.; Zou, W.; Howcroft, T. K.; Woodhouse, E. C.; Weinberg, R. A.; Krummel, M. F., Understanding the tumor immune microenvironment (TIME) for effective therapy. *Nature medicine* **2018,** *24* (5), 541-550.
28. Bonaventura, P.; Shekarian, T.; Alcazer, V.; Valladeau-Guilemond, J.; Valsesia-Wittmann, S.; Amigorena, S.; Caux, C.; Depil, S., Cold Tumors: A Therapeutic Challenge for Immunotherapy. *Frontiers in immunology* **2019,** *10*, 168-168.
29. Barber, G. N., STING: infection, inflammation and cancer. *Nature Reviews Immunology* **2015,** *15* (12), 760-770.
30. Li, K.; Qu, S.; Chen, X.; Wu, Q.; Shi, M., Promising targets for cancer immunotherapy: TLRs, RLRs, and STING-mediated innate immune pathways. *Int J Mol Sci* **2017,** *18* (2), 404.
31. Corrales, L.; Glickman, L. H.; McWhirter, S. M.; Kanne, D. B.; Sivick, K. E.; Katibah, G. E.; Woo, S. R.; Lemmens, E.; Banda, T.; Leong, J. J.; Metchette, K.; Dubensky, T. W., Jr.; Gajewski, T. F., Direct Activation of STING in the Tumor Microenvironment Leads to Potent and Systemic Tumor Regression and Immunity. *Cell Reports* **2015,** *11* (7), 1018-1030.
32. Motwani, M.; Pesiridis, S.; Fitzgerald, K. A., DNA sensing by the cGAS–STING pathway in health and disease. *Nature Reviews Genetics* **2019,** *20* (11), 657-674.
33. Mao, S.; Sun, W.; Kissel, T., Chitosan-based formulations for delivery of DNA and siRNA. *Advanced Drug Delivery Reviews* **2010,** *62* (1), 12-27.
34. Shukla, S. K.; Mishra, A. K.; Arotiba, O. A.; Mamba, B. B., Chitosan-based nanomaterials: A state-of-the-art review. *International Journal of Biological Macromolecules* **2013,** *59*, 46-58.
35. Agnihotri, S. A.; Mallikarjuna, N. N.; Aminabhavi, T. M., Recent advances on chitosan-based micro- and nanoparticles in drug delivery. *J. Control. Release* **2004,** *100* (1), 5-28.
36. Ali, A.; Ahmed, S., A review on chitosan and its nanocomposites in drug delivery. *International Journal of Biological Macromolecules* **2018,** *109*, 273-286.
37. Zhang, H.; Neau, S. H., In vitro degradation of chitosan by bacterial enzymes from rat cecal and colonic contents. *Biomaterials* **2002,** *23* (13), 2761-2766.
38. Escott, G. M.; Adams, D. J., Chitinase activity in human serum and leukocytes. *Infection and Immunity* **1995,** *63* (12), 4770.

39. Shahidi, F.; Synowiecki, J., Isolation and characterization of nutrients and value-added products from snow crab (Chionoecetes opilio) and shrimp (Pandalus borealis) processing discards. *Journal of Agricultural and Food Chemistry* **1991,** *39* (8), 1527-1532.
40. Ragelle, H.; Vandermeulen, G.; Préat, V., Chitosan-based siRNA delivery systems. *J. Control. Release* **2013,** *172* (1), 207-218.
41. Noh, S. M.; Park, M. O.; Shim, G.; Han, S. E.; Lee, H. Y.; Huh, J. H.; Kim, M. S.; Choi, J. J.; Kim, K.; Kwon, I. C., Pegylated poly-l-arginine derivatives of chitosan for effective delivery of siRNA. *J. Control. Release* **2010,** *145* (2), 159-164.
42. Şalva, E.; Kabasakal, L.; Eren, F.; Özkan, N.; Çakalağaoğlu, F.; Akbuğa, J., Local delivery of chitosan/VEGF siRNA nanoplexes reduces angiogenesis and growth of breast cancer in vivo. *Nucleic acid therapeutics* **2012,** *22* (1), 40-48.
43. Han, H. D.; Mangala, L. S.; Lee, J. W.; Shahzad, M. M.; Kim, H. S.; Shen, D.; Nam, E. J.; Mora, E. M.; Stone, R. L.; Lu, C., Targeted gene silencing using RGD-labeled chitosan nanoparticles. *Clinical Cancer Research* **2010,** *16* (15), 3910-3922.
44. Lee, J.; Yun, K.-S.; Choi, C. S.; Shin, S.-H.; Ban, H.-S.; Rhim, T.; Lee, S. K.; Lee, K. Y., T cell-specific siRNA delivery using antibody-conjugated chitosan nanoparticles. *Bioconjugate chemistry* **2012,** *23* (6), 1174-1180.
45. Rezvantalab, S.; Keshavarz Moraveji, M., Microfluidic assisted synthesis of PLGA drug delivery systems. *RSC Advances* **2019,** *9* (4), 2055-2072.
46. Stroock, A. D.; Dertinger, S. K. W.; Ajdari, A.; Mezic, I.; Stone, H. A.; Whitesides, G. M., Chaotic mixer for microchannels. *Science (New York, N.Y.)* **2002,** *295* (5555), 647-651.
47. Chiesa, E.; Dorati, R.; Pisani, S.; Conti, B.; Bergamini, G.; Modena, T.; Genta, I., The Microfluidic Technique and the Manufacturing of Polysaccharide Nanoparticles. *Pharmaceutics* **2018,** *10* (4), 267.
48. Singh, J.; Ou, K.; Thomas, A.; Garg, S.; Ma, M.; Armstead, A.; Leaver, T. J.; Wild, A. W.; Ip, S.; Taylor, R.; Ramsay, E., A Scalable Microfluidics Platform for the Development of Nanoparticles. *Precision NanoSystems Inc., Vancouver, BC, Canada* **2018**.
49. Ramazani, F.; Chen, W.; van Nostrum, C. F.; Storm, G.; Kiessling, F.; Lammers, T.; Hennink, W. E.; Kok, R. J., Strategies for encapsulation of small hydrophilic and amphiphilic drugs in PLGA microspheres: State-of-the-art and challenges. *International Journal of Pharmaceutics* **2016,** *499* (1), 358-367.
50. Wischke, C.; Schwendeman, S. P., Principles of encapsulating hydrophobic drugs in PLA/PLGA microparticles. *International Journal of Pharmaceutics* **2008,** *364* (2), 298-327.
51. Rafiei, P.; Haddadi, A., Docetaxel-loaded PLGA and PLGA-PEG nanoparticles for intravenous application: pharmacokinetics and biodistribution profile. *Int J Nanomedicine* **2017,** *12*, 935-947.
52. Mu, L.; Feng, S. S., A novel controlled release formulation for the anticancer drug paclitaxel (Taxol®): PLGA nanoparticles containing vitamin E TPGS. *J. Control. Release* **2003,** *86* (1), 33-48.
53. Kim, S.; Kim, J. C.; Sul, D.; Hwang, S. W.; Lee, S. H.; Kim, Y. H.; Tae, G., Nanoparticle formulation for controlled release of capsaicin. *Journal of Nanoscience and Nanotechnology* **2011,** *11* (5), 4586-4591.
54. Javadzadeh, Y.; Ahadi, F.; Davaran, S.; Mohammadi, G.; Sabzevari, A.; Adibkia, K., Preparation and physicochemical characterization of naproxen-PLGA nanoparticles. *Colloids and Surfaces B: Biointerfaces* **2010,** *81* (2), 498-502.
55. Nafea, E. H.; El-Massik, M. A.; El-Khordagui, L. K.; Marei, M. k.; Khalafallah, N. M., Alendronate PLGA microspheres with high loading efficiency for dental applications. *Journal of Microencapsulation* **2007,** *24* (6), 525-538.

56. Xu, Q.; Crossley, A.; Czernuszka, J., Preparation and characterization of negatively charged poly(lactic-co-glycolic acid) microspheres. *Journal of Pharmaceutical Sciences* **2009,** *98* (7), 2377-2389.
57. Parikh, R. H.; Parikh, J. R.; Dubey, R. R.; Soni, H. N.; Kapadia, K. N., Poly(D,L-Lactide-Co-Glycolide) microspheres containing 5-fluorouracil: Optimization of process parameters. *AAPS PharmSciTech* **2003,** *4* (2), 14-21.
58. Chaisri, W.; Ghassemi, A. H.; Hennink, W. E.; Okonogi, S., Enhanced gentamicin loading and release of PLGA and PLHMGA microspheres by varying the formulation parameters. *Colloids and Surfaces B: Biointerfaces* **2011,** *84* (2), 508-514.
59. Ubrich, N.; Bouillot, P.; Pellerin, C.; Hoffman, M.; Maincent, P., Preparation and characterization of propranolol hydrochloride nanoparticles: A comparative study. *J. Control. Release* **2004,** *97* (2), 291-300.
60. Sharma, D.; Gabrani, R.; Sharma, S. K.; Ali, J.; Dang, S., Development of midazolam loaded poly(D, L-lactide-co-glycolic acid) nanoparticles for treatment of status epilepticus. *Advanced Science Letters* **2014,** *20* (7-9), 1526-1530.
61. Li, J. L.; Zheng, C. L.; Liu, J. P.; Zhu, J. B., Formulation and process optimization of doxorubicin-loaded PLGA nanoparticles and its in vitro release. *Yaoxue Xuebao* **2013,** *48* (5), 759-766.
62. Ashton, S.; Song, Y. H.; Nolan, J.; Cadogan, E.; Murray, J.; Odedra, R.; Foster, J.; Hall, P. A.; Low, S.; Taylor, P.; Ellston, R.; Polanska, U. M.; Wilson, J.; Howes, C.; Smith, A.; Goodwin, R. J.; Swales, J. G.; Strittmatter, N.; Takats, Z.; Nilsson, A.; Andren, P.; Trueman, D.; Walker, M.; Reimer, C. L.; Troiano, G.; Parsons, D.; De Witt, D.; Ashford, M.; Hrkach, J.; Zale, S.; Jewsbury, P. J.; Barry, S. T., Aurora kinase inhibitor nanoparticles target tumors with favorable therapeutic index in vivo. *Sci Transl Med* **2016,** *8* (325), 325ra17.
63. Strack, P.; Külzer, R.; Sommer, F.; Bretschneider, T.; Merkel, O. M.; Grube, A., A smart approach to enable preclinical studies in pharmaceutical industry: PLGA-based extended release formulation platform for subcutaneous applications. *Drug Development and Industrial Pharmacy* **2020**, 1-11.
64. Greim, H.; Bury, D.; Klimisch, H. J.; Oeben-Negele, M.; Ziegler-Skylakakis, K., Toxicity of aliphatic amines: structure-activity relationship. *Chemosphere* **1998,** *36* (2), 271-295.
65. Carthew, R. W.; Sontheimer, E. J., Origins and Mechanisms of miRNAs and siRNAs. *Cell* **2009,** *136* (4), 642-655.
66. Tseng, Y. C.; Mozumdar, S.; Huang, L., Lipid-based systemic delivery of siRNA. *Advanced Drug Delivery Reviews* **2009,** *61* (9), 721-731.
67. Wang, J.; Lu, Z.; Wientjes, M. G.; Au, J. L. S., Delivery of siRNA therapeutics: Barriers and carriers. *AAPS Journal* **2010,** *12* (4), 492-503.
68. Yin, H.; Kanasty, R. L.; Eltoukhy, A. A.; Vegas, A. J.; Dorkin, J. R.; Anderson, D. G., Non-viral vectors for gene-based therapy. *Nature Reviews Genetics* **2014,** *15* (8), 541-555.
69. Höbel, S.; Aigner, A., Polyethylenimines for siRNA and miRNA delivery in vivo. *Wiley Interdisciplinary Reviews: Nanomedicine and Nanobiotechnology* **2013,** *5* (5), 484-501.
70. Nimesh, S., Polyethylenimine as a promising vector for targeted siRNA delivery. *Current Clinical Pharmacology* **2012,** *7* (2), 121-130.
71. Jiang, H. L.; Islam, M. A.; Xing, L.; Firdous, J.; Cao, W.; He, Y. J.; Zhu, Y.; Cho, K. H.; Li, H. S.; Cho, C. S., Degradable Polyethylenimine-Based Gene Carriers for Cancer Therapy. In *Topics in Current Chemistry*, 2017; Vol. 375.
72. Dehousse, V.; Garbacki, N.; Jaspart, S.; Castagne, D.; Piel, G.; Colige, A.; Evrard, B., Comparison of chitosan/siRNA and trimethylchitosan/siRNA complexes behaviour in vitro. *International journal of biological macromolecules* **2010,** *46* (3), 342-349.

73. Katas, H.; Raja, M. A. G.; Lam, K. L., Development of Chitosan Nanoparticles as a Stable Drug Delivery System for Protein/siRNA. *Int J Biomater* **2013,** *2013*, 146320-146320.
74. Dhandapani, R. K.; Gurusamy, D.; Howell, J. L.; Palli, S. R., Development of CS-TPP-dsRNA nanoparticles to enhance RNAi efficiency in the yellow fever mosquito, Aedes aegypti. *Scientific Reports* **2019,** *9* (1), 8775.
75. Abdul Ghafoor Raja, M.; Katas, H.; Jing Wen, T., Stability, Intracellular Delivery, and Release of siRNA from Chitosan Nanoparticles Using Different Cross-Linkers. *PLOS ONE* **2015,** *10* (6), e0128963.
76. Nasti, A.; Zaki, N. M.; de Leonardis, P.; Ungphaiboon, S.; Sansongsak, P.; Rimoli, M. G.; Tirelli, N., Chitosan/TPP and Chitosan/TPP-hyaluronic Acid Nanoparticles: Systematic Optimisation of the Preparative Process and Preliminary Biological Evaluation. *Pharmaceutical research* **2009,** *26* (8), 1918-1930.
77. Zhang, H.; Mardyani, S.; Chan, W. C. W.; Kumacheva, E., Design of Biocompatible Chitosan Microgels for Targeted pH-Mediated Intracellular Release of Cancer Therapeutics. *Biomacromolecules* **2006,** *7* (5), 1568-1572.
78. Hassani, S.; Laouini, A.; Fessi, H.; Charcosset, C., Preparation of chitosan–TPP nanoparticles using microengineered membranes – Effect of parameters and encapsulation of tacrine. *Colloids and Surfaces A: Physicochemical and Engineering Aspects* **2015,** *482*, 34-43.
79. Maluin, F. N.; Hussein, M. Z.; Yusof, N. A.; Fakurazi, S.; Idris, A. S.; Hilmi, N. H. Z.; Jeffery Daim, L. D., A Potent Antifungal Agent for Basal Stem Rot Disease Treatment in Oil Palms Based on Chitosan-Dazomet Nanoparticles. *Int J Mol Sci* **2019,** *20* (9), 2247.
80. Jarudilokkul, S.; Tongthammachat, A.; Boonamnuayvittaya, V., Preparation of chitosan nanoparticles for encapsulation and release of protein. *Korean Journal of Chemical Engineering* **2011,** *28* (5), 1247.
81. Yeh, C.-H.; Lin, P.-W.; Lin, Y.-C., Chitosan microfiber fabrication using a microfluidic chip and its application to cell cultures. *Microfluidics and Nanofluidics* **2009,** *8* (1), 115.
82. Pessoa, A. C. S. N.; Sipoli, C. C.; de la Torre, L. G., Effects of diffusion and mixing pattern on microfluidic-assisted synthesis of chitosan/ATP nanoparticles. *Lab on a chip* **2017,** *17* (13), 2281-2293.
83. Majedi, F. S.; Hasani-Sadrabadi, M. M.; Emami, S. H.; Shokrgozar, M. A.; VanDersarl, J. J.; Dashtimoghadam, E.; Bertsch, A.; Renaud, P., Microfluidic assisted self-assembly of chitosan based nanoparticles as drug delivery agents. *Lab on a chip* **2013,** *13* (2), 204-207.
84. Cetin, B.; Taze, S.; Asik, M. D.; Tuncel, S. A. In *Microfluidic Device for Synthesis of Chitosan Nanoparticles*, ASME 2013 Fluids Engineering Division Summer Meeting, 2013.
85. Li, J.; Huang, Q., Rheological properties of chitosan–tripolyphosphate complexes: From suspensions to microgels. *Carbohydrate Polymers - CARBOHYD POLYM* **2012,** *87*.
86. Cao, Y.; Tan, Y. F.; Wong, Y. S.; Liew, M. W. J.; Venkatraman, S., Recent Advances in Chitosan-Based Carriers for Gene Delivery. *Mar Drugs* **2019,** *17* (6), 381.
87. De Smedt, S. C.; Demeester, J.; Hennink, W. E., Cationic Polymer Based Gene Delivery Systems. *Pharmaceutical research* **2000,** *17* (2), 113-126.
88. Garg, S. M.; Thomas, A.; Heuck, G.; Armstead, A.; Singh, J.; Leaver, T. J.; Wild, A. W.; Ip, S.; Taylor, R. J.; Ramsay, E. C. *PLGA Nanoparticles, Tuning Particle Size UsingThe NanoAssemblr™ Benchtop Instrument*; 2017.
89. La Spina, R.; Spampinato, V.; Gilliland, D.; Ojea-Jimenez, I.; Ceccone, G., Influence of different cleaning processes on the surface chemistry of gold nanoparticles. *Biointerphases* **2017,** *12* (3), 031003-031003.
90. Erickson, H. P., Size and shape of protein molecules at the nanometer level determined by sedimentation, gel filtration, and electron microscopy. *Biol Proced Online* **2009,** *11*, 32-51.

91. Gan, Q.; Wang, T.; Cochrane, C.; McCarron, P., Modulation of surface charge, particle size and morphological properties of chitosan–TPP nanoparticles intended for gene delivery. *Colloids and Surfaces B: Biointerfaces* **2005,** *44* (2), 65-73.
92. MacLaughlin, F. C.; Mumper, R. J.; Wang, J.; Tagliaferri, J. M.; Gill, I.; Hinchcliffe, M.; Rolland, A. P., Chitosan and depolymerized chitosan oligomers as condensing carriers for in vivo plasmid delivery. *J. Control. Release* **1998,** *56* (1), 259-272.
93. Huang, M.; Fong, C.-W.; Khor, E.; Lim, L.-Y., Transfection efficiency of chitosan vectors: Effect of polymer molecular weight and degree of deacetylation. *J. Control. Release* **2005,** *106* (3), 391-406.
94. Liu, X.; Howard, K. A.; Dong, M.; Andersen, M. Ø.; Rahbek, U. L.; Johnsen, M. G.; Hansen, O. C.; Besenbacher, F.; Kjems, J., The influence of polymeric properties on chitosan/siRNA nanoparticle formulation and gene silencing. *Biomaterials* **2007,** *28* (6), 1280-1288.
95. Yang, Y.; Guo, M.; Qian, R.; Liu, C.; Zong, X.; Li, Y.-Q.; Li, W., Binding efficacy and kinetics of chitosan with DNA duplex: The effects of deacetylation degree and nucleotide sequences. *Carbohydrate Polymers* **2017,** *169*, 451-457.
96. Alameh, M.; Lavertu, M.; Tran-Khanh, N.; Chang, C.-Y.; Lesage, F.; Bail, M.; Darras, V.; Chevrier, A.; Buschmann, M. D., siRNA Delivery with Chitosan: Influence of Chitosan Molecular Weight, Degree of Deacetylation, and Amine to Phosphate Ratio on in Vitro Silencing Efficiency, Hemocompatibility, Biodistribution, and in Vivo Efficacy. *Biomacromolecules* **2018,** *19* (1), 112-131.
97. Howard, K. A.; Rahbek, U. L.; Liu, X.; Damgaard, C. K.; Glud, S. Z.; Andersen, M. Ø.; Hovgaard, M. B.; Schmitz, A.; Nyengaard, J. R.; Besenbacher, F.; Kjems, J., RNA interference in vitro and in vivo using a novel chitosan/siRNA nanoparticle system. *Mol Ther* **2006,** *14* (4), 476-484.
98. Ragelle, H.; Riva, R.; Vandermeulen, G.; Naeye, B.; Pourcelle, V.; Le Duff, C. S.; D'Haese, C.; Nysten, B.; Braeckmans, K.; De Smedt, S. C.; Jérôme, C.; Préat, V., Chitosan nanoparticles for siRNA delivery: Optimizing formulation to increase stability and efficiency. *J. Control. Release* **2014,** *176*, 54-63.
99. Cho, Y. W.; Kim, J.-D.; Park, K., Polycation gene delivery systems: escape from endosomes to cytosol. *Journal of Pharmacy and Pharmacology* **2003,** *55* (6), 721-734.
100. Thibault, M.; Nimesh, S.; Lavertu, M.; Buschmann, M. D., Intracellular Trafficking and Decondensation Kinetics of Chitosan–pDNA Polyplexes. *Molecular Therapy* **2010,** *18* (10), 1787-1795.
101. Yue, Z.-G.; Wei, W.; Lv, P.-P.; Yue, H.; Wang, L.-Y.; Su, Z.-G.; Ma, G.-H., Surface Charge Affects Cellular Uptake and Intracellular Trafficking of Chitosan-Based Nanoparticles. *Biomacromolecules* **2011,** *12* (7), 2440-2446.
102. Huang, M.; Ma, Z.; Khor, E.; Lim, L.-Y., Uptake of FITC-Chitosan Nanoparticles by A549 Cells. *Pharmaceutical research* **2002,** *19* (10), 1488-1494.
103. Wilson, D. R.; Sen, R.; Sunshine, J. C.; Pardoll, D. M.; Green, J. J.; Kim, Y. J., Biodegradable STING agonist nanoparticles for enhanced cancer immunotherapy. *Nanomedicine: Nanotechnology, Biology and Medicine* **2018,** *14* (2), 237-246.
104. Ruponen, M.; Honkakoski, P.; Tammi, M.; Urtti, A., Cell-surface glycosaminoglycans inhibit cation-mediated gene transfer. *The Journal of Gene Medicine* **2004,** *6* (4), 405-414.
105. Danielsen, S.; Strand, S.; de Lange Davies, C.; Stokke, B. T., Glycosaminoglycan destabilization of DNA–chitosan polyplexes for gene delivery depends on chitosan chain length and GAG properties. *Biochimica et Biophysica Acta (BBA) - General Subjects* **2005,** *1721* (1), 44-54.

106. Mao, H.-Q.; Roy, K.; Troung-Le, V. L.; Janes, K. A.; Lin, K. Y.; Wang, Y.; August, J. T.; Leong, K. W., Chitosan-DNA nanoparticles as gene carriers: synthesis, characterization and transfection efficiency. *J. Control. Release* **2001,** *70* (3), 399-421.
107. Suk, J. S.; Xu, Q.; Kim, N.; Hanes, J.; Ensign, L. M., PEGylation as a strategy for improving nanoparticle-based drug and gene delivery. *Advanced drug delivery reviews* **2016,** *99* (Pt A), 28-51.
108. Buyens, K.; De Smedt, S. C.; Braeckmans, K.; Demeester, J.; Peeters, L.; van Grunsven, L. A.; de Mollerat du Jeu, X.; Sawant, R.; Torchilin, V.; Farkasova, K.; Ogris, M.; Sanders, N. N., Liposome based systems for systemic siRNA delivery: Stability in blood sets the requirements for optimal carrier design. *J. Control. Release* **2012,** *158* (3), 362-370.
109. Lee, H.; Jeong, J. H.; Park, T. G., PEG grafted polylysine with fusogenic peptide for gene delivery: high transfection efficiency with low cytotoxicity. *J. Control. Release* **2002,** *79* (1), 283-291.
110. Rudzinski, W. E.; Palacios, A.; Ahmed, A.; Lane, M. A.; Aminabhavi, T. M., Targeted delivery of small interfering RNA to colon cancer cells using chitosan and PEGylated chitosan nanoparticles. *Carbohydrate Polymers* **2016,** *147*, 323-332.
111. Mao, H. Q.; Roy, K.; Troung-Le, V. L.; Janes, K. A.; Lin, K. Y.; Wang, Y.; August, J. T.; Leong, K. W., Chitosan-DNA nanoparticles as gene carriers: synthesis, characterization and transfection efficiency. *J Control Release* **2001,** *70* (3), 399-421.
112. Chinedu, C. O.; Mahdi, G., Berberine Encapsulated PLGA-PEG Nanoparticles Modulate PCSK-9 in HepG2 Cells. *Cardiovascular & Hematological Disorders-Drug Targets* **2018,** *18* (1), 61-70.
113. Locatelli, E.; Comes Franchini, M., Biodegradable PLGA-b-PEG polymeric nanoparticles: synthesis, properties, and nanomedical applications as drug delivery system. *Journal of Nanoparticle Research* **2012,** *14* (12), 1316.
114. Fan, S.; Zheng, Y.; Liu, X.; Fang, W.; Chen, X.; Liao, W.; Jing, X.; Lei, M.; Tao, E.; Ma, Q.; Zhang, X.; Guo, R.; Liu, J., Curcumin-loaded PLGA-PEG nanoparticles conjugated with B6 peptide for potential use in Alzheimer's disease. *Drug Delivery* **2018,** *25* (1), 1091-1102.
115. Cheng, J.; Teply, B. A.; Sherifi, I.; Sung, J.; Luther, G.; Gu, F. X.; Levy-Nissenbaum, E.; Radovic-Moreno, A. F.; Langer, R.; Farokhzad, O. C., Formulation of functionalized PLGA-PEG nanoparticles for in vivo targeted drug delivery. *Biomaterials* **2007,** *28* (5), 869-876.
116. Rezvantalab, S.; Drude, N. I.; Moraveji, M. K.; Güvener, N.; Koons, E. K.; Shi, Y.; Lammers, T.; Kiessling, F., PLGA-Based Nanoparticles in Cancer Treatment. *Frontiers in Pharmacology* **2018,** *9* (1260).
117. Gholizadeh, S.; Kamps, J. A. A. M.; Hennink, W. E.; Kok, R. J., PLGA-PEG nanoparticles for targeted delivery of the mTOR/PI3kinase inhibitor dactolisib to inflamed endothelium. *International Journal of Pharmaceutics* **2018,** *548* (2), 747-758.
118. Albisa, A.; Piacentini, E.; Sebastian, V.; Arruebo, M.; Santamaria, J.; Giorno, L., Preparation of Drug-Loaded PLGA-PEG Nanoparticles by Membrane-Assisted Nanoprecipitation. *Pharmaceutical research* **2017,** *34* (6), 1296-1308.
119. De Rosa, G.; Bochot, A.; Quaglia, F.; Besnard, M.; Fattal, E., A new delivery system for antisense therapy: PLGA microspheres encapsulating oligonucleotide/polyethyleneimine solid complexes. *International Journal of Pharmaceutics* **2003,** *254* (1), 89-93.
120. Hsu, Y. Y.; Hao, T.; Hedley, M. L., Comparison of process parameters for microencapsulation of plasmid DNA in poly(D,L-lactic-co-glycolic) acid microspheres. *J Drug Target* **1999,** *7* (4), 313-323.

121. Oster, C. G.; Kissel, T., Comparative study of DNA encapsulation into PLGA microparticles using modified double emulsion methods and spray drying techniques. *Journal of Microencapsulation* **2005,** *22* (3), 235-244.
122. Walter, E.; Merkle, H. P., Microparticle-mediated transfection of non-phagocytic cells in vitro. *J Drug Target* **2002,** *10* (1), 11-21.
123. Elsaid, N.; Jackson, T. L.; Elsaid, Z.; Alqathama, A.; Somavarapu, S., PLGA Microparticles Entrapping Chitosan-Based Nanoparticles for the Ocular Delivery of Ranibizumab. *Molecular pharmaceutics* **2016,** *13* (9), 2923-2940.
124. Patil, Y.; Panyam, J., Polymeric nanoparticles for siRNA delivery and gene silencing. *International journal of pharmaceutics* **2009,** *367* (1-2), 195-203.
125. Sirsi, S. R.; Schray, R. C.; Wheatley, M. A.; Lutz, G. J., Formulation of polylactide-co-glycolic acid nanospheres for encapsulation and sustained release of poly(ethylene imine)-poly(ethylene glycol) copolymers complexed to oligonucleotides. *Journal of Nanobiotechnology* **2009,** *7* (1), 1.
126. Stigliano, C.; Aryal, S.; de Tullio, M. D.; Nicchia, G. P.; Pascazio, G.; Svelto, M.; Decuzzi, P., siRNA-Chitosan Complexes in Poly(lactic-co-glycolic acid) Nanoparticles for the Silencing of Aquaporin-1 in Cancer Cells. *Molecular Pharmaceutics* **2013,** *10* (8), 3186-3194.
127. Snehalatha, M.; Kolachina, V.; Saha, R. N.; Babbar, A. K.; Sharma, N.; Sharma, R. K., Enhanced tumor uptake, biodistribution and pharmacokinetics of etoposide loaded nanoparticles in Dalton's lymphoma tumor bearing mice. *J Pharm Bioallied Sci* **2013,** *5* (4), 290-297.
128. Schluep, T.; Hwang, J.; Hildebrandt, I. J.; Czernin, J.; Choi, C. H. J.; Alabi, C. A.; Mack, B. C.; Davis, M. E., Pharmacokinetics and tumor dynamics of the nanoparticle IT-101 from PET imaging and tumor histological measurements. *Proceedings of the National Academy of Sciences* **2009,** *106* (27), 11394-11399.
129. Hoshyar, N.; Gray, S.; Han, H.; Bao, G., The effect of nanoparticle size on in vivo pharmacokinetics and cellular interaction. *Nanomedicine (Lond)* **2016,** *11* (6), 673-692.
130. Dhar, S.; Kolishetti, N.; Lippard, S. J.; Farokhzad, O. C., Targeted delivery of a cisplatin prodrug for safer and more effective prostate cancer therapy in vivo. *Proceedings of the National Academy of Sciences* **2011,** *108* (5), 1850.
131. Huang, J.; Zhang, H.; Yu, Y.; Chen, Y.; Wang, D.; Zhang, G.; Zhou, G.; Liu, J.; Sun, Z.; Sun, D.; Lu, Y.; Zhong, Y., Biodegradable self-assembled nanoparticles of poly (d,l-lactide-co-glycolide)/hyaluronic acid block copolymers for target delivery of docetaxel to breast cancer. *Biomaterials* **2014,** *35* (1), 550-566.
132. Fong, D.; Hoemann, C. D., Chitosan immunomodulatory properties: perspectives on the impact of structural properties and dosage. *Future Sci OA* **2017,** *4* (1), FSO225-FSO225.
133. Koshy, S. T.; Cheung, A. S.; Gu, L.; Graveline, A. R.; Mooney, D. J., Liposomal Delivery Enhances Immune Activation by STING Agonists for Cancer Immunotherapy. *Adv Biosyst* **2017,** *1* (1-2), 1600013.
134. Nakamura, T.; Miyabe, H.; Hyodo, M.; Sato, Y.; Hayakawa, Y.; Harashima, H., Liposomes loaded with a STING pathway ligand, cyclic di-GMP, enhance cancer immunotherapy against metastatic melanoma. *J Control Release* **2015,** *216*, 149-157.
135. Shae, D.; Becker, K. W.; Christov, P.; Yun, D. S.; Lytton-Jean, A. K. R.; Sevimli, S.; Ascano, M.; Kelley, M.; Johnson, D. B.; Balko, J. M.; Wilson, J. T., Endosomolytic polymersomes increase the activity of cyclic dinucleotide STING agonists to enhance cancer immunotherapy. *Nat Nanotechnol* **2019,** *14* (3), 269-278.

CHAPTER III

LIVER TARGETED NANOPARTICLES FOR NASH TREATMENT

Parts of the following chapter are intended to be published.

The personal contribution covers manufacturing, characterization, and optimization of the described nanoparticulate formulations. Animal experiments were performed by Stefan Scheuerer.

Developing a nanoparticulate formulation for NASH treatment: Manufacturing, characterization, optimization and *in vivo* proof of concept

Patrick Strack[a, b], Stefan Scheuerer[a], Manuel Baader[a], Ralph Budzinski[a], Olivia M. Merkel[b] and Achim Grube[a]

[a]*Boehringer Ingelheim Pharma GmbH & Co. KG, Birkendorfer Straße 65, 88400 Biberach an der Riss, Germany;*
[b]*Ludwig-Maximilians Universität München, Butenandtstr. 5-13, Haus B, 81377 München, Germany,*

Abstract

The non-alcoholic steatohepatitis (NASH) is currently one of the most common liver diseases worldwide. Without proper treatment, NASH can lead to life-threatening complications such as fibrosis, cirrhosis and finally liver failure. Until this date, there is no approved pharmacotherapy available for NASH. Systemic side effects upon administration are often limiting applicability of a potential drug. Here, a targeted delivery of the active pharmaceutical ingredient (API) into the liver tissue using nanoparticulate formulation was developed in order to address this issue.

Two research compounds were encapsulated into PLGA-based nanoparticles, utilizing microfluidic mixing, and further optimized with regard to particle size, polydispersity index, surface charge, drug loading and *in vitro* release. The final formulations were extensively characterized for their applicability *in vivo* and subsequently tested in a proof of concept PK study.

Optimized nanoparticulate formulations, suitable for *in vivo* studies were manufactured with both model APIs. Uniform particles with a Z-average of 160 nm, zeta potential of -16 mV, drug release up to 4 hours and 2% drug loading were obtained as the final formulation. The following PK study demonstrated high local concentration of the API in the hepatic tissue strongly suggesting successful targeting of the liver by the nanoparticles.

1 Introduction

One of the most common causes for chronic liver disorder worldwide is the nonalcoholic fatty liver disease (NAFLD) [1]. It is present in approximately 25% of the world population [2], with a high prevalence in industrialized nations such as the United States [3, 4] and Europe [5]. NAFLD is defined as an excessive accumulation of fat built-up in the liver [6], caused by any factor other than excessive alcohol use; mostly obesity, diabetes or hyperlipidemia [7].

The most aggressive subtype of NAFLD, the non-alcoholic steatohepatitis (NASH), is marked by cell injury, leading to inflammation and fibrosis, that in turn may progress into irreversible liver cirrhosis [8]. The end-stage of this disease makes a liver transplantation inevitable [9]. Despite the significant burden for patients, to this day no pharmacological treatment has received approval [10].

The standard of care in NASH involves a change in lifestyle, mainly increased physical activity and permanent weight loss [11]. However, due to lack of patient compliance when it comes to implementing life-style alterations, the need for a pharmacotherapy remains.

Currently there are many potential pharmacotherapeutic options in preclinical and clinical trials [12]. One of the promising approaches is the inhibition of the *de novo* lipogenesis in the hepatic stellate cells [13]. Hereby, excessive fatty accumulation in the liver can be prevented by reducing levels of liver triglycerides. Fatty acid synthase inhibitors (FASi) and acetyl-CoA carboxylase inhibitors (ACCi) are two potential classes of research compounds available for this approach. However, both types of APIs show adverse effects when applied systemically, which might be attributed to the additional inhibition of lipogenesis in cells other than hepatic ones. Furthermore, administration of ACCi results in an increase of triglyceride levels in plasma [14]. Therefore, a targeted delivery of the APIs into the hepatic tissue is highly desirable.

Nanoparticles form one plausible strategy for this purpose. The liver acts as a biological filtration system, incorporating 30 - 99% of administered nanoparticles, particularly in a size range between 50 and 250 nm [15]. The high local concentration of nanoparticulate therapeutics in perisinusoidal space (space of disse), following intravenous administration, is caused by the presence of sinusoidal fenestrations along the endothelial wall and the absence of basal lamina in the liver tissue [16].

Nanomedicines for targeting the liver are mainly formulated utilizing liposomes or polymer encapsulation [17]. One of the most commonly utilized and well-established polymers in drug delivery is poly(lactic-co-glycolic acid) (PLGA) [18]. Due to its excellent biocompatibility, biodegradability and low systemic toxicity it has been approved by the FDA in products for various stages of clinical trials, as well as in some commercial formulations [19]. In PLGA nanoparticles, the compound is encapsulated within the polymeric matrix, whereby the drug is protected during circulation and slowly released after reaching the targeted organ [18].

The objective of this work was to develop a PLGA-based nanoparticlulate formulation targeting hepatic tissue for NASH treatment. This manuscript describes the manufacturing, characterization and optimization of API-loaded (FASi/ACCi) nanoparticles and a subsequent *in vivo* proof of concept study.

2 Material and Methods

2.1 Materials

Two research compounds, BI 99179 (FAS inhibitor) and EX00010187 (ACC inhibitor) were provided by Boehringer Ingelheim Pharma GmbH & Co. KG (Biberach an der Riß, Germany).

Poly (lactic-co-glycolic acid) (PLGA) Resomer® RG 752 H (RG752H), Resomer® RG 653 H (RG653H) Resomer® RG 503 H (RG503H) were obtained from Evonik Industries AG (Essen, Germany). A sample of PEGylated PLGA, EXPANSORB® DLG 50-6P (PLGA-PEG) was graciously provided by Merck KGaA (Darmstadt, Germany). Deionized distilled (DI) water was produced in-house with an ultrapure water purification system by PURELAB Ultra Ionic (ELGA, High Wycombe, United Kingdom). Acetonitrile (ACN), dichloromethane (DCM), ethanol (EtOH), polyvinyl alcohol, 90% hydrolyzed, Mw 9000-10000 (PVA), sodium chloride (NaCl) and trehalose were obtained from Merck KGaA (Darmstadt, Germany). All solvents used were of HPLC purity grade.

2.2 Manufacturing methods

2.2.1 Single Emulsion Evaporation

API loaded nanoparticles were prepared using a single emulsion evaporation method. Stock solutions containing 5 or 10 mg/mL RG503H in DCM were prepared. The solution was added dropwise in a 1:20 volume ratio to an aqueous 1 or 10 mg/mL PVA solution obtaining a total volume of 1, 4 and 10 mL. The resulting mixture was homogenized under ice-cooling using a Model 120 Sonic Dismembrator (Thermo Fisher, Waltham, USA) for 1 min at 50% power output. After homogenization, the resulting emulsion was stirred for 1 h to let the organic solvent evaporate. The hardened particles were subsequently washed three times by centrifugation (14000 rpm, 4 °C, 30 min) and redispersed in DI water. Directly after this process the nanoparticle suspension was lyophilized.

2.2.2 Microfluidic mixing

PLGA-based nanoparticles were manufactured using the microfluidic mixer Nanoassemblr Benchtop Instrument (Precision NanoSystems, Inc., Vancouver, Canada) by mixing designated

volumes of an aqueous PVA and organic PLGA solutions. Microfluidic cartridges were pre-processed before every run by washing both channels with DI water, ACN and a DI water/ACN mixture consequently. PVA was dissolved in DI water at a concentration of 0.1 – 20 mg/mL. PLGA (RH503H, RG653H and RG752H) was dissolved in ACN at concentrations of 4.5 – 10 mg/mL. PLGA-PEG was added to the PLGA-solution at concentrations of 0.25 – 1mg/mL relative to the PLGA concentration, as specified throughout the text. The two APIs (FASi and ACCi) were added to the PLGA or PLGA/PLGA-PEG solution in concentrations of 0.5 to 2.5 mg/mL as mentioned in the text. All prepared solutions were filtered through a 0.45 µm cellulose acetate membrane (Sartorius AG, Göttingen, Germany). For manufacturing of PLGA-based nanoparticles, the ACN solution was injected through one inlet of the microfluidic mixer, whereas PVA solution was injected through the other inlet. The complexes were prepared at organic/aqueous solution ratio of 1:1 with a flow rate of 1 mL/min. A total volume of 1 - 10 mL of stock solution was injected through the microfluidic mixer, including an initial waste volume of 0.25 mL and a final waste volume of 0.05 mL.

The manufactured complexes were purified by Spectra/Por™ Float-A-Lyzer™ G2 Dialysis Devices (Repligen, Waltham, USA). The dialysis devices were prepared by submerging the filter membrane in 10% ethanol solution for 10 min and subsequently soaked in DI water for 30 minutes. The manufactured nanoparticles were loaded into the prepared device and kept floating in 1 liter DI water 2 hours. The floating media were changed after 0.5 and 1 hour. Directly after this process the nanoparticle suspension was lyophilized.

2.2.3 Lyophilization

The manufactured nanoparticle suspension were filled into semi-stoppered glass vials at a maximal height of 25 mm. The formulation was flash frozen in liquid nitrogen for 10 minutes and then transferred to an Epsilon 2-4 LSCplus freeze-dryer (Christ, Osterode am Harz, Germany). The initial freeze-drying cycle was performed according to an established generic protocol. Primary drying was performed at a shelf temperature of - 60 °C and a pressure of 1 mbar for 2 hours, followed by a secondary drying step at 20 °C and a pressure of 0.01 mbar for 24 hours. For the optimized protocol, the samples were kept at a shelf temperature of - 60 °C for 1 hour, subsequently primary drying was performed at a pressure of 0.001 mbar for 10 hours. This was followed by a secondary drying step, gradually increasing the temperature to 4 °C in 5 hours. The samples were kept in this atmosphere until complete dehydration. After

aeration, the vials were sealed and stored in a desiccator. When applying the optimized protocol, trehalose was added to the nanoparticle suspension at a concentration of 0.1 – 2.5 mg/mL.

2.3 Physicochemical characterization

2.3.1 Particle size measurement

The hydrodynamic diameter and size distribution of particles dispersed in DI water were determined by dynamic light scattering (DLS) using a NanoPartica SZ-100 (Horiba, Kyoto, Japan). All measurements were conducted at 25°C with a detection angle of 173° for 120 sec. Z-average and polydispersity index (PDI) were estimated from autocorrelation using the cumulant analysis. For each sample, the measurement was recorded in triplicates, and the average of the measurements was calculated. All values of Z-average and PDI were expressed as the mean standard deviation.

2.3.2 Zeta Potential

Surface charge of the nanoparticles dispersed in 1 mM NaCl solution was measured in carbon-coated microelectronics cells (Horiba, Kyoto, Japan) using the NanoPartica SZ-100 (Horiba, Kyoto, Japan). The measurements were repeated at least three times without sample dilution. The zeta potential was calculated from electrophoretic mobility using the Helmholtz-Smoluchowski equation.

2.3.3 Determination of drug loading

Next, 1 mg of the lyophilized sample was resuspended in 1 mL ethanol and sonicated in an ultrasonication bath for 60 min, as to extract the API from the nanoparticles. The resulting mixture was centrifuged (60 min, 14000 rpm, 4°C), and the concentration in the supernatant was measured by HPLC. Drug loading (DL) was calculated as shown here:

Drug loading: $\left(\frac{amount\ of\ drug\ present\ in\ formulation}{total\ weight\ of\ formulation}\right)$ x 100%

2.3.4 *In vitro* drug release assay

Subsequently, 1 mL of the manufactured nanoparticle suspension or 5 mg of the lyophilized nanoparticles resuspended in 1 mL DI water were added to 9 mL phosphate-buffered saline

(PBS, pH =7.4). The resulting mixture was aliquoted in 1.5 mL Eppendorf™ reaction tubes and incubated at 700 rpm and at 37°C in an Eppendorf™ ThermoMixer (Eppendorf AG, Hamburg, Germany) for 24 hours. At each predetermined sampling point, the supernatant was separated by centrifugation (45 min, 14000 rpm, 4°C) and the concentration was measured by HPLC. Due to the high compound consumption necessary for the release assay, FASi-nanoparticle release profiles determination were not performed in triplicate.

2.3.5 Differential scanning calorimetry (DSC)

Modulated DSC (MDSC) was used to determine the mid-point of the glass transition. MDSC was performed using a Q2000® (TA Instruments Ltd., New Castle, USA). For each sample, 0.5 mg of the lyophilized nanoparticles was placed on an aluminum pan and hermetically sealed. The samples were heated from - 40 °C to 120 °C at a rate of 3 K/min in a modulation temperature amplitude of 1 °C over 60 seconds modulation period.

2.3.6 Transmission electron microscopy (TEM)

Negative staining TEM was applied for the evaluation of the nanoparticle morphology. Of each sample 2 µL were diluted in 98 µL water and placed on a carbon film coated copper grid. Excess sample solution was removed with a filter paper. The grid was stained with 10 µL of 2% phosphotungstic acid vapor for 1 minute. The surplus staining solution was removed afterwards with a filter paper and the sample was dried at ambient environment before imaging using a LEO 912 AB (Carl Zeiss AG, Jena, Germany) operating at an acceleration voltage of 80 kV.

2.3.7 High-performance liquid chromatography (HPLC)

All HPLC measurements were performed on an Agilent 1100 Series (Agilent Technologies, Santa Clara, USA). For each HPLC run, 2 µL of sample solution was aliquoted and analyzed with a Synergi™ 4 µm Fusion-RP 80 Å, LC Column 100 x 2 mm (Phenomenex Inc., Torrance, USA), at a flow rate of 1 mL/min. A gradient method was used to elute the API, starting with 95% 20 mM filtered ammonium acetate buffer (pH 4.5). The ratio of acetonitrile was increased progressively until the mobile phase consisted of 85% acetonitrile after 9 min. Finally, the amount of acetonitrile was increased to 95% in the last minute of the run. The overall runtime was 10 min with a retention time of 5 min for the API. *Empower 3* software (Waters, Milford, USA) was used to process and quantify sample peaks.

2.3.8 Statistical Analysis:

All results are given as mean value ± standard deviation (SD). All experiments were performed in triplicates unless stated otherwise.

2.4 PK study

2.4.1 Animal experiments

The different formulations were administered intravenously (i.v.) to fed BALB/c mice (17 – 24 g body weight, three female animals per treatment group, respectively) in a dose of 1 µmol/kg (control NaCL formulation) and 0.79 µmol/kg (nanoparticle formulation) on day one and day four of the study. Blood samples were collected at specified time points via puncture of the saphenous vein using ethylenediaminetetraacetic acid (EDTA)-coated microvettes. Plasma was captured after centrifugation and immediately frozen at -20 °C until LC-MS/MS analysis. 15 min after the second dosing (mice were euthanized. Liver and spleen were removed and homogenized in an aqueous buffer prior to protein precipitation with acetonitrile. The samples were stored at −20 °C until LC-MS/MS analysis.

Animal experiments were approved by the local animal ethics committee and were in agreement with the German Animal Welfare Act.

2.4.2 LC-MS/MS analysis

Plasma aliquots of 5 µL were supplemented with 400 nM of BI-1052 (internal standard). Plasma proteins were precipitated by the addition of 70 µL 50% acetonitrile : 50% methanol and subsequent centrifugation at 4000 rpm, 4 °C for 10 min in an Eppendorf 5810 centrifuge (Eppendorf AG, Hamburg, Germany). From the resulting supernatant 30 µL were diluted in 170 µL 0.1% formic acid in a 96-well plate (Greiner, Frickenhausen, Germany).

An API 6500 mass spectrometer (ABSciex, Darmstadt, Germany) was equipped with an Agilent 1290 LC system, a CTC autosampler and a Kinetex 30 x 2.1 mm, 2.6 µm C18 LC column (Phenomenex, Aschaffenburg, Germany). The MS conditions were set as follows: Positive mode, 400 °C source heating, curtain gas = 40, gas 1 = 50, gas 2 = 50, a capillary voltage of 5000 V. The following MS transitions were recorded: EX 7123: 473.3/256.2, DP = 81, CE = 19; internal standard: 453.0/275.0, DP = 91, CE = 29. Solvent A consisted of 0.1% aqueous formic

acid and solvent B of 0.1% formic acid in 50% acetonitrile: 50% methanol. The gradient started at 90% solvent A, which increased within 2.6 min to 5%. After 0.7 min solvent A was set to 90% for re-equilibration. The flow rate was set to 0.400 mL/min and the injection volume was 20 µL.

3 Results and Discussion

In order to enable delivery of an API directly into the hepatic tissue, a number of nanoparticle properties is required. Properties most important for an effective formulation are particle size and uniform size distribution, surface charge, drug load and drug release profile. Therefore, the manufacturing parameters are optimized with regard to the above-mentioned properties and extensively characterized, as to obtain an applicable nanoparticulate formulation.

3.1 Identification and validation of suitable manufacturing methodology

Initially, the establishment of a suitable manufacturing method was necessary for producing the PLGA-based nanoparticles. Based on previous in-house studies, single emulsion evaporation and microfluidic mixing were identified for robust particle preparation (Chapter II). In order to determine the optimal manufacturing method for liver targeting, both procedures were compared with regard to resulting nanoparticle size and size distribution. These initial experiments were performed with different concentrations of polymers without API to produce placebo particles and reduce the compound consumption.

In Figure 1 the Z-average and PDI values of the nanoparticles, manufactured with both techniques, are shown.

1

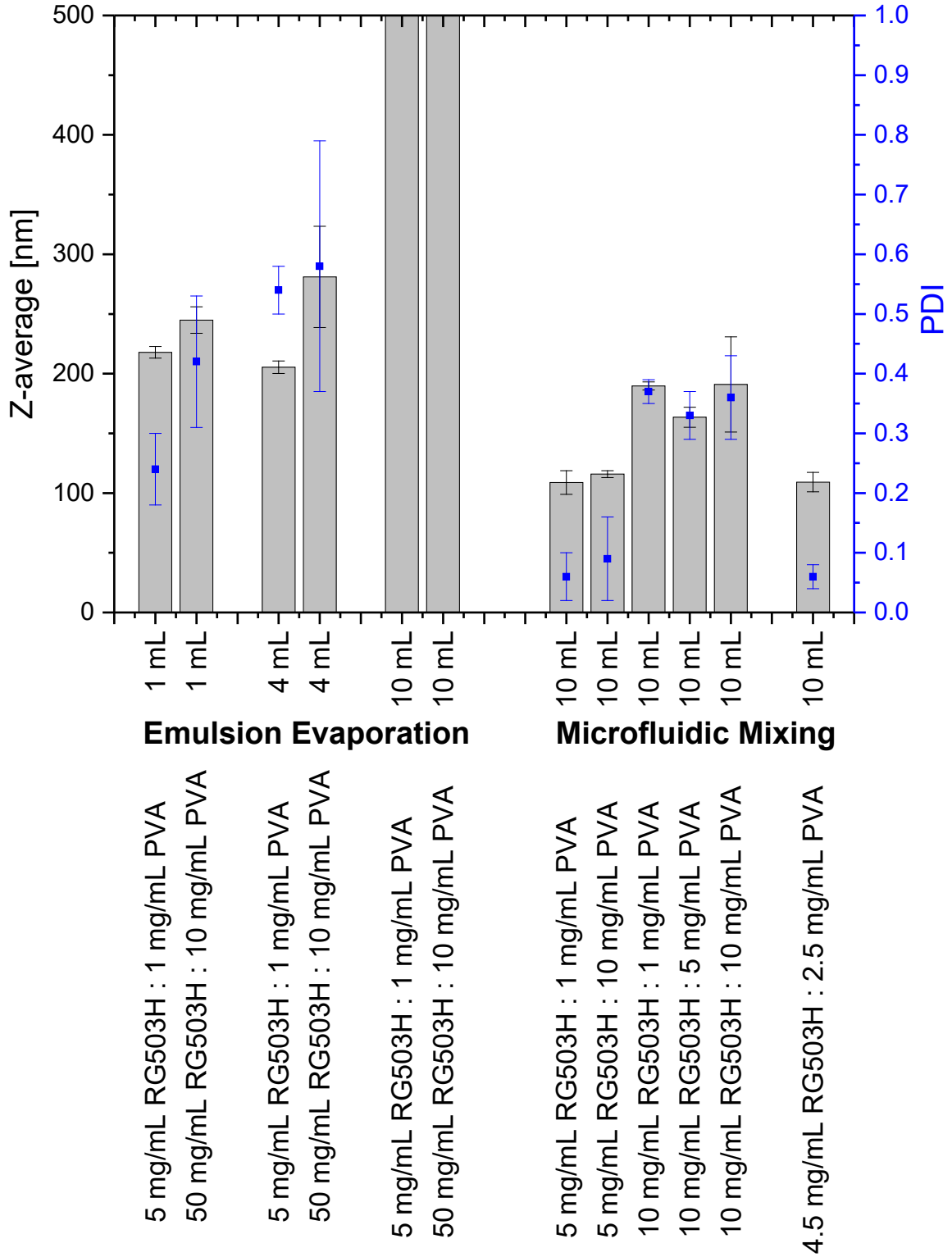

Figure 1 Influence of RG503H concentration, PVA concentration, and produced volume on Z-average and PDI for single emulsion evaporation (left) and microfluidic mixing method (right).

Both methods allow for production of nanoparticles in the desired size range. With single emulsion evaporation method, a Z-average between 200 and 300 nm was achieved, whereas microfluidic mixing generated approximately 100-200 nm particles. The reduction of particle size when using microfluidic mixing compared to single emulsion evaporation has been described in the literature as a result of mixing solutions under laminar flow conditions, ensuring controlled precipitation[20].

A higher relative amount of polymers (PVA, as well as PLGA) leads to a particle size growth from approximately 110 to 190 nm with microfluidic mixing and 220 to 280 nm with single emulsion evaporation. The influence of polymer concentration on particle size has been precedent for other PLGA-based nanoparticles [20, 21]. Fessi, Puisieux [22] attributed this behavior to the Marangoni effect occurring during nanoprecipitation, predicting that the concentration of the polymers plays an influential role for nanoparticle properties.

Another difference between both manufacturing methods is the amount of formulation product yield. As evident from Figure 1, a high volume of nanoparticle suspension of 10 mL was reproducibly obtained utilizing microfluidic mixing, whereas agglomerations were observed when producing 10 mL of formulation with single emulsion evaporation, with comparable concentrations. Further optimization of the single emulsion evaporation method might have prevented agglomeration, however it was shown that microfluidic mixing allows for manufacturing of larger batches in an easy and reproducible manner and was chosen as an optimal procedure [23]. Additionally, microfluidic mixing showed an overall smaller PDI compared to single emulsion evaporation, indicating a more monodisperse particle size distribution. Another advantage in case of the industrial pharmaceutical research, is the possibility of scaling-up the manufacturing simply by increasing the number of parallel mixing-chambers [24].

Keeping with the discussion above, microfluidic mixing was used and further optimized in the subsequent steps. The nanoparticulate formulation obtained from 4.5 mg/mL RG503H and 2.5 mg/mL PVA achieved a suitable Z-average of 109 nm and a very low PDI of 0.06. Therefore, subsequent approaches were based on nanoparticles manufactured with those parameters.

After determination of a suitable manufacturing method, further influential parameters were investigated.

3.2 Formulation Optimization

3.2.1 Addition of PLGA-PEG

For i.v. administration, the nanoparticles have to be protected from the immune system. Immobilization of PEG on a surface (PEGylation) can shield nanoparticles from aggregation, opsonization, and phagocytosis [25, 26]. Furthermore, especially Kuppfer Cells (specialized macrophages located in the liver), are known to phagocytize non-PEGylated nanoparticles [27, 28]. These macrophages are mainly located on the walls of the liver sinusoids and might prevent nanoparticles from reaching the space of disse where the targeted stellate cells are situated [16].

Therefore, PLGA-PEG block copolymer was added to the PLGA solution in a ratio of 1:10 (+ 0.5 mg/mL DLG 50-6P) and 1:20 (+ 0.25 mg/mL DLG 50-6P). As described by Rezvantalab and Keshavarz Moraveji [23], microfluidic mixing utilizing PLGA-PEG results in controlled precipitation in the aqueous phase. Herby, the hydrophobic PLGA-block aligns to the hydrophobic PLGA-core, whereas the hydrophilic PEG-block is facing the aqueous phase. This allows the desired shielding of the nanoparticle by PEG-chains.

In order to determine how addition of PLGA-PEG affects the PLGA-based nanoparticulate formulation, Z-average and PDI of the PEGylated nanoparticles were measured.

As shown in Figure 2 A, a slight increase in Z-average and PDI in comparison to the pure PLGA formulation was observed. This increase might be explained with the additional PEG-coating on the particle surface, contributing to a more voluminous nanoparticle. Nevertheless, the particle sizes were still in a suitable range, and further optimization approaches were performed with the PEGylated particles. Based on the low PDI of 0.19 for the 1:10 DLG 50-6P : RG503H ratio formulation, these parameters were chosen for all following procedures .

3.2.2 Influence of API concentration

For an effective formulation, the nanoparticles have to be loaded with a high amount of the proposed API. In literature, a drug load between 0.9 and 3.8% are described for similar PLGA-PEG based nanoparticles [29-32]. Therefore, a FAS inhibitor (FASi) was introduced to the manufacturing procedure in different concentrations (0.5 mg/mL – 2.5 mg/mL), aiming for a

drug load at a minimum of 1%. Consequently, drug loading (Figure 2 B) was measured in addition to Z-average and PDI analysis (Figure 2 A).

A

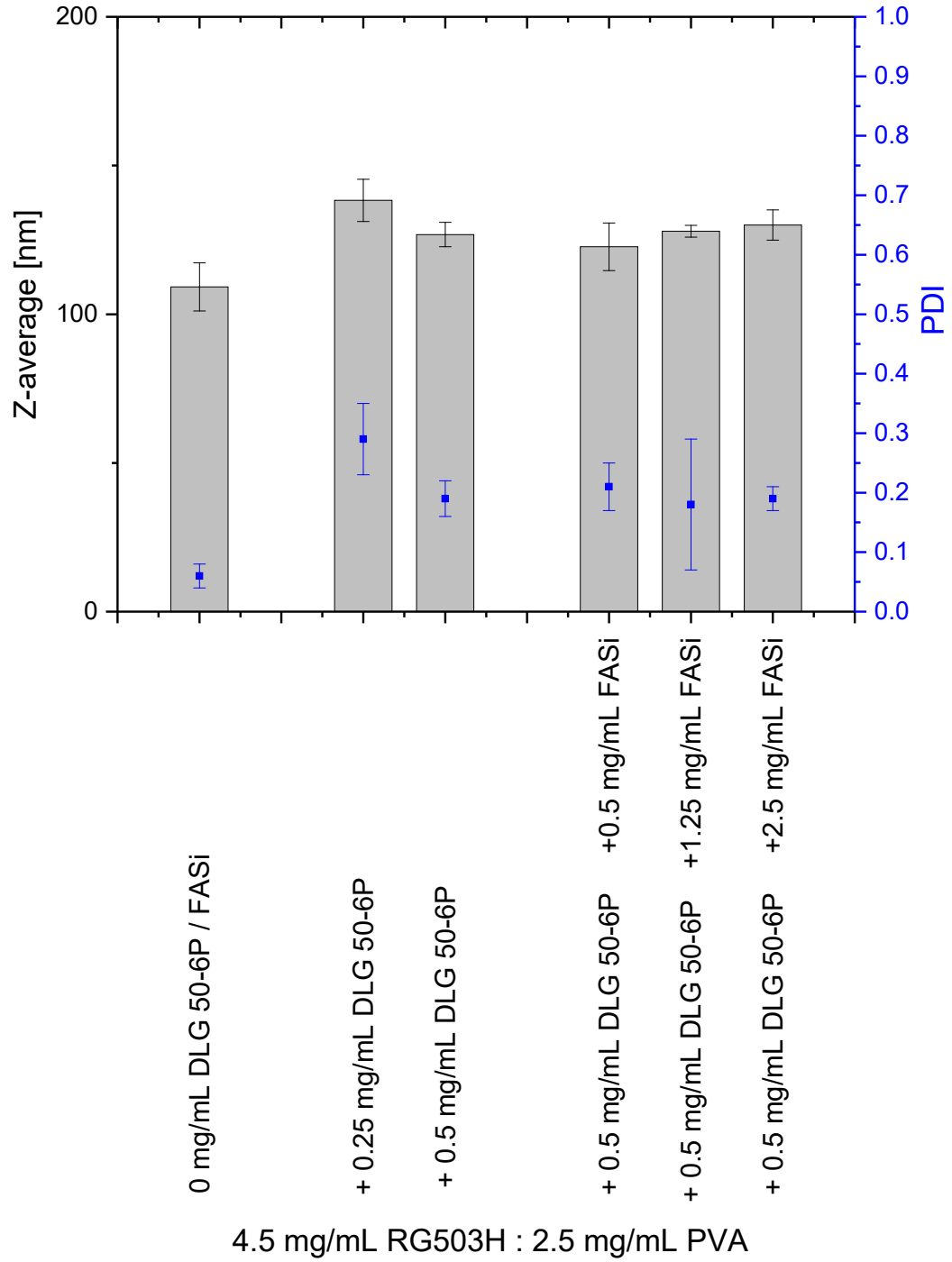

B

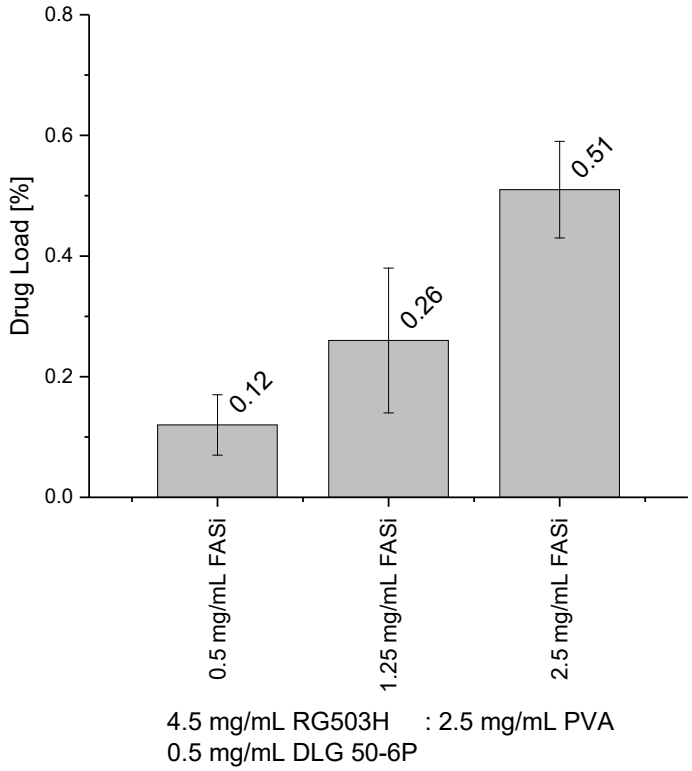

Figure 2 Influence of API amount (0.5 mg/mL – 2.5 mg/mL) and PLGA : PLGA-PEG ratio (1:10, 1:20) on Z-average, PDI (A) and drug load (B).

The Z-Average and PDI of all formulations were in a similar range of 120 – 130 nm and it leads to reason, that loading the nanoparticles with an API does not alter the particle size significantly. Noticeable differences were observed with regard to drug loading. As expected, a higher amount of API leads to an increased drug loading. Here, the encapsulation efficiency remains constant, which might be explained by the high loading capacity of the nanoparticles. By applying an API concentration of 2.5 mg/mL, a maximum drug loading of 0.51% was achieved. Since a higher drug loading was desired for an *in vivo* administration, further approaches were evaluated to increase the drug loading. One possibility to achieve a higher absolute drug loading is the use of higher amounts of API**.** However, owing to the limited availability of the compound and the constant encapsulation efficiency, independent of the API feed, other approaches to enhance the drug load were examined.

3.2.3 Influence of PVA concentration

The amphiphilic polymer PLGA-PEG acts as an emulsifier and stabilizer for the nanoparticles. Therefore, less amount of the originally used emulsifier, PVA might be necessary to form stable particles. It was rationalized that a reduced PVA concentration relative to the API amount would be sufficient and aid an overall higher drug load.

Therefore, the influence of reduced PVA concentration (0 –2.5 mg/mL) on Z-Average, PDI, zeta potential and drug load were investigated.

A

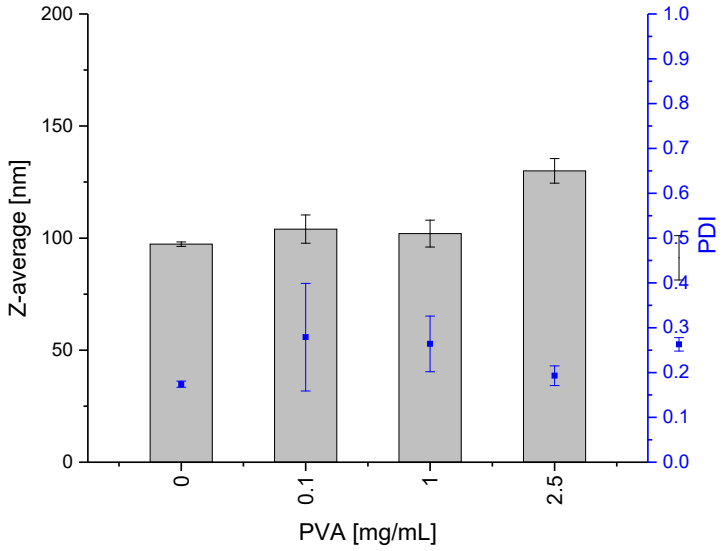

B

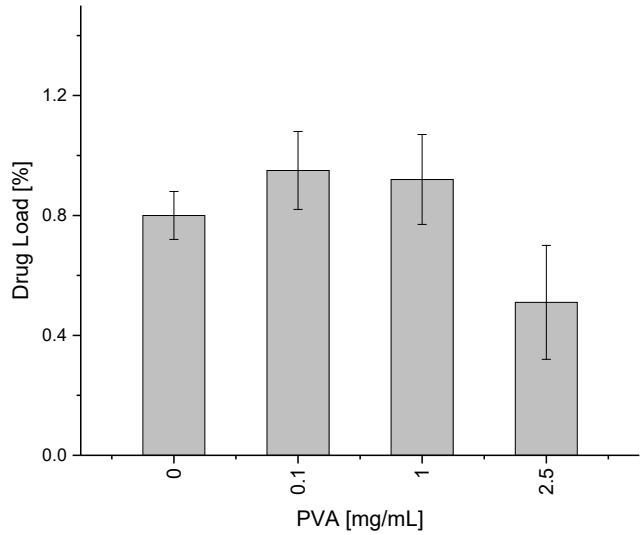

C

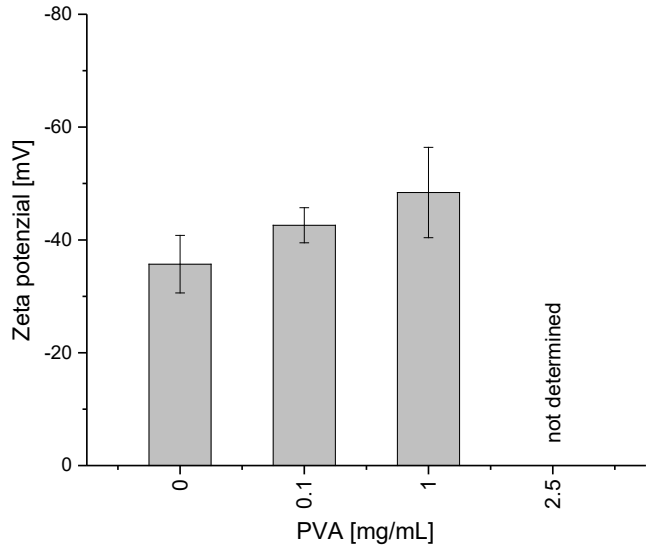

Figure 3 Influence of PVA concentration on Z-average and PDI (A), drug load (B) and zeta potential (C).

As shown in Figure 3 A, Z-Average decreases slightly with a lower amount of PVA, but is still in a suitable range of approximately 100 nm. A higher drug loading of nearly 1% was achieved for all PVA concentration lower than 2.5 mg/mL (Figure 3 B). Therefore, PVA concentrations up to 1 mg/mL were further investigated.

In order to identify the most stable particles, zeta potential measurements were conducted. Nanoparticles with a high value zeta potential are electrically stabilized due to repulsion between similarly charged particles. According to Kumar and Dixit [33] a zeta potential between (positive or negative) 40 and 60 mV indicates good stability. Since the nanoparticle formulation with 1 mg/mL PVA achieved the highest zeta potential of -48.4 (Figure 3 C), it was rationalized that with these parameters, the most stable nanoparticles with a comparably high drug load can be achieved, and this formulation was further analyzed.

3.2.4 *In vitro* drug release profile

One of the most important properties for a successful targeted delivery formulation, is the capability of reaching the target without significant loss of API from the nanoparticles. After i.v. injection, the nanoparticles are transported into the hepatic tissue in a matter of minutes [34, 35]. Nevertheless, an extended *in vitro* total release time is desired, since preparation and administration of the nanoparticles might take a considerable amount of time with the worst-

case scenario being the API already released before the nanoparticulate formulation is administered.

Measuring the *in vitro* drug release profile is a suitable indicator to estimate the behavior of the nanoparticles. Therefore, the API release from the nanoparticles in PBS buffer was analyzed for 4 hours as shown in Figure 4.

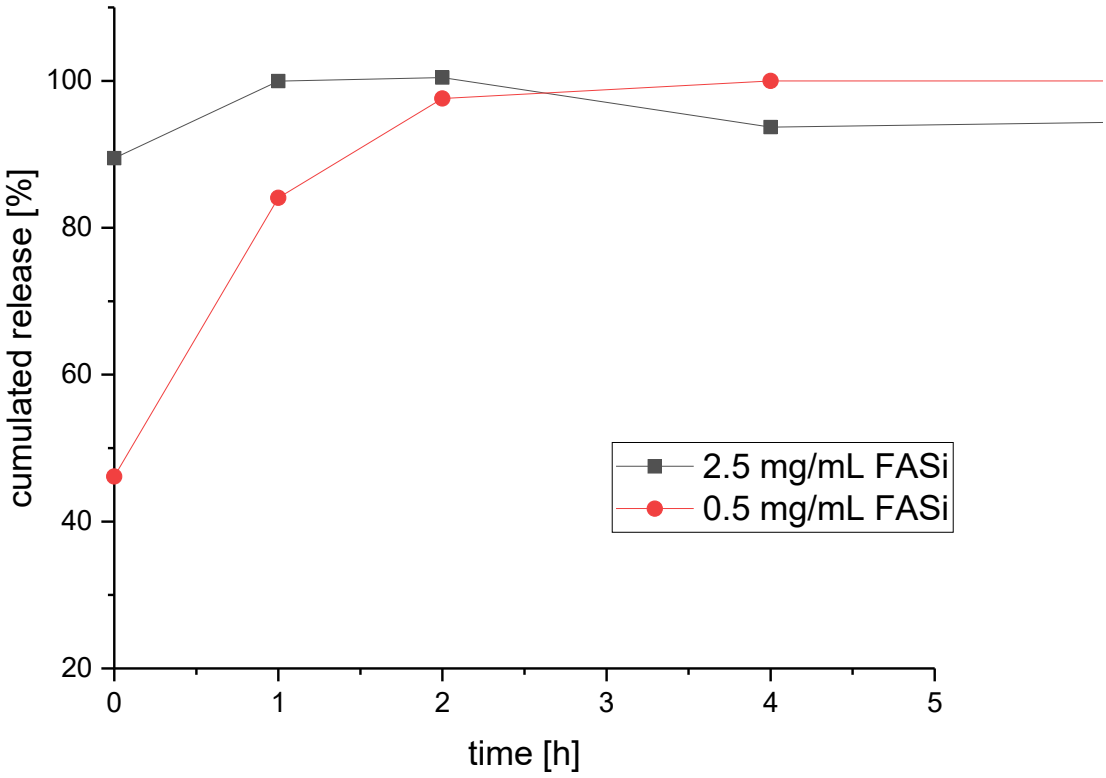

Figure 4 *In vitro* drug release profile of 2.5 mg/mL and 0.5 mg/mL FASi formulation.

The *in vitro* release profile for the 2.5 mg/mL FASi formulation shows an almost immediate release of the drug from the developed nanoparticles. Over 90% of the API was released at the start of the measurement and after 1 hour, nearly 100% of the FASi was detected.

It was assumed that a high amount of the API wasn't encapsulated in a stable manner. Hereby, the drug release profile is mainly directed by dissolution of the API and not the release from the particle. This initial burst effect has been widely described for PLGA-based formulations previously [36]. One possibility to reduce the initial burst is lowering the amount of API in the formulation.

Thus, the API concentration was reduced to 0.5 mg/mL in a next step and the resulting nanoparticles were characterized. As expected, shown in Figure 5 A, Z-average remained at a constant level of about 100 nm and PDI was reduced to < 0.2. As anticipated, due to the lower amount of API applied, a drug loading of 0.44% was achieved (Figure 5 B).

The effect of the reduced API concentration on the *in vitro* release profile is illustrated in Figure 5 C. Here, a reduced initial burst of under 50% and an extended drug release of up to 2 hours was observed. A similar influence of the drug loading on the *in vitro* release profile for PLGA-based formulations was shown in previous work [37]. In order to further improve the release and loading properties of the nanoparticles, different PLGA types are explored [38].

3.2.4.1 *Variants of PLGA*

In preceding work it was demonstrated, that a more hydrophobic PLGA with a higher lactic acid (LA)-content (RG752H) could increase drug loading and extend the release profile for microparticulate formulations [37]. In order to examine if these findings are also transferable to this study, nanoparticles composed of 3 different PLGA-types, ranging from relatively fast release (503H) to relatively slow release (752H) were manufactured and tested regarding their size, drug loading, and most importantly release profile.

A

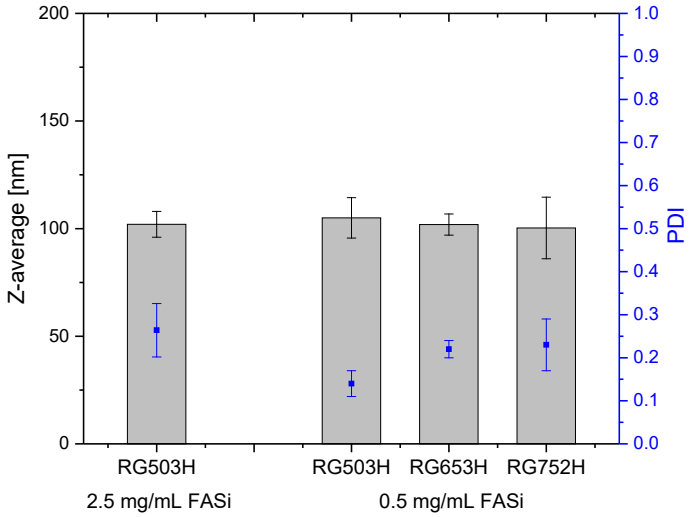

B

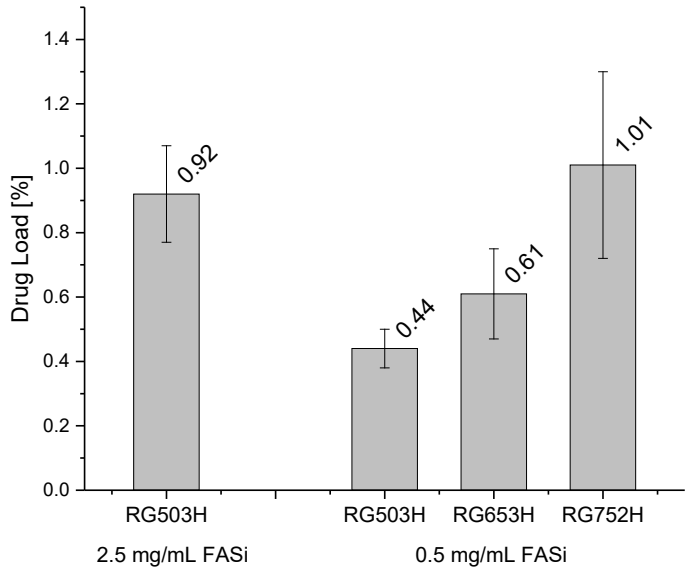

C

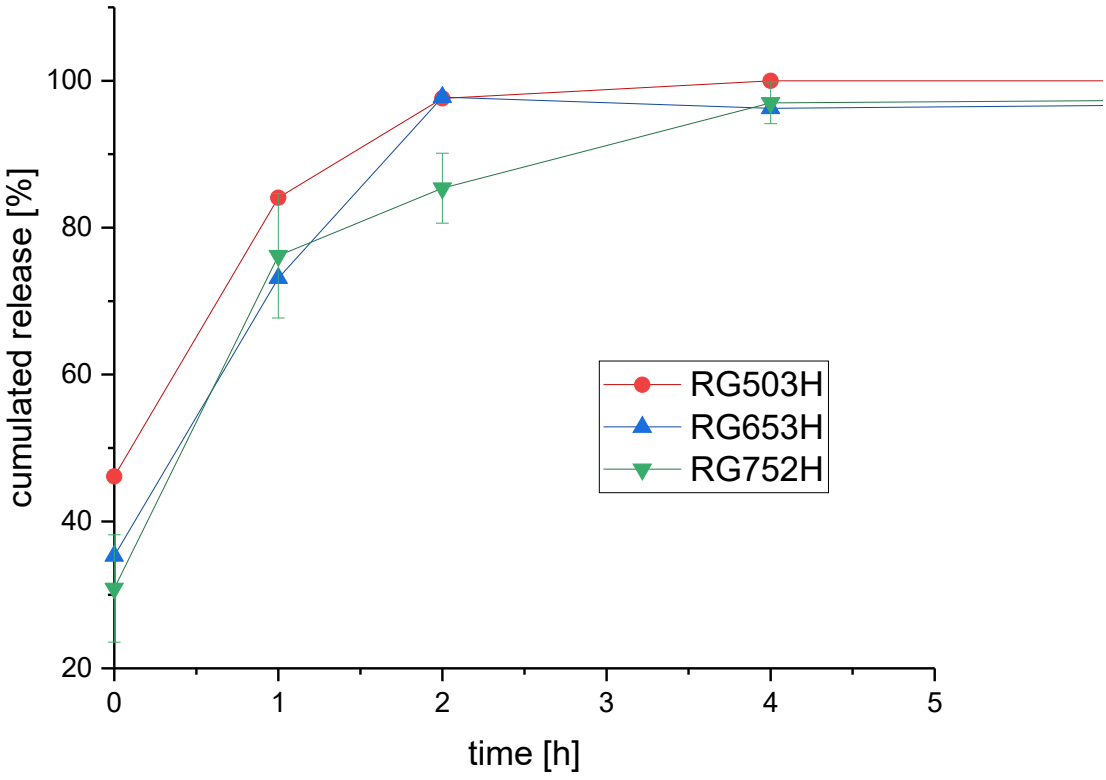

Figure 5 Influence of PLGA type (RG503H, RG653H, and RG752H) and FASi concentration (0.5 mg/mL and 2.5 mg/mL FASi) on Z-Average, PDI (A), drug load (B) and *in vitro* drug release profile (C).

Changing the polymer type only slightly affects particle size, as shown in Figure 5 C. With all formulations, a Z-average of approximately 100 nm and a PDI of under 0.3 was achieved.

As expected, PLGA with a higher amount of LA (RG752H, RG653H) further extended the drug release time. By utilizing the polymer with the highest LA ratio (RG752H), the initial burst at the start of the measurement was reduced to 30%. After 1 and 2 hours, only 76 and 85% of the API were release, respectively, compared to nearly 100% for both other formulations after 2 hours (Figure 5 C). Additionally, utilizing RG752H doubled the drug loading to 1% compared to 0.44% resulting with RG503H (Figure 5 B).

Both extended release and increased encapsulation might be explained with the more hydrophobic nature of the RG752H polymer, which leads to a higher DL and slower release for hydrophobic compounds. As mentioned previously, similar effects were noticed in previous in-house work, as well as reported in literature [22].

With the described optimization steps, an applicable formulation for hepatic targeting was successfully developed. However, despite the utilized FAS inhibitor ACC inhibitors are in the focus for NASH treatment whereby a delivery into the liver tissue is highly desired. It was assumed that the developed optimized manufacturing and screening method could be transferred to other compounds.

3.3 Use of an alternative API

A molecule from the ACC inhibitor (ACCi) class forms another potential candidate to treat NASH. Similar to FASi, systemic administration of the free API leads to adverse effects, and delivery into hepatic tissue is required. In the previous part, a suitable nanoparticulate formulation was developed for the FAS inhibitor molecule. Due to similar physico-chemical properties of both APIs (Table 1) it was suspected, that the manufacturing procedure can be applied to the new compound, and ACCi-loaded nanoparticles were manufactured with the same parameters.

Table 1 Structural formula and physicochemical parameters of FASi and ACCi.

Compound	Structural formula	Molecular weight	Solubility in aqueous media pH 6.8 at 25° C	logP predicted
FASi	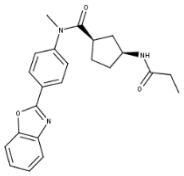	391.5 g/mol	0.035 mg/mL	3.0
ACCi	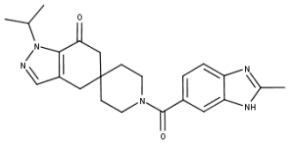	405.5 g/mol	0.077 mg/mL	1.59

Using a different API while applying the same parameters led to a comparable Z-average of 113.5 nm and PDI of 0.08. However, a higher drug loading of 1.4% was observed with the ACC inhibitor. It was assumed, that the higher molecular weight might contribute to the increased drug loading.

Another parameter that can influence the drug loading is the particle size. As described by Kohane [39], larger particles might allow a higher drug loading. It has been shown in the previous part of this work that an increased polymer concentration results in an increased particle size. Therefore, the PLGA/PLGA-PEG and PVA concentration were doubled in the next step. In order to keep the drug loading high, the API concentration was doubled as well.

As expected, the particle size was increased to 147 nm with a PDI of 0.21. Additionally, a drug loading of nearly 2% was achieved (Table 2). A similar drug loading – between 0.9 and 3.8% – are described for PLGA-PEG based nanoparticles of comparable size in literature as well [29-32].

Due to the high drug loading and suitable particle size, this formulation was considered the most promising for an *in vivo* proof of concept study. Therefore, further experiments were performed with nanoparticles manufactured by the established parameters, shown in Figure 6.

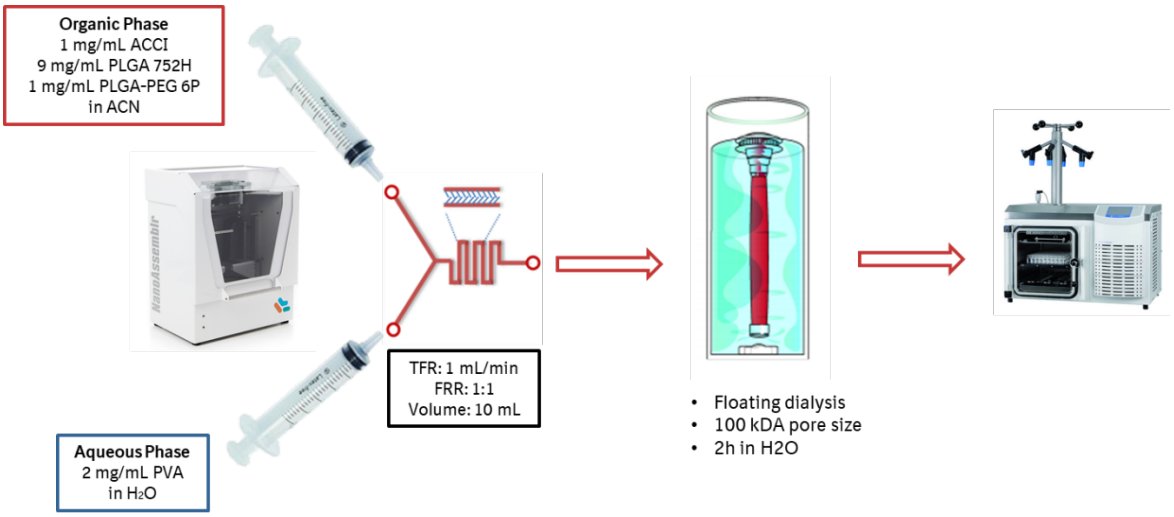

Figure 6 Graphical representation of manufacturing method for final nanoparticulate formulation.

3.4 Lyophilization

The hydrolytic degradation of PLGA in aqueous environments during short storage period is one of the main problems that limit the use of PLGA-based nanoparticles. In order to enhance the storage stability, the water contained in the formulation has to be removed [40]. Lyophilization (or freeze-drying) is one of the milder procedures commonly utilized for this purpose.

The most significant complication that can occur during freeze-drying is agglomeration of the nanoparticles due to the considerable stress during the process [41]. This effect was also observed in this work, when using a default lyophilization procedure. Therefore, an optimized freeze-drying method had to be developed.

As described in literature, addition of cryoprotectants such as glucose, sorbitol and trehalose can prevent agglomeration [42]. According to Alkilany, Abulateefeh [43] cryoprotectants form an amorphous glassy matrix that inhibits the mobility and thus agglomeration of the nanoparticles. Since Holzer, Vogel [44] demonstrated improved particle integrity utilizing trehalose, the influence of various amounts of this cryoprotectant on particle agglomeration

were tested. Additionally, the parameters for primary and secondary drying were optimized in order to accelerate the procedure (see Materials and Methods).

Addition of 0.0 to 1.25% trehalose to the nanoparticulate formulation was not sufficient to prevent agglomeration; large agglomerates were detected upon resuspension. When 2.5% trehalose was applied, the freeze-dried samples did not show any sign of agglomeration. The freeze-dried cakes were white and easily resuspendable by manual shaking, showing no visible agglomerates. Additionally, only a minimal particle size increase after lyophilization and redispersion from 147 to 160 nm was detected with DLS. According to these data, optimal lyophilized nanoparticles were obtained, suggesting that the utilized cryoprotectant and freeze-drying procedure allows preservation of the nanoparticulate formulation.

3.5 Characterization of the final formulation

Prior to the proof of concept *in vivo* study, the established nanoparticulate formulation was fully characterized. A drug loading of 1.93%, particle size of 160.7 nm, zeta potential of -16 mV and a Tg of 51.2 °C were initially determined, as shown in Table 2.

Table 2 Drug load, Z-average, PDI, glass transition temperature and zeta potential of final formulation.

Nanoparticle characterization	
Drug load	1.93 ± 0.15%
Z-Average	160.7 ± 10.6 nm
PDI	0.24 ± 0.06
Glas transition	51.2 °C
Zeta potential	-16.0 ± 3.8 mV

A Particle size distribution

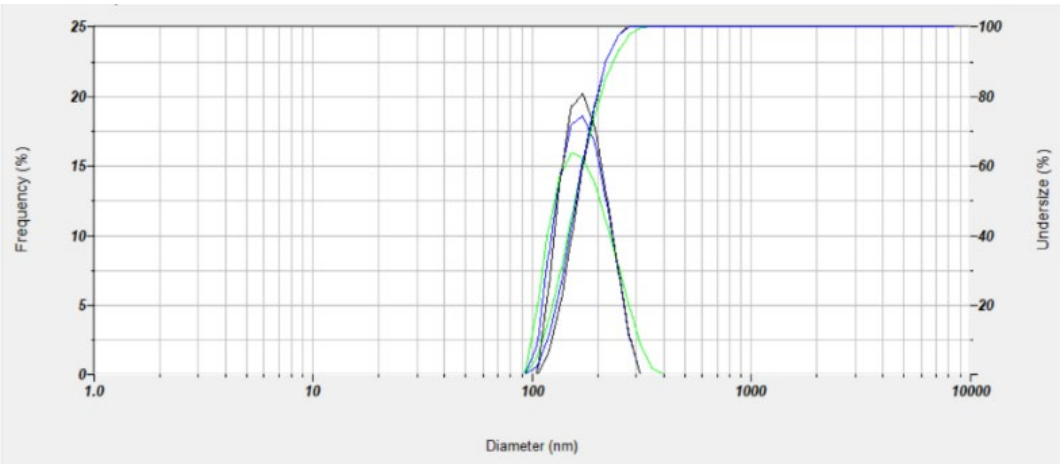

B TEM-pictures

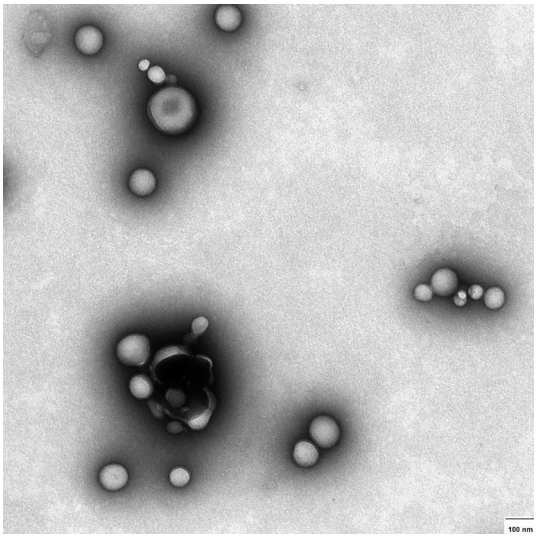

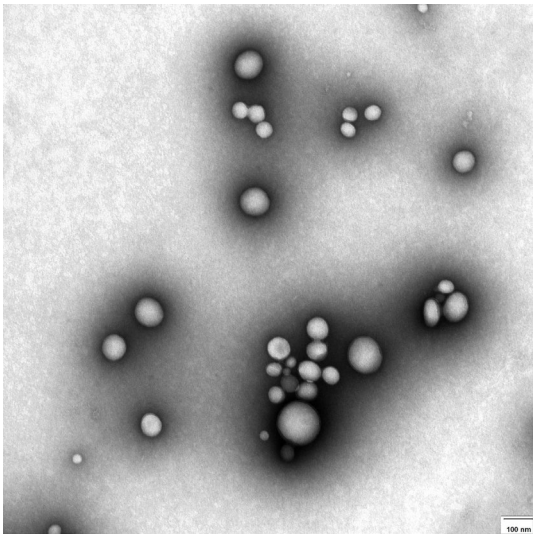

C Zeta potential

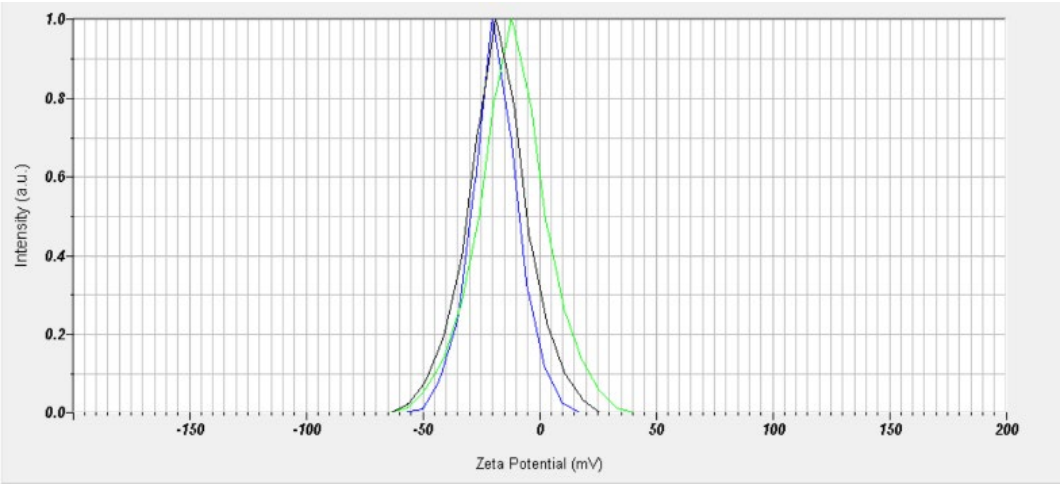

D MDSC thermograph

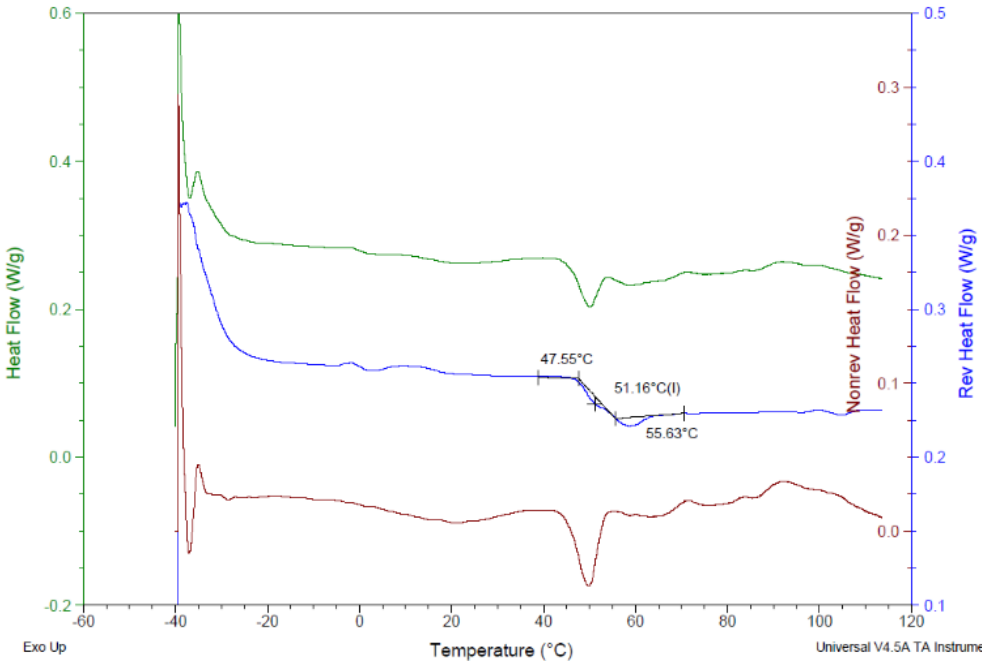

E *In vitro* drug release profile

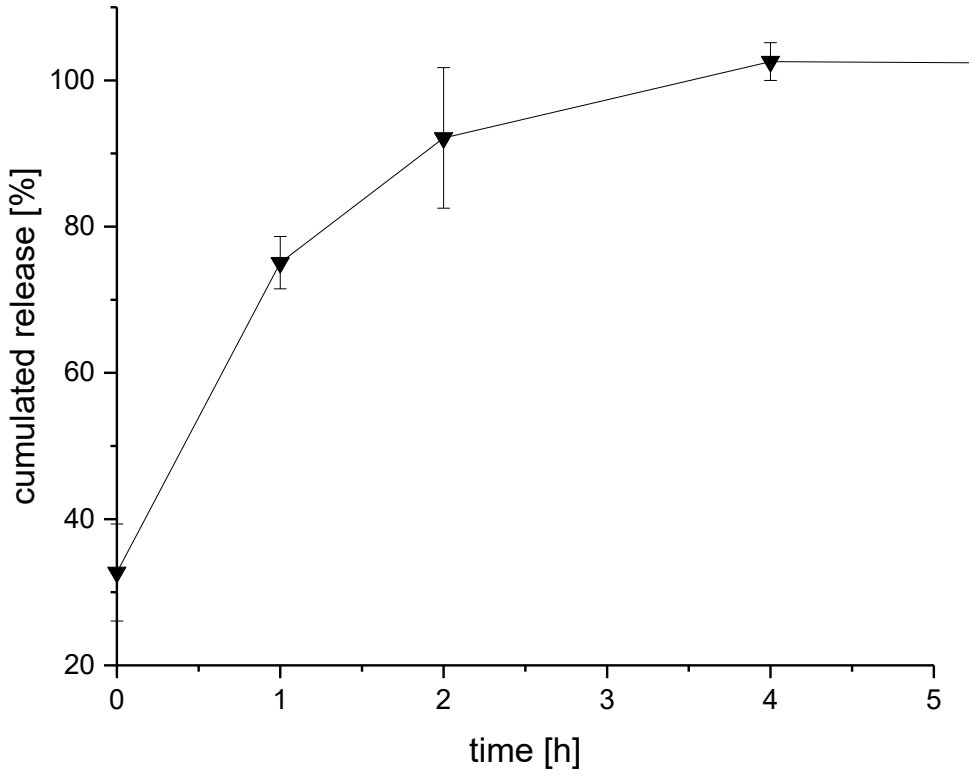

Figure 7 Characterization of the final formulation: Particle size distribution (A), TEM-pictures (B), Zeta potential (C), MDSC thermograph (D) and *in vitro* drug release profile (E).

3.5.1 Particle size and Morphology

In order to confirm the DLS results and to visualize the particle morphology, TEM images of the nanoparticles were acquired.

In Figure 7 B nanoparticles after lyophilization are demonstrated. In all pictures, nanoparticles are clearly visible, and show spherical structures. Comparable results are described by other authors, who also obtained spherical nanoparticles with a similar particle size [44-46]. However, the particle diameter appears to be smaller than the Z-average obtained from DLS measurement (Figure 7 A). This might be induced to some extent by the sample preparation procedure, which may have caused shrinking of the air-dried particles. Additionally, this type of discrepancy is not uncommon between DLS and microscopical data. DLS determines the hydrodynamic diameter of a particle and weights the size distribution differently, overrating larger particles due to the stronger scattered light intensity [47]. Therefore, bigger particles are given more weight, and the Z-average appears to be larger than the particles observed via TEM.

3.5.2 Glass transition temperature

Another defining parameter for polymeric nanoparticles is the glass transition temperature (Tg). A Tg lower than normal body temperature (37 °C) can alter the nanoparticle behavior after administration, since nanoparticles will not remain in their solid, “glassy” state but transition into a viscous or rubbery state during *in vivo* experiments**.** According to the PLGA supplier, the RG752H has a Tg between 42 and 46 °C. However, it cannot be ruled out, that the manufacturing process and additives such as trehalose affects the Tg of the nanoparticles and therefore Tg of the final formulation was measured. Hereby a Tg of 51 °C was detected, and it can be assumed, that under normal physiological condition, glass transition will not occur (Figure 7 D). The increased Tg might be explained by the addition of other excipients including the cryoprotectant. A similar effect was observed by Holzer, Vogel [44], who measured a Tg increase from 40.1 °C to 60.9 °C after addition of 3% trehalose.

3.5.3 Zeta potential

As described previously, zeta potential measurement is a good indicator of particle stability. The developed formulation has a zeta potential of -16.0 mV (Figure 7 C) and according to Kumar and Dixit [33] only incipient stability can be expected. However, in various publications

similar zeta potentials between -8.0 and -16 mV [46, 48, 49] were described for PLGA-PEG coated nanoparticles depending on the suspension medium. Since the PEG-coating also stabilizes the nanoparticles, it was assumed, that the achieved results are sufficient for a stable formulation cumulatively.

3.5.4 *In vitro* drug release profile

Finally, the drug release profile of the freeze-dried nanoparticles was investigated, as shown in Figure 7 C. Similar to the FASi-nanoparticles, a low initial burst of only 33% was achieved. After 1 and 2 hours, 75% and 92% of the API were released, and 100% release was observed after 4 hours (Figure 7 E).

A wide range of different *in vitro* release rates for nanoparticulate formulations, ranging from a few hours [50-52] to several days [49, 53, 54] are reported in the literature. Similar to the drug loading, extension of the release time is highly dependent on the type of API and the fabrication method. Additionally, the differences might also be explained with the utilized methods to quantify the release. Most published reports apply the dynamic dialysis method, where the release from the nanoparticles into the dialysis chamber is followed by diffusion across the dialysis membrane. The API transport across the dialysis membrane leads to a slower overall apparent release rate which may lead to the flawed conclusion that the nanoparticles will provide a more extended release [55]. Therefore, it was assumed, that the utilized method (despite the fast release) has a better transferability for upcoming *in vivo* studies.

3.6 *In vivo* PK study

In order to investigate how these elaborate characterization results translate into *in vivo* conditions, a PK study was conducted. The nanoparticulate suspensions and a control solution of API in 0.9% NaCl were injected i.v., and the plasma profile was measured for 8 hours. The dose normalized mean plasma concentrations versus time profiles for the first two hours are illustrated in Figure 8.

Directly upon administration, the API plasma concentration of the nanoparticulate formulation is nearly 3-fold lower than that of the NaCl control. Up to 30 min, the measured plasma concentrations observed with API/NaCl control were higher than those obtained after

treatment with the nanoparticulate formulation. AUD and AUC (0-Inf) after administration of the control NaCl formulation is nearly doubled compared to the nanoparticle formulation.

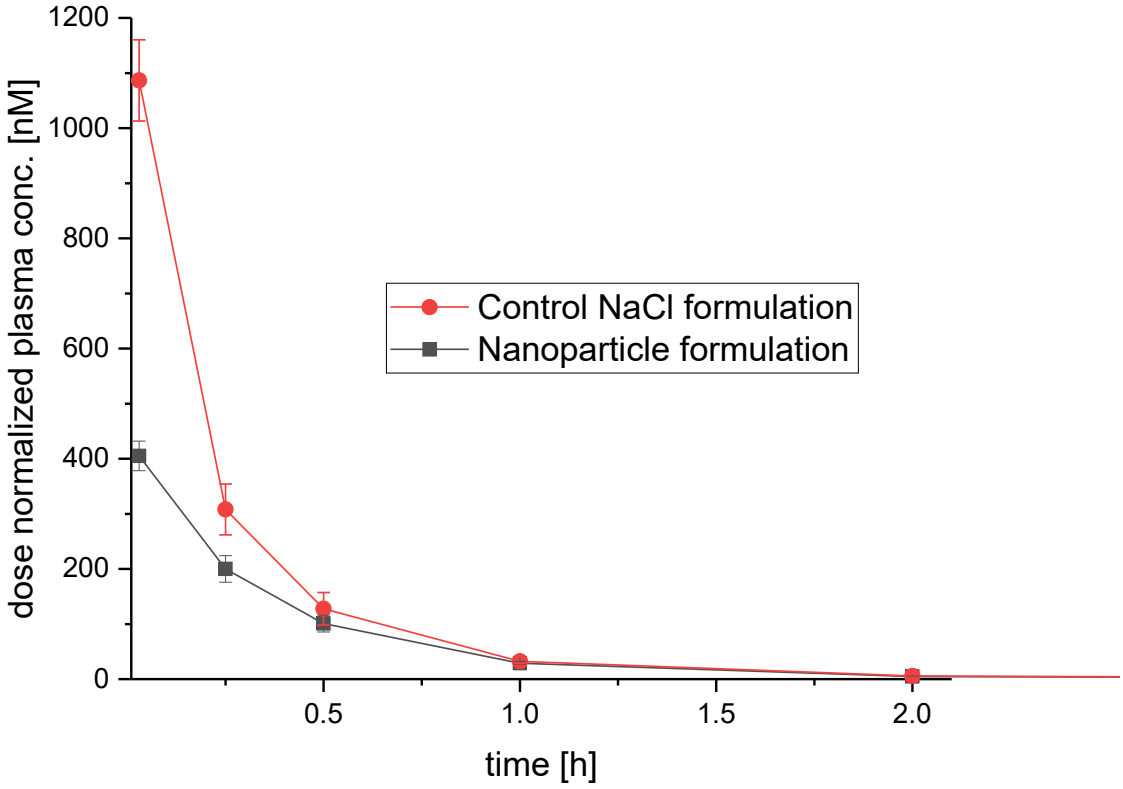

Formulation	AUD [nM*h]	AUC(0-Inf) [nM*h]	Clearance [mL/min/kg]	MRT [h]
Control NaCl	276 ± 51.6	277 ± 51.2	61 ± 10.7	0.32 ± 0.06
Nanoparticle	159 ± 19.4	160 ± 19.4	122 ± 13.4	0.45 ± 0.04

Figure 8 Dose normalized PK profile and parameters after i.v. administration of control NaCl formulation and final nanoparticulate formulation.

This reduced API concentration in the plasma might be explained with the passive accumulation of the nanoparticles in the hepatic tissue. As described previously, nanoparticles tend to accumulate in the space of disse due to fenestration in the liver sinusoids [16]. Ideally

the API remains in the nanoparticles during circulation and is than mainly released after its delivery into the liver tissue.

The minimal amount of ACCi detected in the plasma might additionally be caused by a premature drug release within the nanoparticulate formulation, which was also observed in the *in vitro* release study. An overall low systemic bioavailability could, however, bear the benefit of lower systemic side effects.

The delivery of the API into the liver tissue by the developed nanoparticulate formulation, on the other hand, was further endorsed with an additional biodistribution study. Here, concentration of the ACCi in liver and spleen were measured 15 min after administration and compared with plasma concentration.

Table 3 ACCi concentration after i.v. administration of final nanoparticulate formulation in plasma, spleen and liver.

PK properties	
ACCi concentration in plasma:	321 ± 119 nM
ACCi concentration in spleen:	338 ± 180 nM
ACCi concentration in liver:	2986 ± 1193 nM
Spleen : plasma ratio	0.98
Liver : plasma ratio	9.14

As shown in Table 3, similar concentrations of API were found in spleen and plasma. This is in contrast with literature data, where capturing of nanoparticles by splenic macrophages is described [56, 57]. This observation might be explained with the PEGylation of the nanoparticles, leading to a reduced accumulation of the macrophages in the spleen. Compared to spleen and plasma, a 10-fold higher amount of API was detected in the hepatic tissue. It can be assumed, that the nanoparticles were successfully delivered into the hepatic space of disse, where the API is then released.

Similar results, targeting the liver with PLGA-based nanoparticles, are reported in the literature [35, 58-60]. In these studies, Liang, Chen [60] showed an additional increase in liver accumulation of the API when conjugating galactosamine with the nanoparticles. These results might be promising for subsequent optimization of the developed nanoparticulate formulation. In order to enhance the liver uptake galactosylated-PLGA could be utilized in future approaches. Another advantage of nanoparticles for NASH treatment was demonstrated by Lin Ts, Gao [59]. They observed an increased uptake of PLGA-PEG based nanoparticles into fibrotic liver tissue compared to normal liver. Especially in the progressive states of NASH, which is characterized by a highly fibrotic liver, an enhanced accumulation in the liver tissue might offer additional therapeutic benefits.

Consequently, the achieved results strongly indicate the desired hepatic targeting of the API-loaded nanoparticles for the treatment of NASH.

4 Conclusion

In this work, a nanoparticulate formulation targeting hepatic tissue, for delivery of FAS and ACC inhibitors associated with NASH treatment, was developed. An initial formulation was optimized with regard to particle size, zeta potential, drug load and *in vitro* release, until applicable FASi-loaded nanoparticles were obtained. By successfully translating the established manufacturing method and characterization screening to an additional API (ACCi), a general applicability for numerous research compounds can be assumed.

After extensive characterization of the developed formulation, an *in vivo* PK proof of concept study was conducted. The obtained results strongly suggested accumulation of the ACCi-loaded nanoparticles in the hepatic tissue. Herby, adverse reaction of the NASH treatment after systemic administration may be reduced, enhancing efficacy of the drug.

Based on these results, subsequent work will investigate active cell targeting of hepatocytes utilizing manose-6-phosphate decorated nanoparticles, to further optimize the formulation

5 References

1. Oseini, A. M.; Sanyal, A. J., Therapies in non-alcoholic steatohepatitis (NASH). *Liver Int* **2017,** *37 Suppl 1* (Suppl 1), 97-103.
2. Marjot, T.; Moolla, A.; Cobbold, J. F.; Hodson, L.; Tomlinson, J. W., Nonalcoholic Fatty Liver Disease in Adults: Current Concepts in Etiology, Outcomes, and Management. *Endocrine reviews* **2020,** *41* (1).
3. Browning, J. D.; Szczepaniak, L. S.; Dobbins, R.; Nuremberg, P.; Horton, J. D.; Cohen, J. C.; Grundy, S. M.; Hobbs, H. H., Prevalence of hepatic steatosis in an urban population in the United States: impact of ethnicity. *Hepatology (Baltimore, Md.)* **2004,** *40* (6), 1387-95.
4. Williams, C. D.; Stengel, J.; Asike, M. I.; Torres, D. M.; Shaw, J.; Contreras, M.; Landt, C. L.; Harrison, S. A., Prevalence of nonalcoholic fatty liver disease and nonalcoholic steatohepatitis among a largely middle-aged population utilizing ultrasound and liver biopsy: a prospective study. *Gastroenterology* **2011,** *140* (1), 124-31.
5. Pimpin, L.; Cortez-Pinto, H.; Negro, F.; Corbould, E.; Lazarus, J. V.; Webber, L.; Sheron, N., Burden of liver disease in Europe: Epidemiology and analysis of risk factors to identify prevention policies. *J Hepatol* **2018,** *69* (3), 718-735.
6. Puri, P.; Sanyal, A. J., Nonalcoholic fatty liver disease: Definitions, risk factors, and workup. *Clinical Liver Disease* **2012,** *1* (4), 99-103.
7. Younossi, Z.; Anstee, Q. M.; Marietti, M.; Hardy, T.; Henry, L.; Eslam, M.; George, J.; Bugianesi, E., Global burden of NAFLD and NASH: trends, predictions, risk factors and prevention. *Nature reviews. Gastroenterology & hepatology* **2018,** *15* (1), 11-20.
8. Karlas, T.; Wiegand, J.; Berg, T., Gastrointestinal complications of obesity: non-alcoholic fatty liver disease (NAFLD) and its sequelae. *Best practice & research. Clinical endocrinology & metabolism* **2013,** *27* (2), 195-208.
9. Noureddin, M.; Vipani, A.; Bresee, C.; Todo, T.; Kim, I. K.; Alkhouri, N.; Setiawan, V. W.; Tran, T.; Ayoub, W. S.; Lu, S. C.; Klein, A. S.; Sundaram, V.; Nissen, N. N., NASH Leading Cause of Liver Transplant in Women: Updated Analysis of Indications For Liver Transplant and Ethnic and Gender Variances. *The American journal of gastroenterology* **2018,** *113* (11), 1649-1659.
10. Weiss, J.; Rau, M.; Geier, A., Non-alcoholic fatty liver disease: epidemiology, clinical course, investigation, and treatment. *Deutsches Arzteblatt international* **2014,** *111* (26), 447-52.
11. Huang, M. A.; Greenson, J. K.; Chao, C.; Anderson, L.; Peterman, D.; Jacobson, J.; Emick, D.; Lok, A. S.; Conjeevaram, H. S., One-year intense nutritional counseling results in histological improvement in patients with non-alcoholic steatohepatitis: a pilot study. *The American journal of gastroenterology* **2005,** *100* (5), 1072-81.
12. Konerman, M. A.; Jones, J. C.; Harrison, S. A., Pharmacotherapy for NASH: Current and emerging. *J Hepatol* **2018,** *68* (2), 362-375.
13. Paglialunga, S.; Dehn, C. A., Clinical assessment of hepatic de novo lipogenesis in non-alcoholic fatty liver disease. *Lipids Health Dis* **2016,** *15* (1), 159-159.
14. Kim, C. W.; Addy, C.; Kusunoki, J.; Anderson, N. N.; Deja, S.; Fu, X.; Burgess, S. C.; Li, C.; Ruddy, M.; Chakravarthy, M.; Previs, S.; Milstein, S.; Fitzgerald, K.; Kelley, D. E.; Horton, J. D., Acetyl CoA Carboxylase Inhibition Reduces Hepatic Steatosis but Elevates Plasma Triglycerides in Mice and Humans: A Bedside to Bench Investigation. *Cell metabolism* **2017,** *26* (2), 394-406.e6.

15. Zhang, Y. N.; Poon, W.; Tavares, A. J.; McGilvray, I. D.; Chan, W. C. W., Nanoparticle-liver interactions: Cellular uptake and hepatobiliary elimination. *J Control Release* **2016,** *240*, 332-348.
16. Li, L.; Wang, H.; Ong, Z. Y.; Xu, K.; Ee, P. L. R.; Zheng, S.; Hedrick, J. L.; Yang, Y.-Y., Polymer- and lipid-based nanoparticle therapeutics for the treatment of liver diseases. *Nano Today* **2010,** *5* (4), 296-312.
17. Poilil Surendran, S.; George Thomas, R.; Moon, M. J.; Jeong, Y. Y., Nanoparticles for the treatment of liver fibrosis. *Int J Nanomedicine* **2017,** *12*, 6997-7006.
18. Makadia, H. K.; Siegel, S. J., Poly lactic-co-glycolic acid (PLGA) as biodegradable controlled drug delivery carrier. *Polymers* **2011,** *3* (3), 1377-1397.
19. Wang, Y., FDA's regulatory science program for generic PLA/PLGA-based drug products. *American Pharmaceutical Review* **2016,** *20*.
20. Lababidi, N.; Sigal, V.; Koenneke, A.; Schwarzkopf, K.; Manz, A.; Schneider, M., Microfluidics as tool to prepare size-tunable PLGA nanoparticles with high curcumin encapsulation for efficient mucus penetration. *Beilstein Journal of Nanotechnology* **2019,** *10*, 2280-2293.
21. Wagh, V. D.; Apar, D. U., Cyclosporine A Loaded PLGA Nanoparticles for Dry Eye Disease: In Vitro Characterization Studies. *Journal of Nanotechnology* **2014,** *2014*, 683153.
22. Fessi, H.; Puisieux, F.; Devissaguet, J. P.; Ammoury, N.; Benita, S., Nanocapsule formation by interfacial polymer deposition following solvent displacement. *International Journal of Pharmaceutics* **1989,** *55* (1), R1-R4.
23. Rezvantalab, S.; Keshavarz Moraveji, M., Microfluidic assisted synthesis of PLGA drug delivery systems. *RSC Advances* **2019,** *9* (4), 2055-2072.
24. Singh, J.; Ou, K.; Thomas, A.; Garg, S.; Ma, M.; Armstead, A.; Leaver, T. J.; Wild, A. W.; Ip, S.; Taylor, R.; Ramsay, E., A Scalable Microfluidics Platform for the Development of Nanoparticles. *Precision NanoSystems Inc., Vancouver, BC, Canada* **2018**.
25. Suk, J. S.; Xu, Q.; Kim, N.; Hanes, J.; Ensign, L. M., PEGylation as a strategy for improving nanoparticle-based drug and gene delivery. *Advanced drug delivery reviews* **2016,** *99* (Pt A), 28-51.
26. Jokerst, J. V.; Lobovkina, T.; Zare, R. N.; Gambhir, S. S., Nanoparticle PEGylation for imaging and therapy. *Nanomedicine (Lond)* **2011,** *6* (4), 715-728.
27. Sadauskas, E.; Wallin, H.; Stoltenberg, M.; Vogel, U.; Doering, P.; Larsen, A.; Danscher, G., Kupffer cells are central in the removal of nanoparticles from the organism. *Particle and Fibre Toxicology* **2007,** *4* (1), 10.
28. Tavares, A. J.; Poon, W.; Zhang, Y. N.; Dai, Q.; Besla, R.; Ding, D.; Ouyang, B.; Li, A.; Chen, J.; Zheng, G.; Robbins, C.; Chan, W. C. W., Effect of removing Kupffer cells on nanoparticle tumor delivery. *Proc Natl Acad Sci U S A* **2017,** *114* (51), E10871-e10880.
29. Rafiei, P.; Haddadi, A., Docetaxel-loaded PLGA and PLGA-PEG nanoparticles for intravenous application: pharmacokinetics and biodistribution profile. *Int J Nanomedicine* **2017,** *12*, 935-947.
30. Gryparis, E. C.; Hatziapostolou, M.; Papadimitriou, E.; Avgoustakis, K., Anticancer activity of cisplatin-loaded PLGA-mPEG nanoparticles on LNCaP prostate cancer cells. *European Journal of Pharmaceutics and Biopharmaceutics* **2007,** *67* (1), 1-8.
31. Lancheros, R.; Guerrero, C. A.; Godoy-Silva, R. D., Improvement of N-Acetylcysteine Loaded in PLGA Nanoparticles by Nanoprecipitation Method. *Journal of Nanotechnology* **2018,** *2018*.

32. Lee, S.-M.; Park, H.; Yoo, K.-H., Synergistic Cancer Therapeutic Effects of Locally Delivered Drug and Heat Using Multifunctional Nanoparticles. *Advanced Materials* **2010,** *22* (36), 4049-4053.
33. Kumar, A.; Dixit, C. K., 3 - Methods for characterization of nanoparticles. In *Advances in Nanomedicine for the Delivery of Therapeutic Nucleic Acids*, Nimesh, S.; Chandra, R.; Gupta, N., Eds. Woodhead Publishing: 2017; pp 43-58.
34. Quini, C. C.; Próspero, A. G.; Calabresi, M. F. F.; Moretto, G. M.; Zufelato, N.; Krishnan, S.; Pina, D. R.; Oliveira, R. B.; Baffa, O.; Bakuzis, A. F.; Miranda, J. R. A., Real-time liver uptake and biodistribution of magnetic nanoparticles determined by AC biosusceptometry. *Nanomedicine : nanotechnology, biology, and medicine* **2017,** *13* (4), 1519-1529.
35. Hoshyar, N.; Gray, S.; Han, H.; Bao, G., The effect of nanoparticle size on in vivo pharmacokinetics and cellular interaction. *Nanomedicine (Lond)* **2016,** *11* (6), 673-692.
36. Thote, A. J.; Chappell, J. T., Jr.; Gupta, R. B.; Kumar, R., Reduction in the initial-burst release by surface crosslinking of PLGA microparticles containing hydrophilic or hydrophobic drugs. *Drug Dev Ind Pharm* **2005,** *31* (1), 43-57.
37. Strack, P.; Külzer, R.; Sommer, F.; Bretschneider, T.; Merkel, O. M.; Grube, A., A smart approach to enable preclinical studies in pharmaceutical industry: PLGA-based extended release formulation platform for subcutaneous applications. *Drug Development and Industrial Pharmacy* **2020**, 1-11.
38. Han, F. Y.; Thurecht, K. J.; Whittaker, A. K.; Smith, M. T., Bioerodable PLGA-Based Microparticles for Producing Sustained-Release Drug Formulations and Strategies for Improving Drug Loading. *Frontiers in Pharmacology* **2016,** *7* (185).
39. Kohane, D. S., Microparticles and nanoparticles for drug delivery. *Biotechnology and Bioengineering* **2007,** *96* (2), 203-209.
40. Abrego, G.; Alvarado, H. L.; Egea, M. A.; Gonzalez-Mira, E.; Calpena, A. C.; Garcia, M. L., Design of Nanosuspensions and Freeze-Dried PLGA Nanoparticles as a Novel Approach for Ophthalmic Delivery of Pranoprofen. *Journal of Pharmaceutical Sciences* **2014,** *103* (10), 3153-3164.
41. Abdelwahed, W.; Degobert, G.; Stainmesse, S.; Fessi, H., Freeze-drying of nanoparticles: Formulation, process and storage considerations. *Advanced Drug Delivery Reviews* **2006,** *58* (15), 1688-1713.
42. Fonte, P.; Soares, S.; Sousa, F.; Costa, A.; Seabra, V.; Reis, S.; Sarmento, B., Stability study perspective of the effect of freeze-drying using cryoprotectants on the structure of insulin loaded into PLGA nanoparticles. *Biomacromolecules* **2014,** *15* (10), 3753-65.
43. Alkilany, A. M.; Abulateefeh, S. R.; Mills, K. K.; Yaseen, A. I.; Hamaly, M. A.; Alkhatib, H. S.; Aiedeh, K. M.; Stone, J. W., Colloidal stability of citrate and mercaptoacetic acid capped gold nanoparticles upon lyophilization: effect of capping ligand attachment and type of cryoprotectants. *Langmuir : the ACS journal of surfaces and colloids* **2014,** *30* (46), 13799-808.
44. Holzer, M.; Vogel, V.; Mantele, W.; Schwartz, D.; Haase, W.; Langer, K., Physico-chemical characterisation of PLGA nanoparticles after freeze-drying and storage. *Eur J Pharm Biopharm* **2009,** *72* (2), 428-37.
45. Han, J.; Michel, A. R.; Lee, H. S.; Kalscheuer, S.; Wohl, A.; Hoye, T. R.; McCormick, A. V.; Panyam, J.; Macosko, C. W., Nanoparticles Containing High Loads of Paclitaxel-Silicate Prodrugs: Formulation, Drug Release, and Anticancer Efficacy. *Molecular Pharmaceutics* **2015,** *12* (12), 4329-4335.
46. Gholizadeh, S.; Kamps, J. A. A. M.; Hennink, W. E.; Kok, R. J., PLGA-PEG nanoparticles for targeted delivery of the mTOR/PI3kinase inhibitor dactolisib to inflamed endothelium. *International Journal of Pharmaceutics* **2018,** *548* (2), 747-758.

47. Fissan, H.; Ristig, S.; Kaminski, H.; Asbach, C.; Epple, M., Comparison of different characterization methods for nanoparticle dispersions before and after aerosolization. *Analytical Methods* **2014,** *6* (18), 7324-7334.
48. Jia-Gen, W.; Tingting, G.; Hong-Yuan, Z., Preparation and Optimization of PEG-PLGA Loaded with Vincristine Sulfate and its In vitro Release. *Journal of Bioequivalence & Bioavailability* **2011,** *03*.
49. Ramanlal Chaudhari, K.; Kumar, A.; Megraj Khandelwal, V. K.; Ukawala, M.; Manjappa, A. S.; Mishra, A. K.; Monkkonen, J.; Ramachandra Murthy, R. S., Bone metastasis targeting: A novel approach to reach bone using Zoledronate anchored PLGA nanoparticle as carrier system loaded with Docetaxel. *J. Control. Release* **2012,** *158* (3), 470-478.
50. Günday Türeli, N.; Torge, A.; Juntke, J.; Schwarz, B. C.; Schneider-Daum, N.; Türeli, A. E.; Lehr, C.-M.; Schneider, M., Ciprofloxacin-loaded PLGA nanoparticles against cystic fibrosis P. aeruginosa lung infections. *European Journal of Pharmaceutics and Biopharmaceutics* **2017,** *117*, 363-371.
51. Öztürk, A. A.; Namlı, İ.; Güleç, K.; Kıyan, H. T., Diclofenac sodium loaded PLGA nanoparticles for inflammatory diseases with high anti-inflammatory properties at low dose: Formulation, characterization and in vivo HET-CAM analysis. *Microvascular Research* **2020,** *130*, 103991.
52. Babos, G.; Biró, E.; Meiczinger, M.; Feczkó, T., Dual Drug Delivery of Sorafenib and Doxorubicin from PLGA and PEG-PLGA Polymeric Nanoparticles. *Polymers* **2018,** *10* (8), 895.
53. Yoo, H. S.; Park, T. G., Biodegradable polymeric micelles composed of doxorubicin conjugated PLGA–PEG block copolymer. *J. Control. Release* **2001,** *70* (1), 63-70.
54. Piazza, J.; Hoare, T.; Molinaro, L.; Terpstra, K.; Bhandari, J.; Selvaganapathy, P. R.; Gupta, B.; Mishra, R. K., Haloperidol-loaded intranasally administered lectin functionalized poly(ethylene glycol)–block-poly(d,l)-lactic-co-glycolic acid (PEG–PLGA) nanoparticles for the treatment of schizophrenia. *European Journal of Pharmaceutics and Biopharmaceutics* **2014,** *87* (1), 30-39.
55. Modi, S.; Anderson, B. D., Determination of Drug Release Kinetics from Nanoparticles: Overcoming Pitfalls of the Dynamic Dialysis Method. *Molecular Pharmaceutics* **2013,** *10* (8), 3076-3089.
56. Cataldi, M.; Vigliotti, C.; Mosca, T.; Cammarota, M.; Capone, D., Emerging Role of the Spleen in the Pharmacokinetics of Monoclonal Antibodies, Nanoparticles and Exosomes. *Int J Mol Sci* **2017,** *18* (6), 1249.
57. Demoy, M.; Andreux, J. P.; Weingarten, C.; Gouritin, B.; Guilloux, V.; Couvreur, P., In vitro evaluation of nanoparticles spleen capture. *Life sciences* **1999,** *64* (15), 1329-37.
58. Avgoustakis, K.; Beletsi, A.; Panagi, Z.; Klepetsanis, P.; Livaniou, E.; Evangelatos, G.; Ithakissios, D. S., Effect of copolymer composition on the physicochemical characteristics, in vitro stability, and biodistribution of PLGA–mPEG nanoparticles. *International Journal of Pharmaceutics* **2003,** *259* (1), 115-127.
59. Lin Ts, T.; Gao, D. Y.; Liu, Y. C.; Sung, Y. C.; Wan, D.; Liu, J. Y.; Chiang, T.; Wang, L.; Chen, Y., Development and characterization of sorafenib-loaded PLGA nanoparticles for the systemic treatment of liver fibrosis. *J Control Release* **2016,** *221*, 62-70.
60. Liang, H. F.; Chen, C. T.; Chen, S. C.; Kulkarni, A. R.; Chiu, Y. L.; Chen, M. C.; Sung, H. W., Paclitaxel-loaded poly(gamma-glutamic acid)-poly(lactide) nanoparticles as a targeted drug delivery system for the treatment of liver cancer. *Biomaterials* **2006,** *27* (9), 2051-9.

CHAPTER IV

PLGA-BASED EXTENDED RELEASE FORMULATION PLATFORM

The following chapter has been published in Drug Development and Industrial Pharmacy

DRUG DEVELOPMENT AND INDUSTRIAL PHARMACY
2020, VOL. 46, NO. 4, 635–645
https://doi.org/10.1080/03639045.2020.1742146

Taylor & Francis
Taylor & Francis Group

RESEARCH ARTICLE

Check for updates

A smart approach to enable preclinical studies in pharmaceutical industry: PLGA-based extended release formulation platform for subcutaneous applications

Patrick Strack[a,b], Raimund Külzer[a], Florian Sommer[a], Tom Bretschneider[a], Olivia M. Merkel[b] and Achim Grube[a]

[a]Boehringer Ingelheim Pharma GmbH & Co. KG, Biberach an der Riss, Germany; [b]Ludwig-Maximilians Universität München, München, Germany

The personal contribution covers manufacturing and characterization of *der p 1* inhibitor formulations and establishing of the formulation platform. Spray drying experiments were performed by Florian Sommer. Animal experiments were performed by Raimund Külzer.

A smart approach to enable preclinical studies in pharmaceutical industry: PLGA-based extended release formulation platform for subcutaneous applications

Abstract

Objective: Validation of a prospective new therapeutic concept in a proof of concept study is costly and time-consuming. In particular, pharmacologically active tool compounds often lack suitable pharmacokinetic (PK) properties for subsequent studies. The current work describes a PLGA-based formulation platform, encapsulating different preclinical research compounds into extended release microparticles, to optimize their PK properties after subcutaneous administration.

Significance: Developing a PLGA-based formulation platform offers the advantage of enabling early proof of concept studies in pharmaceutical research for a variety of preclinical compounds by providing a tailormade PK profile.

Methods: Different model compounds were encapsulated into PLGA microparticles, utilizing emulsification solvent evaporation or spray drying techniques. Formulations aiming different release rates were manufactured and characterized. Optimized formulations were assessed in *in vivo* studies to determine their PK properties, with the mean residence time (MRT) as one key PK parameter.

Results: Utilizing both manufacturing methods, tested tool compounds were encapsulated successfully, with a drug load between 5% and 40% w/w, and an extended release time up to 250 h. In the following PK studies, the MRT was extended by a factor of 90, resulting in prolonged coverage of the required target through level. This approach was confirmed to be equally successful for additional internal compounds, verifying a general applicability of the platform.

Conclusion: For different active pharmaceutical ingredients (API), an optimized, tailor-made PK profile was obtained utilizing the described formulation platform. This approach is applicable for a variety of pharmacologically active tool compounds, reducing timelines and costs in preclinical research.

1 Introduction

In industrial preclinical research, an expeditious proof of concept for prospective new compounds is of great importance. One approach to identify these compounds and to determine new targets/projects is literature based. To validate published results, described molecules are tested on in-house models to show efficacy of the published chemical structures in the respective pharmacological *in vivo* model. Positive results of these experiments are the basis to initiate an exploratory research project and to invest capacity in medicinal chemistry to identify other suitable chemical structures. A prerequisite for proof of concept studies is a suitable pharmacokinetic (PK) profile of the tool compound. However, in most cases published compounds are pharmacologically active but lack suitable PK properties. Specifically, many tool compounds exhibit a short mean residence time (MRT), fast clearance and very low oral bioavailability if administered as a pure drug, which is linked in many (but not all) cases to either low aqueous solubility or poor permeability [1]. Chemical modifications to overcome those limitations are costly and time consuming [2]. To avoid an early investment into optimizing chemical structures with regard to PK properties, utilization of tailor-made formulations forms a plausible approach.

One approach, which is often considered to overcome limiting PK properties of a tool compound, is the use of osmotic pumps (Alzet®) or electronic peristaltic pumps (Iprecio®) [3], [4]. Those pumps are typically implanted subcutaneously (or intraperitoneally) and release a solution with the tool compound at a constant rate. One major disadvantage of these pumps is the required high solubility of the applied compounds. Poorly soluble compounds can be solubilized by addition of organic solvents to the pump solution. However, some organic solvents are not compatible with the pumps or are not tolerated by the animals and an extensive solubility testing is required to identify suitable solvents or solvent combinations. Furthermore, using organic solvents as dissolution enhancers often results in clogging of the tip of the flow moderator and finally failure of the pumps. In addition, a surgery including anesthesia is required to implant these devices and withdraw them after depletion of the drug reservoir. However, both surgery and anesthesia could have influences on the *in vivo* pharmacological model in which the tool compound should be tested.

Another way to increase MRT is the administration of a higher dose. However, administering the drug in a solution is often not feasible, due to low aqueous solubility and a high dose in a suspension can be associated with tolerability issues. Furthermore, especially in early phases of preclinical research, only limited amounts of API is usually available, restricting applicability of this approach.

An alternative way is an extended release formulation via incorporation of the API into a specific biocompatible polymer. Here, the compound is encapsulated within a polymeric matrix, whereby the drug is protected and slowly released by diffusion, erosion and/or degradation of the polymer [5]. Varieties of different polymers - natural, semi-synthetic and synthetic - are used as drug delivery systems [6]. One of the most commonly utilized and well-established polymers in controlled drug delivery is poly(lactic-co-glycolic acid) (PLGA) [5]. Due to its excellent biocompatibility, biodegradability and nontoxicity it has been approved by the FDA for various stages of clinical trials, as well as in some formulations on the market [7].

Despite the ubiquitous use and extensive characterization of PLGA, no manufacturing technology has been developed meeting the needs of preclinical research: a fast and user-friendly formulation platform for a variety of structurally different tool compounds on a variable scale. Addressing the above mentioned issues, herein we describe a platform formulation tool for preclinical studies to encapsulate compounds into PLGA based microparticles for subcutaneous application. An advantage of this approach is its independence of solubility of the respective compound. In addition, the presented approach is applicable for low compound amounts on milligram scale for initial screenings, and up to several grams for comprehensive *in vivo* studies. Furthermore, different PLGA derivatives are available, allowing a tailor-made release profile.

Two different manufacturing methods applied herein are emulsification solvent evaporation and spray drying. In this manuscript, we describe application of both methods to formulate water-soluble and practically insoluble compounds in PLGA based microparticles for subcutaneous administration. It is widely known that particle size distribution, morphology and drug load have a significant effect on release properties and these parameters subsequently influence PK properties [8, 9]. Therefore, those parameters were utilized for optimizing the manufactured formulation characteristics. In our studies the antibiotic, trimethoprim, and an inhibitor of the *der p 1* peptidase (a main allergen of house dust mites),

were used as model compounds [10]; trimethoprim served as an example for a slightly soluble API whereas the *der p 1* inhibitor was selected as model for a compound which is practically insoluble in aqueous media (Table 1).

Table 1 Structural formula and physicochemical data of investigated tool compounds

Compound	Structural formula	Solubility in aqueous media pH 6.8 at 25° C	logP predicted
Der p 1 inhibitor	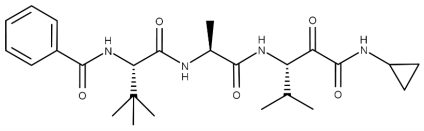	0.067 mg/mL[1]	3.01
Trimethoprim	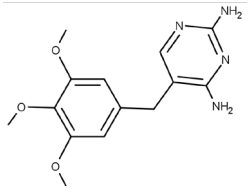	0.4 mg/mL [34]	0.98

[1] determined in house by shake flask method

2 Material and Methods

2.1 Materials

Polyvinyl alcohol, 87-89% hydrolyzed, Mw 13000-23000 (PVA), lauric acid (LA), HPLC grade acetonitrile (ACN) and dichloromethane (DCM) were purchased from Sigma Aldrich (Darmstadt, Germany). Poly (lactic-co-glycolic acid) (PLGA) Resomer® RG 752 H (RG752H) and Resomer® RG 503 H (RG503H) were obtained from Evonik Industries AG (Essen, Germany). Sodium chloride based suspensions were prepared with a 0.9% sodium chloride stock solution from Deltamedica (Reutlingen, Germany). Two model compounds, trimethoprim (Tri) and *der p 1* inhibitor, were provided internally (Boehringer Ingelheim Pharma GmbH).

2.2 Manufacturing Methods

2.2.1 Single Emulsion Evaporation

API loaded microparticles were prepared using a single emulsion evaporation method according to literature [11]. Briefly, stock solutions containing 5% (w/v) RG752H or RG503H and 5% (w/v) API (e.g. *der p 1* inhibitor) were prepared in DCM. The solution was added dropwise in a 1:20 volume ratio to an aqueous 1% (w/v) PVA solution containing 5% NaCl. LA was added in 1:1 and 1:2 weight ratios into the API solution, as specified throughout the text. The mixture was then homogenized using a T 25 digital ULTRA-TURRAX® (IKA, Staufen, Germany) for 2 min at 14.000 rpm. After homogenization, the resulting microparticle suspension was stirred for 3 h to let the organic solvent evaporate. The hardened particles were subsequently washed three times by centrifugation (4500 rcf, 4 °C, 15 min) and redispersed in deionized distilled water. Directly after this process the microparticle suspension was lyophilized. The final formulation yield obtained ranged from 20 mg to 100 mg.

2.2.2 Lyophilisation

The manufactured PLGA microparticles were filled into semi-stoppered glass vials at a maximal height of 25 mm. The formulation was flash frozen in liquid nitrogen for 10 minutes and then transferred to an Epsilon 2-4 LSCplus freeze-dryer (Christ, Osterode am Harz,

Germany). The freeze-drying cycle was performed according to an established generic protocol. Primary drying was performed at a shelf temperature of -60 °C and a pressure of 1 mbar for 2 hours, followed by a secondary drying step at 20 °C and a pressure of 0.01 mbar for 24 hours. After aeration, the vials were sealed and stored in a desiccator.

2.2.3 Spray Drying (SD)

Spray drying (B-90, Büchi, Flawil, Switzerland) was performed to manufacture API loaded microparticles. Briefly, PLGA (RG752H) and API (e.g. Trimethoprim) were dissolved in 95% Acetonitrile : 5% H_2O in a ratio of 5% and 10% API : PLGA. The solution was sprayed using a 7 µm (5%, 10%) nozzle. The process parameters were as follows: inlet temperature = 55 °C, outlet temperature = 27-31 °C, drying gas flow rate = 130 l/min (N_2: 1.5 bar/CO_2: 0.5 bar), relative spray rate = 100%, sprayhead temperature = 61 °C, inside pressure = 36 mbar, aspirator speed = 31.15 Hz. The collected formulations were dried and stored in a sealed desiccator for at least 3 days. The final formulation yield obtained ranged from 100 mg to 5000 mg.

2.3 Physicochemical characterization

2.3.1 Drug load/encapsulation efficiency

1 mg of PLGA/API-formulation was resuspended in 1 mL methanol and sonicated in an ultrasonication bath for 30 min to extract the API from the polymer microparticles. After centrifugation at 14 krpm for 10 minutes, the concentration in the supernatant was measured by HPLC. Drug load (DL) and encapsulation efficiency (EE) were calculated as shown here:

DL: $\left(\frac{amount\ of\ drug\ present\ in\ formulation}{weight\ of\ formulation\ sample\ analyzed}\ \mathrm{x}\ 100\%\right)$

EE: $\left(\frac{actual\ drug\ loading}{theoretical\ drug\ loading}\ \mathrm{x}\ 100\%\right)$

All DL and EE results are expressed in w/w percent throughout the text.

2.3.2 HPLC

All HPLC measurements were performed on an Agilent 1100 Series (Agilent Technologies, Santa Clara, USA). For each HPLC run, 2 µL of sample solution was aliquoted and analyzed with an XBridge Shield RP18 column (3.0 × 50 mm, 3.5 µm; Waters, Milford, USA), with a flow rate

of 0.8 mL/min and a detection wavelength of 246 nm. A gradient method was used to elute the API, starting with 100% 10 mM filtered ammonium acetate buffer (pH not adjusted). The ratio of acetonitrile was increased progressively until the mobile phase consisted of 85% acetonitrile after 9 min. Finally, the amount of acetonitrile was further increased to 95% in the last minute of the run. The overall runtime was 10 min with a retention time of 5 min for the API. *Empower 3* software (Waters, Milford, USA) was used to process and quantify sample peaks.

2.3.3 Size Distribution

Laser diffraction was used to determine the mean particle size and size distributions. Particle size distribution data were obtained as 10% volume percentile (X_{10}), 90% volume percentile (X_{90}) and volume mean diameter (VMD). The HELIOS system (Sympatec GmbH, Clausthal-Zellerfeld, Germany) with a 6 ml cuvette and a R1 lens was used to measure the particle size in an aqueous suspension. Samples were prepared by suspending approximately 10 mg microparticle formulation in 10 mL phosphate buffer (pH 7.4).

2.3.4 Morphology

Scanning electron microscopy (SEM) and optical microscopy were used for the particle size and morphology investigation. Carl Zeiss Model SUPRA-55VP scanning electron microscope and SmartSEM software were used to obtain images. For sample preparation, the dry microparticles were deposited on metal stubs with conductive carbon tape as a substrate. Secondary electron detector and 0.7-1 kV accelerating voltage was used for this purpose.

2.3.5 *In vitro* drug release assay

The dissolution profiles were obtained with the µDiss profiler (pION, Billerica, USA). Measurements were conducted using 5 mm pathlength tips. Approximately 0.2 mg of the samples were weighted carefully and exact weights recorded and suspended in 20 ml phosphate buffer (pH 7.4) at 37° C and 250 rpm. As a standard, a solution of the API in phosphate buffer was prepared. The dissolution profile was recorded for 7 to 14 days for all samples.

2.3.6 Statistical Analysis:

All results are given as mean value ± standard deviation (SD). All experiments were performed in triplicates unless stated otherwise.

2.4 *In vivo* pharmacokinetics

2.4.1 Animal experiments

The different formulations of the *der p 1* inhibitor were administered *subcutaneously* (s.c.) or *per os* (p.o.) to fed BALB/c mice (17 – 24 g body weight, three female animals per treatment group, respectively). The different formulations of trimethoprim were administered *subcutaneously* (s.c.) to RJHAN:WI rats (200 – 250 g body weight, three male animals per treatment group, respectively). Blood samples were collected at specified time points via puncture of the saphenous vein (mice) or the sublingual vein (rats) using Ethylendiamintetraacetic acid (EDTA)-coated microvettes. Plasma was captured after centrifugation and immediately frozen at -20 °C until LC-MS/MS analysis.

Animal experiments were approved by the local animal ethics committee and were in agreement with the German Animal Welfare Act.

2.4.2 LC-MS/MS analysis

Plasma aliquots of 5 µL were supplemented with 400 nM of BI-1052 (internal standard). Plasma proteins were precipitated by the addition of 70 µL 50% acetonitrile : 50% methanol and subsequent centrifugation at 4000 rpm, 4 °C for 10 min in an Eppendorf 5810 centrifuge (Eppendorf AG, Hamburg, Germany). From the resulting supernatant 30 µL were diluted in 170 µL 0.1% formic acid in a 96-well plate (Greiner, Frickenhausen, Germany).

An API 6500 mass spectrometer (ABSciex, Darmstadt, Germany) was equipped with an Agilent 1290 LC system, a CTC autosampler and a Kinetex 30 x 2.1 mm, 2.6 µm C_{18} LC column (Phenomenex, Aschaffenburg, Germany). The MS conditions were set as follows: Positive mode, 400 °C source heating, curtain gas = 40, gas 1 = 50, gas 2 = 50, a capillary voltage of 5000 V. The following MS transitions were recorded: EX 7123: 473.3/256.2, DP = 81, CE = 19; internal standard: 453.0/275.0, DP = 91, CE = 29. Solvent A consisted of 0.1% aqueous formic acid and solvent B of 0.1% formic acid in 50% acetonitrile: 50% methanol. The gradient started

at 90% solvent A, which increased within 2.6 min to 5%. After 0.7 min solvent A was set to 90% for re-equilibration. The flow rate was set to 400 µL·min^{-1} and the injection volume was 20 µL.

3 Results and discussion

3.1 Initial approach using Resomer® RG 503 H

The *der p 1* inhibitor exhibits a peptide like structure and is practically insoluble in water (Table 1). The targeted effective plasma concentration of the *der p 1* inhibitor was a minimum of 150 nM which should be covered for at least 7 days to show a pharmacological effect. To assess the PK properties of the compound, p.o. and s.c. PK studies were conducted in mice. An API/natrosol suspension was administered orally and an API/cyclodextrin solution was administered subcutaneously to mice. The API in both formulations showed a rapid decline of the *der p 1* inhibitor plasma concentrations resulting in a short MRT of only 0.96 hours (following s.c. administration) and 1.7 hours (following p.o. application) (Table 2). At 24 hours post dosing, no API was detectable in plasma (Figure 1).

A: *in vivo* PK profile

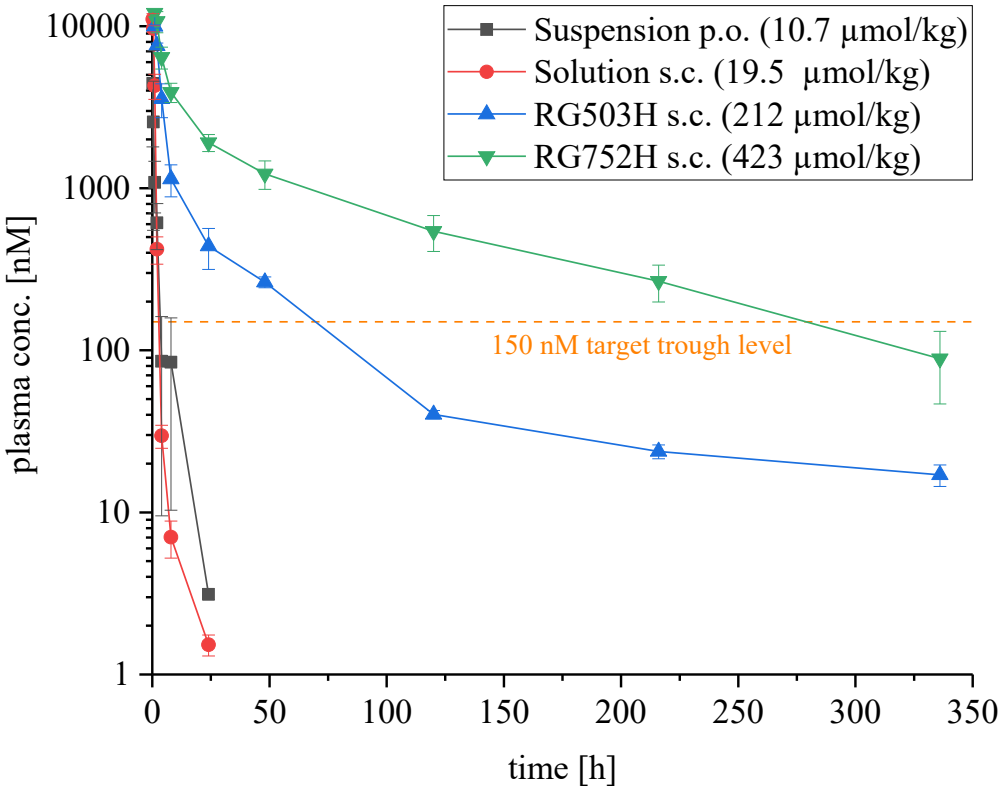

B: dose normalized

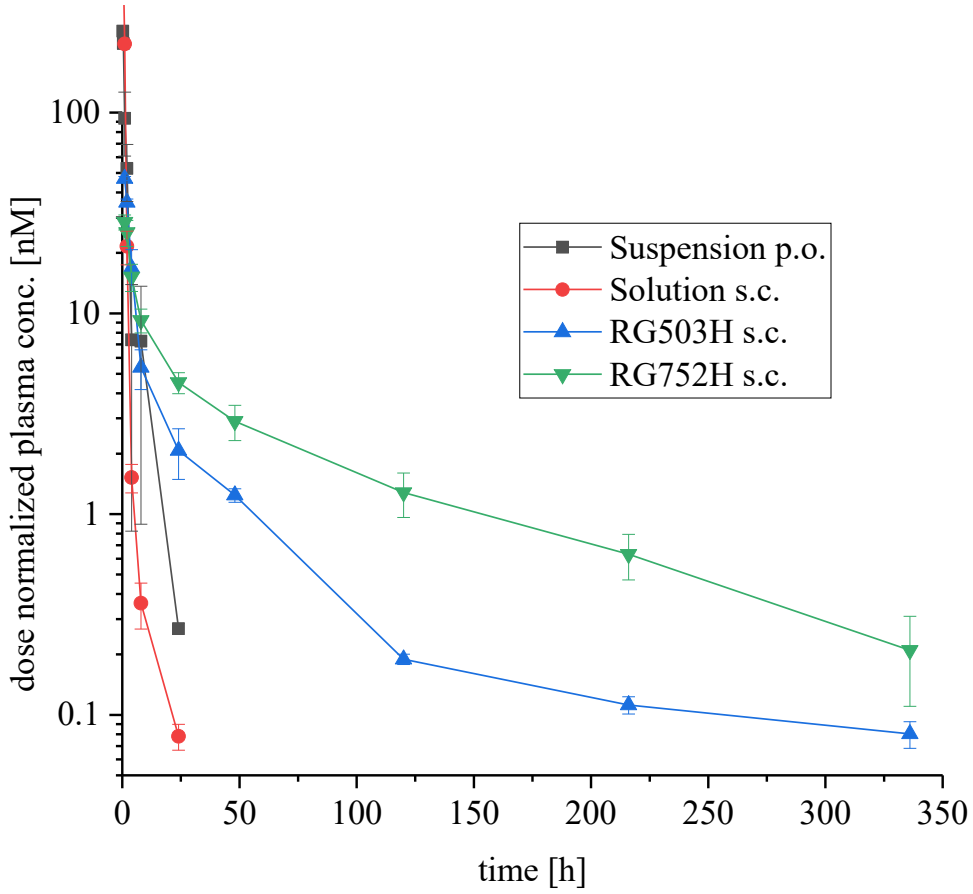

Figure 1 Plasma concentration-time profile of der p 1 inhibitor in mice after administration of different formulations (A) and dose normalized PK profile (B)

Table 2. PK parameters of the *der p 1* inhibitor in mice after p.o. or s,c, administration of different formulations

Formulation	Dose [µmol/kg]	MRT [h]	C_{1h} [nM/ (µmol/kg)]	AUC (0h-inf) [(nM*h)/ (µmol/kg)]	AUC (24h-inf) [(nM*h)/ (µmol/kg)]
Suspension p.o.	10.7	1.7 ± 1.0	93.5 ± 28.1	566.3	0.86
Solution s.c.	19.5	0.96 ± 2	150.8 ± 38.7	497.9	0.51
RG503H s.c.	212	71 ± 14.7	46.9 ± 1.1	334.9	125.5
RG752H s.c.	423	86 ± 22.0	25.3 ± 2.4	621.7	387.7

Due to the observed poor PK properties of the *der p 1* inhibitor, the required coverage of the targeted minimum effective plasma concentration via repeated administration of the suspension/solution was considered as not feasible. As an alternative, an extended release formulation was developed in order to optimize the PK profile of the compound.

In an initial approach, PLGA-microparticles were prepared utilizing the single emulsion evaporation method. Thereby the hydrophobic *der p 1* inhibitor was encapsulated into RG503H polymer and characterization of the manufactured formulation was performed.

The laser diffraction results in Table 3 showed a size distribution between X_{10}: 1.73 µm and X_{90}: 14.55 µm, correlating well with the microscopy images, which demonstrate spherical microparticles with a similar size distribution. (Figure 2)

A: RG503H

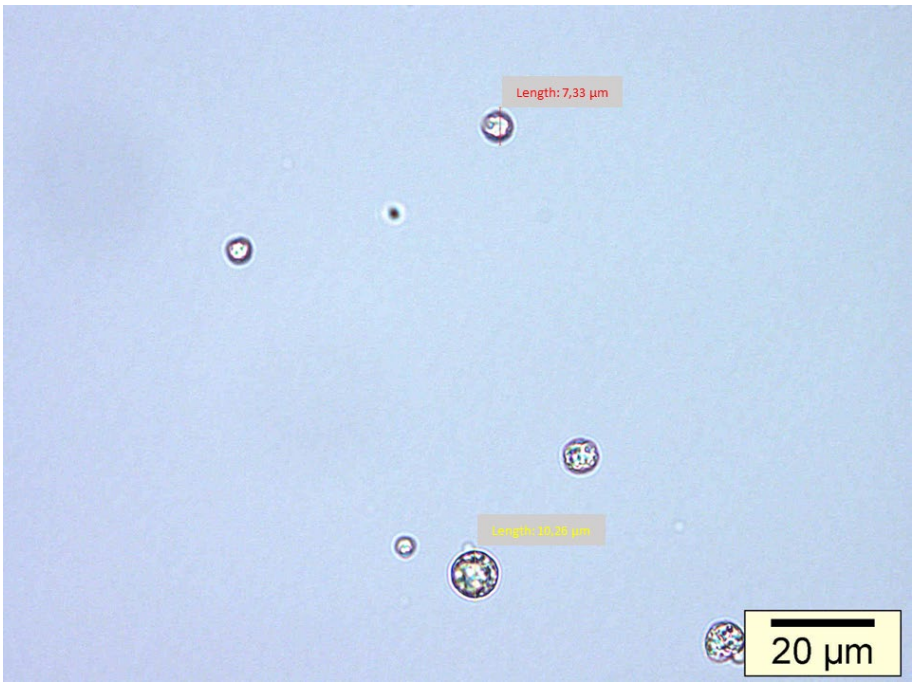

B: RG752H

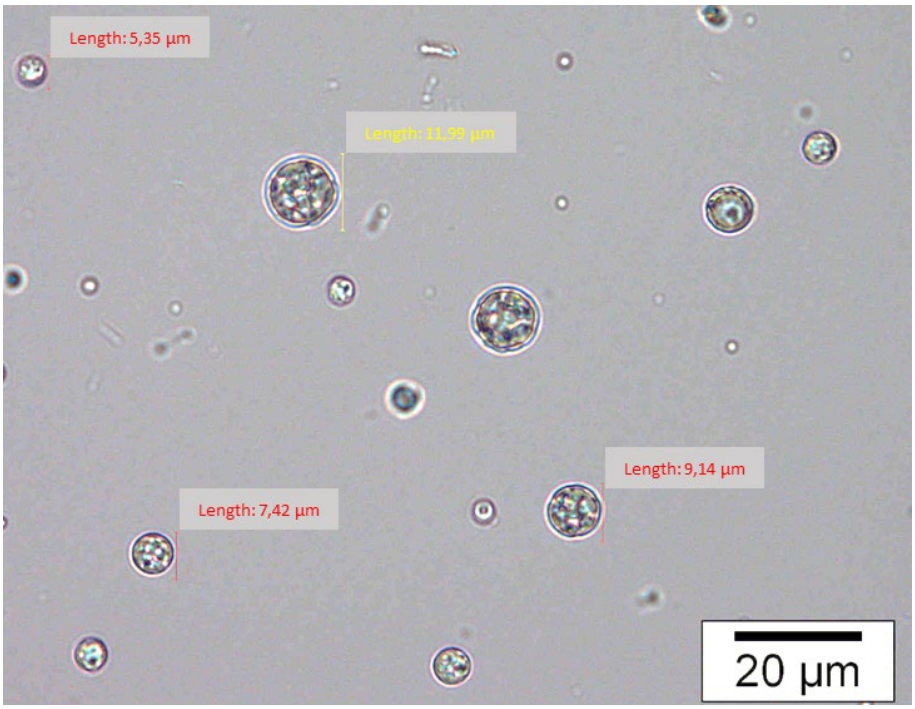

Figure 2 Microscopic images of der p 1 inhibitor formulations (A) Resomer RG503H (B) Resomer RG752H

The high DL of 30.5 ± 5.4% achieved with the RG503H formulation (Table 3) may be linked to the hydrophobic nature of the API, which has a higher affinity to the hydrophobic PLGA-polymer.

Table 3 Characterization of investigated *der p 1* inhibitor formulations

Formulation	DL [%]	EE [%]	VMD [µm]	X_{10} [µm]	X_{90} [µm]
RG503H	30.5 ± 5.4	61 ± 10.8	8.46	1.73	14.55
RG752H	40.4 ± 3.8	80.8 ± 7.6	6.81	1.48	11.41

Similar hydrophobic drugs, e.g. paclitaxel [12], [13], fusic acid [14] and beta-estradiol [15] were reported by others to display a comparably high DL between 18 and 38%.

The size distribution of the manufactured microparticle formulation did not show oversized particles or agglomerates and therefore allowed a subcutaneous injection to mice without blocking of the syringe needle. Furthermore, subcutaneous injection of particles with a size

distribution below 50 µm is considered to minimize discomfort, distress and pain for the animals.

The release profile of the RG503H formulation showed a burst release of approximately 40% in the first hour, followed by a fast, exponential release up to 75% within 24 hours. Terminally, a linear profile from 75 to 100% release was observed for 125 hours. Between 200 and 300 hours, 100% of the API was released and a plateau was reached (Figure 3).

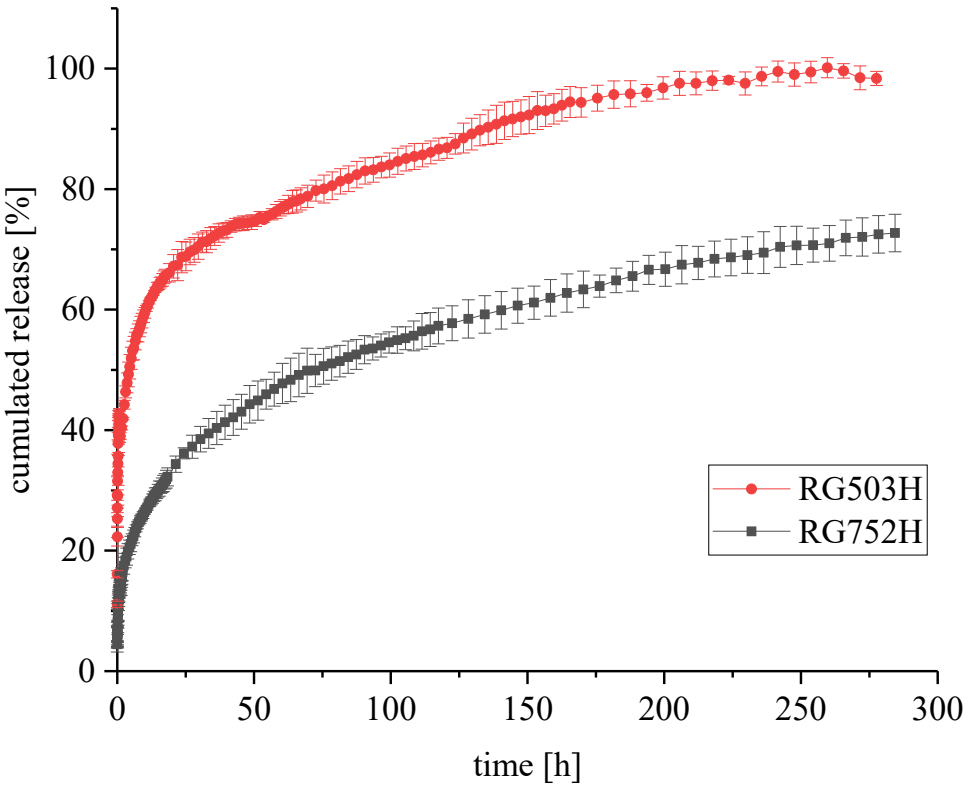

Figure 3 *In vitro* release profile of der p 1 inhibitor formulations

The observed initial burst occurs in several PLGA-based extended release formulation and is mainly caused by API that has been absorbed on the particle surface [16]. In literature, this burst release and particularly the following release profile is highly variable. In other studies, using similar hydrophobic APIs and comparable manufacturing, initial burst ranges from under 10% to nearly 70% and total release from a few hours to several days [12, 13, 14, 15].

In order to demonstrate that the extended release shown in the *in vitro* profile can also be observed *in vivo*, a PK study was performed.

3.1.1 *In vivo* PK study

The PLGA formulation was injected s.c. at a dose of 212 µmol/kg and an extended release of the API from the microparticulate formulation into the plasma was observed. The mean plasma concentrations versus time profiles are illustrated in Figure 1.

Starting from 1 hour, the measured plasma concentrations of the *der p 1* inhibitor obtained after a single administration of the RG503H formulation were higher than those obtained after p.o. dosing of the natrosol suspension or s.c. injection of the solution, as expected. Furthermore, plasma concentration of the *der p 1* inhibitor 24 h after dosing of these standard formulation were below the limit of quantitation whereas *der p 1* inhibitor encapsulated into RG503H polymer exhibited long lasting plasma levels, which were quantifiable up to 336 hours with a final plasma concentration of 16 nM. As shown in Figure 1, the minimum trough plasma level of 150 nM was maintained for at least 48 hours.

The MRT value as key PK parameter of the RG503H formulation increased approximately 36 and 74-fold, respectively, compared to the p.o. suspension and the s.c. solution (Table 2). This MRT increase is well within the range described in literature for similar formulations [17, 18, 19, 20].

Despite the extended release and the subsequent increase of the MRT achieved with RG503H, the targeted 7-day coverage of the effective concentration of 150 nM was not reached. Therefore, the formulation was further optimized to achieve this objective.

3.2 Optimized formulation with Resomer® RG 752 H

One of the parameters that can be tuned to extend the release profile and consequently influence the PK profile, is the polymer type [21]. Therefore, a different PLGA polymer was tested, to investigate the impact on *in vitro* release.

Resomer® RG 752 H (RG752H) has a higher lactic acid ratio and lower molecular weight than RG503H. It is suggested that the more hydrophobic nature of this polymer leads to a higher DL and slower release for hydrophobic compounds [22]. Whereas the lower molecular weight may reduce the initial burst, by forming more compact microparticles due to reduced porosity [23].

The manufacturing of the *der p 1* RG752H formulation was similar to the RG503H formulation, despite changing the type of polymer. Hereby, compared to the first formulation, a higher DL of 40.4% and EE of 80.8% was observed (Table 3). A high DL is beneficial, due to the lower administered dose necessary to reach the target plasma level. Additionally, a high EE is of advantage, in order to reduce API costs.

The laser diffraction measurement provided similar results to the previous findings with RG503H (Table 3) and were corresponding to the microscopic pictures (Figure 2). The slightly smaller size distribution might be caused by the more compact particle structure due to shorter polymer chains in RG752H [5, 24].

Distinct differences were observed in the *in vitro* release profile. Initial burst in the first hour was reduced to approx. 15%. The following exponential phase up to 50% release occurred over 50 h. The terminal linear profile of the RG752H was stopped after 300h with a release of 70% (Figure 3). Herby, the objective of the optimized formulation was achieved. Compared to the RG503H formulation, the *in vitro* release time was extended. Similar findings were reported in previous publications [18, 25, 26]. Here, despite the difference in total release time, the slower release of the drug from microparticles with higher lactic content is clearly noticeable. Ayoub, Elantouny [18] attribute this effect to the increasing hydrophobicity, causing a reduction in hydration and swelling and subsequently a slower diffusion of the API from the polymer matrix.

In order to investigate how these results translate to *in vivo* conditions, another PK study was conducted.

3.2.1 *In vivo* PK study

The optimized PLGA formulation was injected s.c. at a dose of 423 µmol/kg to ensure that the desired plasma level of > 150 nM is maintained for at least 7 days. In Figure 1, the mean plasma concentrations versus time profiles are shown. As expected, the measured plasma concentrations obtained after treatment with the RG752H formulation were higher than those observed after treatment with any of the previously discussed formulations. This effect can be partially attributed to the increased dose administered, but is mainly caused by the improved formulation. The influence of the formulation is especially visible when comparing the dose normalized PK profiles, where API concentration of RG752H is still over 5-fold higher

than RG503H (Figure 1 B). Additionally, the compound residence time was extended to at least 336 hours with a plasma concentration of 65 nM at the last sampling time point.

A comparison of PK parameters of the different formulations is shown in Table 2. The MRT values of the RG752H formulation were further increased about 43-, and 90-fold respectively, compared to the p.o. suspension and the s.c. solution.

Due to the prolonged MRT after administration of the RG752H formulation, the target plasma concentration of 150 nM was covered now for 168 hours. Furthermore, the dose-normalized plasma concentration after one hour was decreased by almost 50% compared to the RG503H formulation. This observation is consistent with the *in vitro* profile, where only a small portion of the RG752H formulation was released in the initial burst. Another parameter of the *in vitro* release, which correlates with the *in vivo* profile, is the total release time. As shown in Figure 3, release time is far more extended for the RG752H formulation than observed with the RG503H particles. Therefore, a good prediction for the *in vivo* study can be derived from the given *in vitro* release profile.

By using two different PLGA copolymers, different release profiles - *in vitro,* as well as *in vivo* – were observed. Based on these results and supported by literature [15, 18, 25, 26], tailor-made formulation can be achieved using RG503H for a faster or RG752H for a slower release formulation. Alternative PLGA types may also be applied to further refine the release profile.

3.3 Encapsulation of a water-soluble tool compound (trimethoprim)

Similar to the *der p 1* inhibitor, discussed in the previous section, trimethoprim is another example showing suboptimal PK properties for proof of concept in preclinical research. After subcutaneous application of an API/cyclodextrin solution with a dose of 34.4 µmol/kg, a fast decline of the trimetoprime plasma concentrations was observed. The MRT was 1.3 hours, and plasma levels were only detectable up to 8 hours after administration (Figure 7). Following this, the desired target through level of 200 nM for at least 3 days was not achieved and another extended release formulation was developed.

Trimethoprim is slightly soluble in water (Table 1), thus encapsulating into hydrophobic PLGA may be challenging, mainly due to partitioning of the API from the polymeric phase into the external phase before solidification of the particles [27]. Initially, encapsulation by single

emulsion evaporation was tested and preliminary characterization revealed a low DL of 1.15%, as expected (Table 4).

Table 4 Characterization of investigated trimethoprim formulations

Formulation	DL [%]	EE [%]	VMD [µm]	X_{10} [µm]	X_{90} [µm]
PLGA/Tri	1.15 ± 0.14	5.7 ± 0.56	ND	ND	ND
PLGA/Tri:LA 1:1	4.1 ± 0.211	20.5 ± 0.84	7.8	1.44	15.1
PLGA/Tri:LA 1:2	3.4 ± 0.45	17 ± 1.80	5.01	1.19	8.77
Spray Dry 10%	9.3 ± 0.29	92.6 ± 2.87	6.65	1.00	13.32
Spray Dry 5%	4.7 ± 0.1	93.0 ± 1.02	6.42	1.00	13.09

Hence, lauric acid (LA) was incorporated, as to form an ionic pair with trimethoprim resulting in an overall more hydrophobic complex, consequently enhancing the DL. A similar approach has been performed in a nanoparticulate formulation described in the literature. Ashton and Song [28] used organic acid counter ions to increase encapsulation efficiency for basic compounds and decrease the release rate out of PLGA-PEG nanoparticles.

3.4 Single emulsion evaporation with lauric acid as the excipient

The same manufacturing procedure as described above was used with addition of LA in 1:1 (PLGA/Tri:LA 1:1) and 1:2 (PLGA/Tri:LA 1:2) molar ratios to the API solution. With this approach, the DL was enhanced to 4.1% and 3.4% respectively, depending on the LA/API ratio (Table 4).

The size distribution and VMD of both formulations were in a similar range (Table 4) and corresponded to the microscopic images, demonstrating spherical microparticles with a uniform distribution (Figure 4).

A: PLGA/Tri:LA 1:1

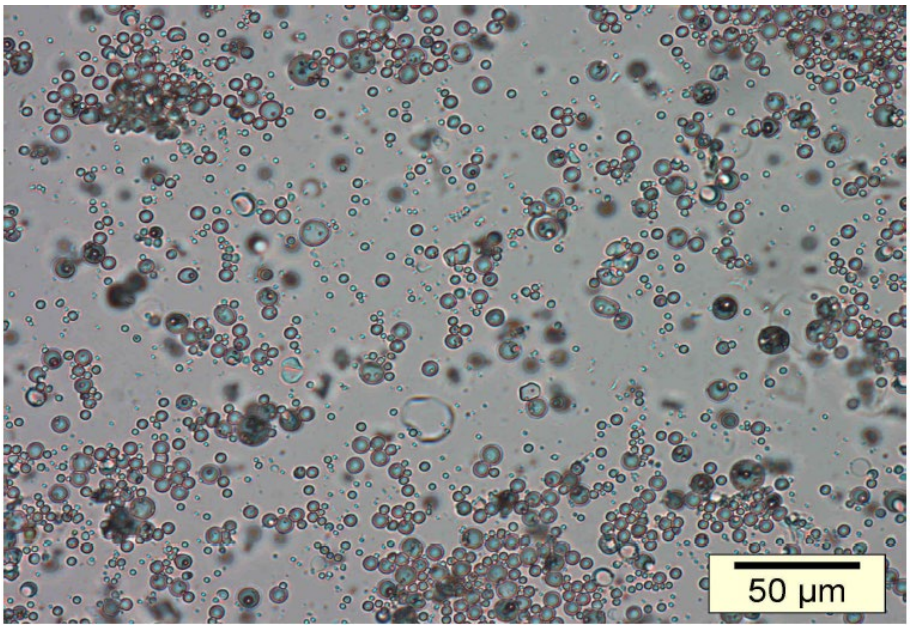

B: PLGA/Tri:LA 1:2

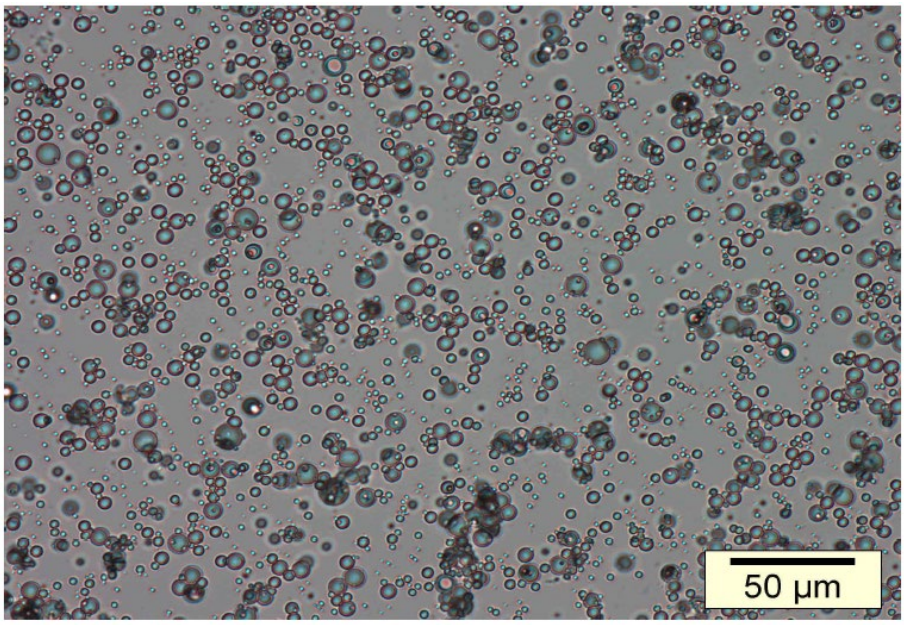

Figure 4 Light microscopic images of trimethoprim formulations (A) PLGA/Tri:LA 1:1 (B) PLGA/Tri:LA 1:2

SEM imaging revealed overall smooth surface morphology, although some abrasive and even porous particles were observed additionally (Figure 5).

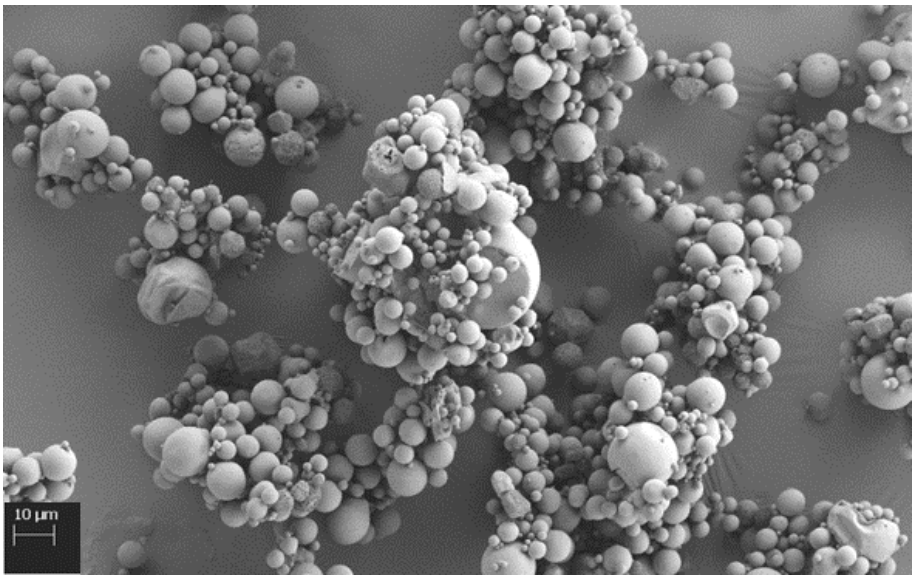

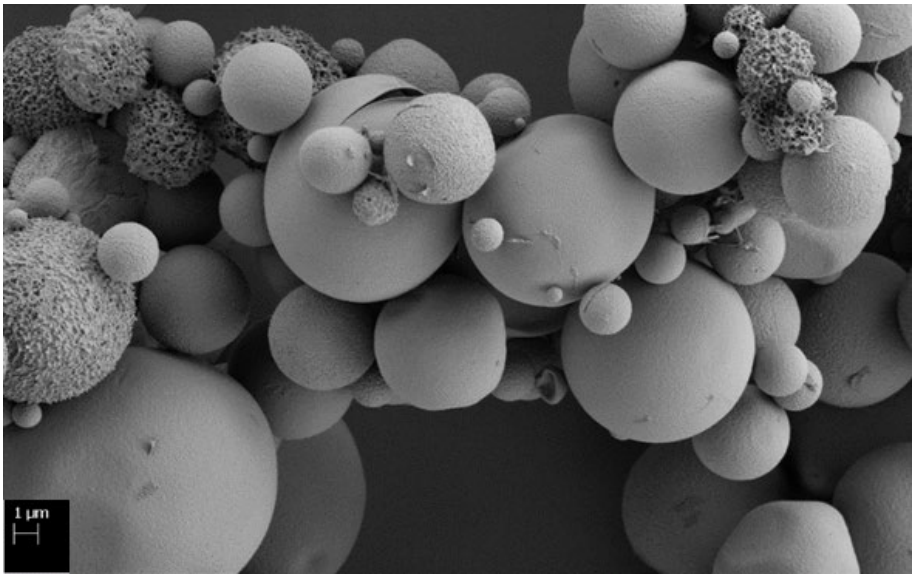

Figure 5 SEM images of PLGA/Tri:LA 1:1 formulation

Most single emulsion manufactured formulations show a smooth surface [17, 18, 25], and primarily the use of a porogen [29, 30] leads to porous structures. Since no porogens were used here, initial signs of degradation of the PLGA on the surface or the sample preparation might explain the abrasive structures.

In vitro release analysis resulted in an initial burst release under 10% for both formulations. This low initial burst could be explained by the reduced PLGA-surface adsorption of the relatively hydrophilic API and the low drug loading [9]. Furthermore, the addition of LA might contribute to the observed release retention, as was anticipated based on literature [28].

The release profile was similar for both formulations. Starting with an exponential release phase in the first 24 hours up to 30%, followed by a linear profile for 150 hours up to 80% release, at which point the measurement was terminated (Figure 6).

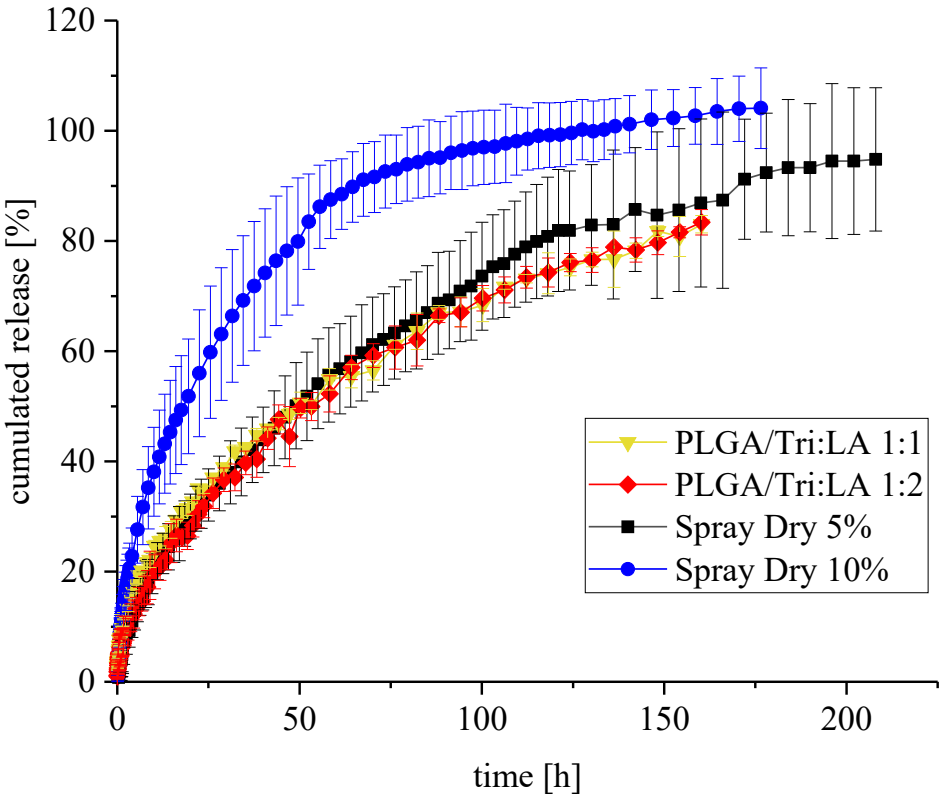

Figure 6 *In vitro* release profile of trimethoprim formulations

As already observed with both *der p 1* formulations, extending the *in vitro* release of the API should translate to an increased MRT *in vivo*. Therefore, similar results with the PLGA/Tri:LA formulations were expected, and an *in vivo* PK study was performed to confirm this.

3.4.1 *In vivo* PK study

Both PLGA-based formulations were applied subcutaneously at a dose of 103 µmol/kg. The mean plasma concentrations versus time profiles are illustrated in Figure 7.

Starting from 4 hours, the measured plasma concentrations observed after treatment with either PLGA/Tri:LA formulation were higher than those obtained after treatment with the cyclodextrin solution. Additionally, trimethoprim solution was cleared from the circulation after 8 hours, whereas decline of trimethoprim plasma concentrations after s.c. administration of the PLGA particles was much slower, leading to measurable plasma concentrations of the tool compound up to 168h. Similar formulations showed an extended circulation time between 2 and 4 weeks [17, 18, 19]. The MRT values of the PLGA/Tri:LA formulation increased approximately 73-fold in plasma compared to the cyclodextrin solution, as shown in Table 5.

A: *in vivo* PK profiles

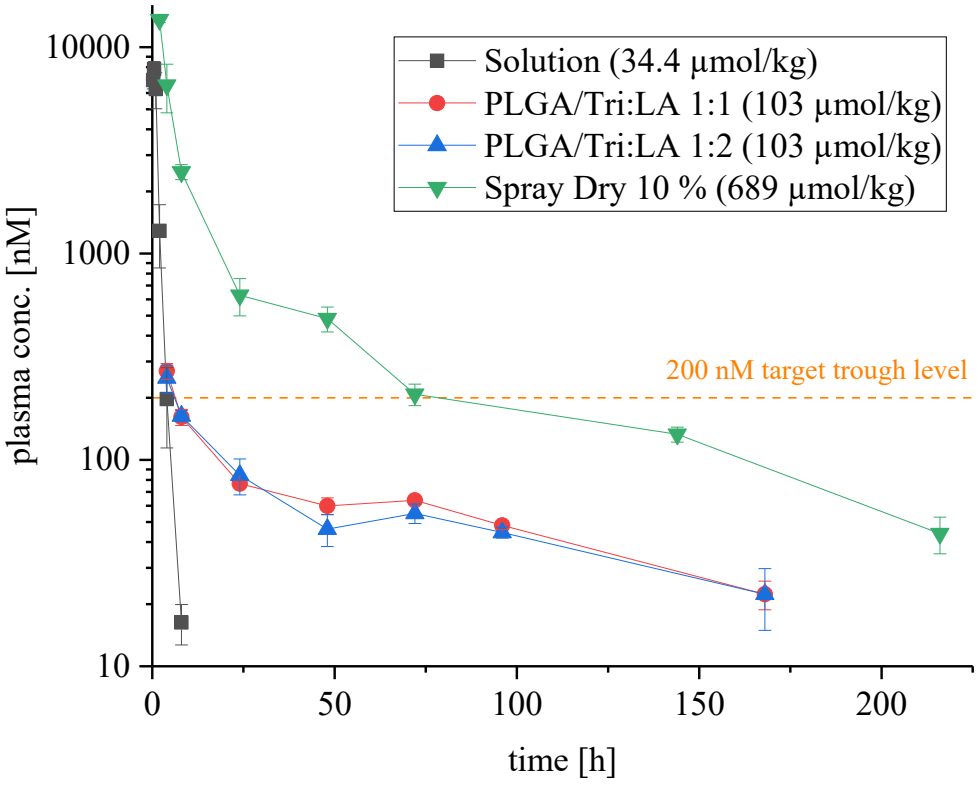

B: dose normalized profiles

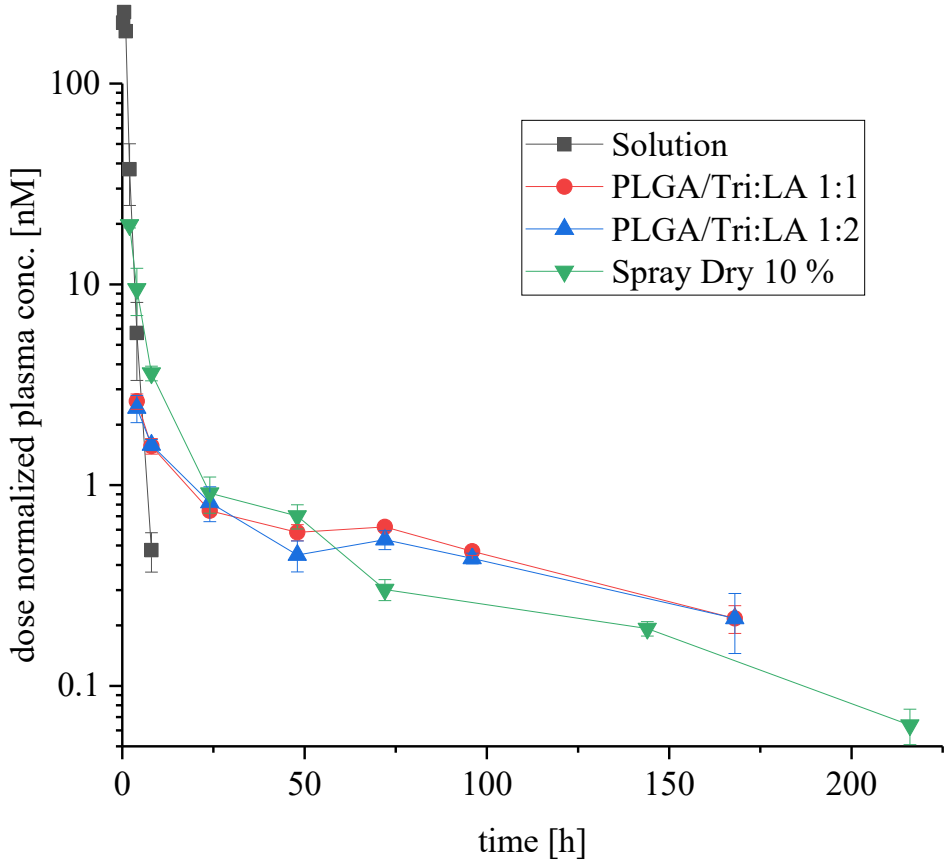

Figure 7 *In vivo* PK profiles of different trimethoprim formulations after s.c. administration to rats (A) and dose normalized profiles (B)

Table 5 PK parameters of trimethoprim in rats after s,c, administration of different formulations

Formulation	Dose [µmol/kg]	MRT [h]	C_{1h} [nM/ (µmol/kg)]	AUC (0h-inf) [(nM*h)/ (µmol/kg)]	AUC (24h-inf) [(nM*h)/ (µmol/kg)]
Solution	34.4	1.3 ± 0.1	5.7 ± 2.4	315	0
PLGA/Tri:LA 1:1	103	95 ± 12.1	2.6 ± 0.2	118	87.4
PLGA/Tri:LA 1:2	103	ND	2.4 ± 0.4	118	87.2
Spray Dry 10%	689	45 ± 4.3	9.4 ± 2.5	167	63.7

Despite the promising results in the PK studies, the intended target minimum effective level of 200 nM was only reached for 4 hours. To achieve the desired plasma level for 3 days, a high dose PK study was planned and thus, a larger formulation quantity was necessary. With the conventional laboratory homogenizer, repeatable manufacturing was only feasible on a small-scale due to obviously different mixing conditions. Scale-up was observed to result in high batch-to-batch variability, particularly with regard to drug loading (data not shown). Furthermore, spontaneous API crystallization was observed in several batches during solvent removal. Needle shaped crystals were visible in and outside of the particles and may have caused perforation of the particle wall, as also rationalized in literature [9].

In order to manufacture a sufficient amount of formulation reproducibly and to avoid the described issues, a spray drying method was utilized.

3.5 Spray drying of trimethoprim PLGA microparticles

Spray drying allows easy manufacturing of higher formulation amounts. Provided an adequate compound availability of at least 100 mg, PLGA-based formulations can be produced in a fast and reproducible manner with this one-step manufacturing method. Furthermore, spray drying is more likely to prevent crystallization of the API during solvent evaporation [31, 32]. This can be mainly explained by the rapid solvent evaporation in the drying chamber of the spray dryer, as opposed to slow evaporation at room temperature taking place using single emulsion method. The rapid transformation of the solution to a solid state, not allowing for ordered conformation, consequently leads to reduced formation of crystals [33].

Drug loading is described to have an impact on the release profile and consequently can be utilized to optimize the PK profile [9, 21]. Therefore, trimethoprim PLGA microparticles with a drug loading of 5% and 10% were manufactured by spray drying.

Since there is no loss of API in the manufacturing procedure, an EE of over 90% was achieved and the intended DL was obtained (Table 4). The EE was increased 5-fold, compared to the single emulsion evaporation method results, even for high DL formulations. In Table 4, the laser diffraction measurements of the spray dried formulations are provided. Formulations with 5% and 10% DL resulted in similar VMD of 6.42 µm and 6.65 µm, respectively, and are thus similar to those manufactured using single emulsion evaporation method.

Spherical particles of similar size distribution were observed via optical microscopy, supporting the laser diffraction findings (Figure 8). A closer look into morphology by SEM revealed the surface appearance of the microparticles. Smooth surface morphology was observed in SEM images, and no abrasive or porous particles were detected (Figure 9).

A Spray Dry 10%

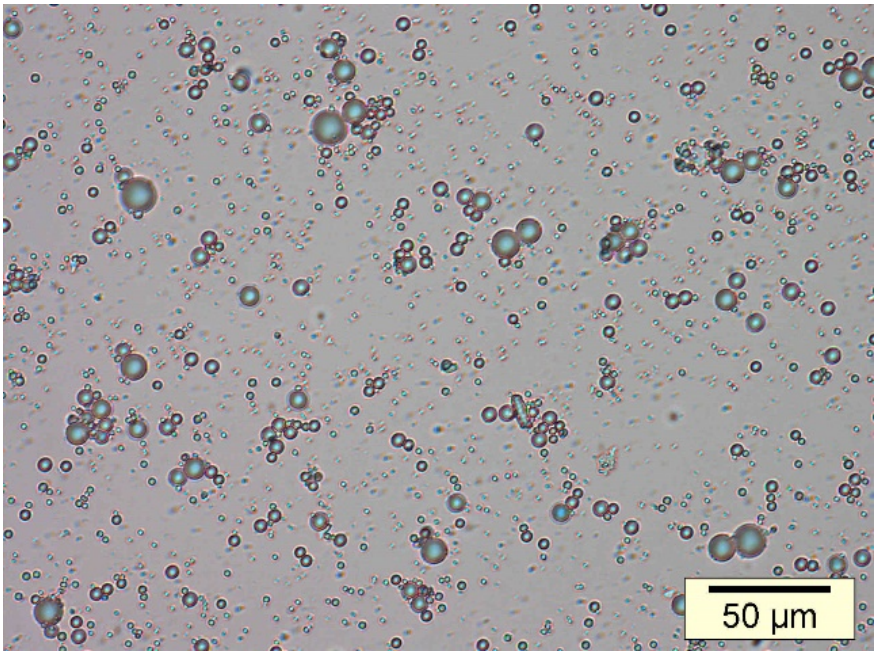

B Spray Dry 5%

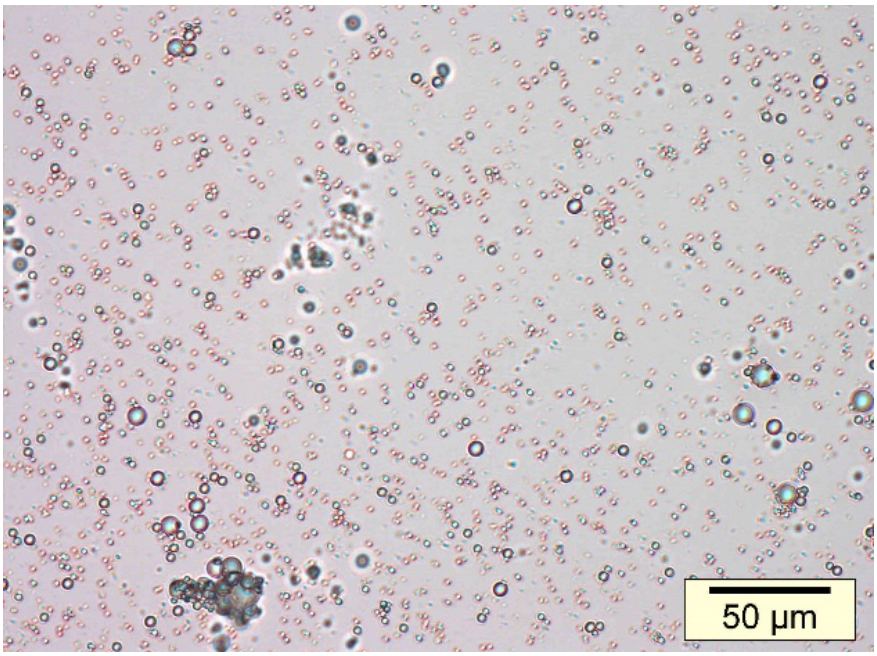

Figure 8 Light microscopic images of spray dried trimethoprim formulations (A) SD 10% (B) SD 5%

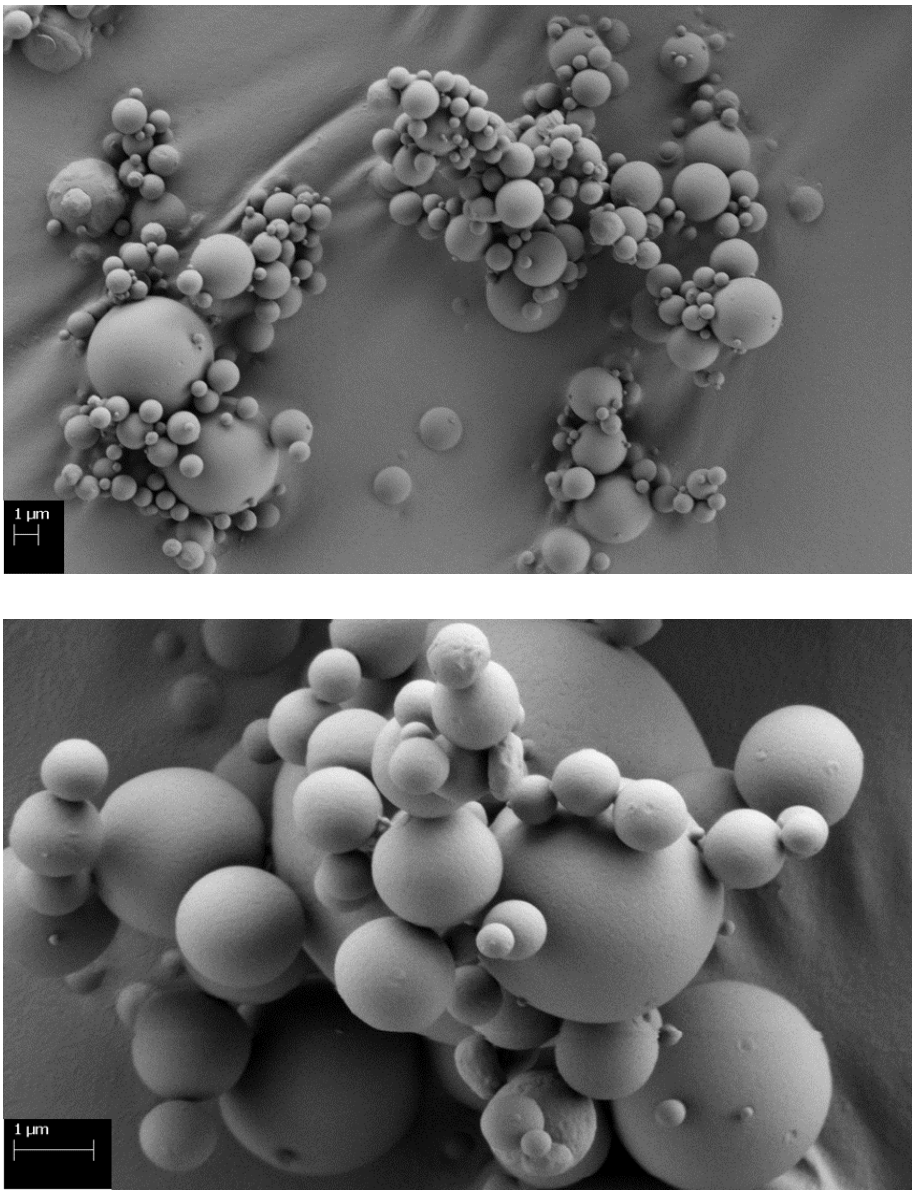

Figure 9 SEM images of Spray Dry 10% formulation

A clear difference was observed in the release profile for the different DL spray dried formulations (Figure 6). With a burst release in the first hour of approximately 10%, and an exponential release phase in the first 24 hours up to 30%, followed by a linear release profile for 170 hours with up to 90% release, the 5% DL formulation was comparable to that of the PLGA/Tri:LA single emulsion formulation with similar DL.

The 10% DL formulation had a similar burst release of 10%, but release continued with an exponential phase up to 85% in 50 hours. The terminal linear profile from 85 to 100% release was observed in the following 100 hours. This behavior can be explained by the lower density

of the polymer on the particle surface, acting as a diffusion barrier and subsequently increasing porosity of the particles upon release of the API [9].

As a result, different release profiles were obtained by utilizing different drug loadings. Hereby, another easy to apply option to customize the release profile was confirmed. The formulation containing 10% DL showed a fast release whereas a slow release formulation was generated with 5% DL. This is in accordance with previously published work, demonstrating that increasing DL may cause a larger burst phase of release leading to a higher overall drug release [14].

With the established spray drying method a sufficient amount of formulation was reproducibly manufactured for a high dose PK study.

3.5.1 *In vivo* PK study

To achieve the desired dose combined with a suitable *in vitro* release profile, the 10% DL formulation was tested. Based on results of previous PK studies, the dose of 689 µmol/kg was expected to achieve the desired minimum plasma concentration of 200 nM for 3 days after s.c. administration.

The mean plasma concentrations versus time profiles are shown in Figure 7. As expected, due to the 7 times higher dose, the measured plasma concentrations obtained after treatment with the spray dried formulation were higher than those observed after treatment with any of the other formulations and the target trough level of 200 nM was maintained for the desired time of 72 hours. The blood circulation time was extended to at least 216 hours with a final plasma concentration of 43 nM and the MRT of the spray dried formulation compared to the cyclodextin formulation was increased 35-fold (Table 2).

Furthermore the dose-normalized PK profile of the spray dried formulation closely matched the PLGA/Tri:LA formulation as can be observed on Figure 7 B, suggesting that both manufacturing methods can be utilized equally.

With these results, it was demonstrated that spray drying is an appropriate methodology choice to manufacture extended release microparticles on a larger scale to optimize PK properties.

3.6 Description of the proposed formulation platform

As shown for two compounds with different physicochemical properties, it is possible to apply presented technologies to enable an early pharmacological proof of principle study without further optimizing the chemical structure. However, this work was focused on the development of a tool platform, to accommodate a wide range of APIs, enabling early preclinical studies.

Hence, in the following the proposed formulation platform is described, which comprises an optimal combination of manufacturing method choices (single emulsion evaporation or spray drying), polymer type and DL, as to facilitate the desired release and the subsequent PK profiles.

As visualized on Figure 10, an adequate API availability of minimum 100 mg allows for spray drying of the formulation. For smaller amounts, solubility has to be taken into consideration. Water-insoluble APIs can be manufactured using single emulsion evaporation method, whereas for water-soluble APIs, this method is not recommended, since without further elaborate modification only a low drug loading can be attained.

In a second step, tailor-made release profiles are feasible by varying the polymer type; high lactic acid ratio and low molecular weight allow a slow release and subsequently a long MRT. A fast release and shorter MRT can be achieved by lower lactic acid ratio and a higher molecular weight of the polymer. Furthermore, by varying the DL the release can be customized. A low drug loading results in a slow release and consequently a long MRT, where a high DL will produce a fast release profile and short MRT.

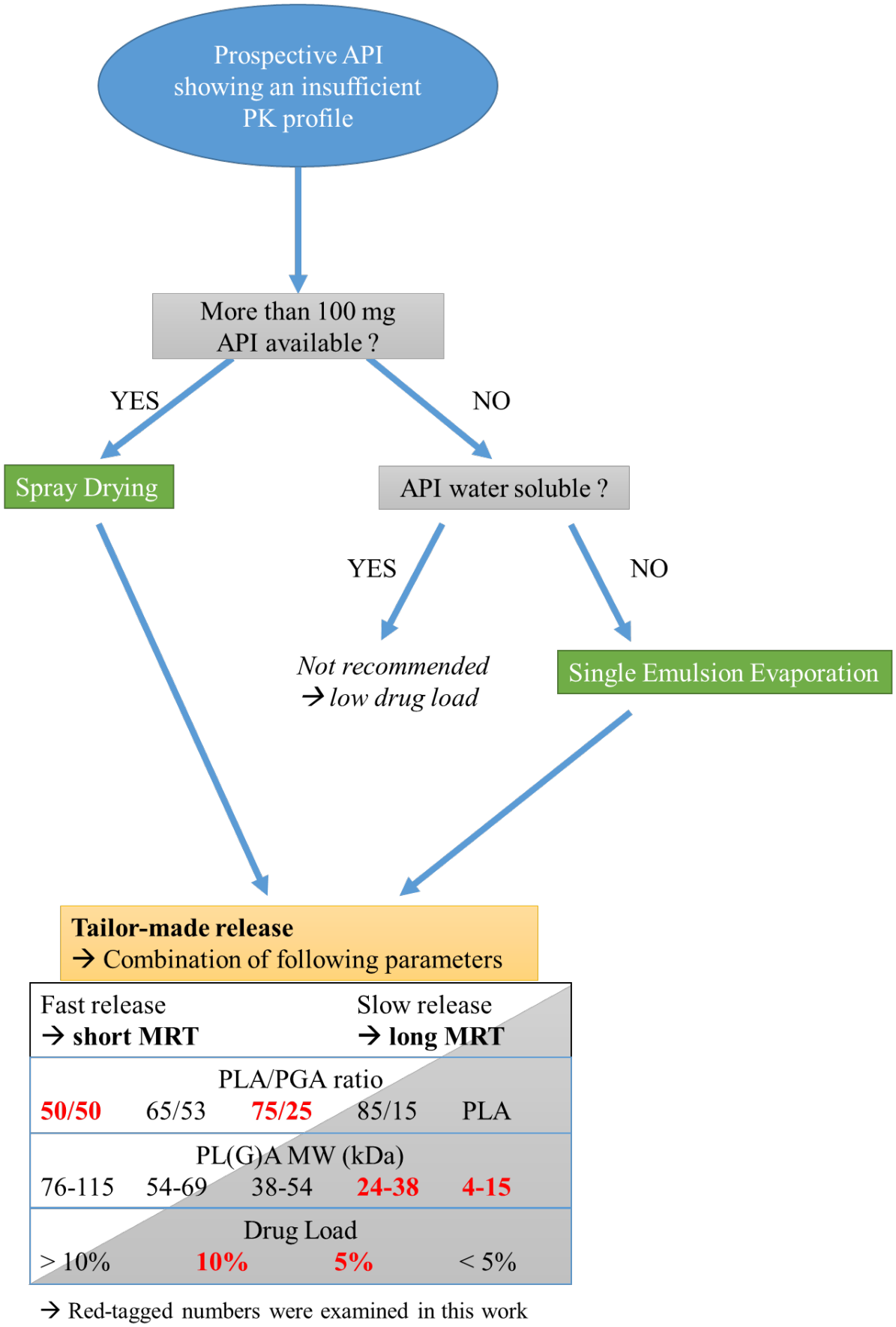

Figure 10 Graphical representation of proposed formulation platform

3.7 Platform applied to further compounds

To support this platform technology, additional compounds exhibiting different physicochemical properties (denominated as compounds G, I, K, L and P) were formulated accordingly (Table 6). By applying the proposed parameters, extended release formulations utilizing mentioned APIs were manufactured. Especially for water-insoluble compounds, this platform proofs to be successful. Here, for compound G, L and P the *in vitro* release time was extended up to 140 hours and MRT in conducted *in vivo* PK studies was increased by 40-fold. Encapsulation of water-soluble compounds resulted in consistently faster release as compared to the corresponding water-insoluble compound formulations. However, using this platform method the minimum of 10% DL and 5-fold MRT increase was achieved for all attempted formulations.

By utilizing the described platform, the *in vitro* release time of all trialed compounds was consistently increased, which translates to increased MRTs in *in vivo* PK experiments in a fast and easily applicable manner. Thus, these studies further testify to the general applicability of the described platform within the scope of preclinical research.

Table 6 Data of additional compounds for which formulations were manufactured using the described formulation platform

API	logP predicted	Solubility [mg/ml]	Manufacturing Method	DL [%]	Polymer properties		*In vitro* release profile		Mean residence time [h] (dose [µmol/kg])		species
					PLA/PGA ratio	**MW (kDa)**	**Initial burst 1 h [%]**	**Total release [h]**	**PLGA-formulation**	**Standard formulation**	
der p 1	3	0.067	Single Emulsion	30	50/50	24 - 38	40	150	71 (212)	1.0 (19)	mouse
			Single Emulsion	40	75/25	4 - 15	15	300 (70%)	86 (423)	1.0 (19)	mouse
trimethoprim	0.98	0.4	Single Emulsion	4	75/25	4 - 15	10	150 (80%)	95 (103)	1.3 (34)	rat
			Spray Dry	10	75/25	4 - 15	10	175	45 (689)	1.3 (34)	mouse
Compound G	3.2	< 0.001	Spray Dry	30	75/25	4 - 15	25	65	76 (70)	1.9 (2)	mouse
Compound I	2	0.081	Spray Dry	10	75/25	4 - 15	55	50	11 (28)	1.4 (10)	rat
Compound K	-0.4	> 0.1	Spray Dry	10	75/25	4 - 15	30	60	8 (28)	1.6 (5)	mouse
Compound L	4.7	< 0.001	Single Emulsion	19	75/25	4 - 15	35	120	100 (200)	ND (63)	mouse
Compound P	2.5	0.011	Single Emulsion	10	75/25	4 - 15	25	140	ND (70)	4.6 (70)	mouse
			Spray Dry	20	75/25	4 - 15	35	60	32 (70)	4.6 (70)	mouse

4 Conclusion

In this work, a platform formulation tool to accommodate a wide range of structurally different compounds, enabling early proof of concept studies is developed. The platform parameters were identified and optimized by utilizing two structurally different model APIs, as to facilitate the formulations for the desired PK profile fitting the requirements of preclinical *in vivo* studies. MRT was extended significantly and the plasma trough level was prolonged for a sufficient period for all of the optimized formulations. Hereby, the well-known antibiotic trimethoprim was successfully encapsulated into PLGA, for the first time. Additionally, a tailor-made release profile, *in vitro* as well as *in vivo*, was enabled.

Based on these results, the described formulation platform was established, successfully encapsulating a variety of early research compounds into extended release microparticles.

Thereby, the proof of concept studies were achieved, by improving the PK properties. The subsequent shortened timelines are particularly critical in industrial research and offer a competitive advantage.

5 References

1. Amidon, G. L.; Lennernäs, H.; Shah, V. P.; Crison, J. R., A Theoretical Basis for a Biopharmaceutic Drug Classification: The Correlation of in Vitro Drug Product Dissolution and in Vivo Bioavailability. *Pharmaceutical Research: An Official Journal of the American Association of Pharmaceutical Scientists* **1995,** *12* (3), 413-420.
2. Sánchez-Serrano, I., Success in translational research: Lessons from the development of bortezomib. *Nature Reviews Drug Discovery* **2006,** *5* (2), 107-114.
3. Gullapalli, R.; Wong, A.; Brigham, E.; Kwong, G.; Wadsworth, A.; Willits, C.; Quinn, K.; Goldbach, E.; Samant, B., Development of ALZET® osmotic pump compatible solvent compositions to solubilize poorly soluble compounds for preclinical studies. *Drug Delivery* **2012,** *19* (5), 239-246.
4. Tan, T.; Watts, S. W.; Davis, R. P., Drug delivery: Enabling technology for drug discovery and development. iPRECIO® Micro Infusion Pump: programmable, refillable, and implantable. *Frontiers in Pharmacology* **2011,** *JUL*.
5. Makadia, H. K.; Siegel, S. J., Poly lactic-co-glycolic acid (PLGA) as biodegradable controlled drug delivery carrier. *Polymers* **2011,** *3* (3), 1377-1397.
6. Vilos, C.; Velasquez, L. A., Therapeutic strategies based on polymeric microparticles. *Journal of Biomedicine and Biotechnology* **2012,** *2012*.
7. Wang, Y., FDA's regulatory science program for generic PLA/PLGA-based drug products. *American Pharmaceutical Review* **2016,** *20*.
8. Shen, J.; Choi, S.; Qu, W.; Wang, Y.; Burgess, D. J., In vitro-in vivo correlation of parenteral risperidone polymeric microspheres. *J. Control. Release* **2015,** *218*, 2-12.
9. Wischke, C.; Schwendeman, S. P., Principles of encapsulating hydrophobic drugs in PLA/PLGA microparticles. *International Journal of Pharmaceutics* **2008,** *364* (2), 298-327.
10. Kobayashi, H.; Watanabe, R.; Choyke, P. L., Improving conventional enhanced permeability and retention (EPR) effects; What is the appropriate target? *Theranostics* **2014,** *4* (1), 81-89.
11. Jain, R. A., The manufacturing techniques of various drug loaded biodegradable poly(lactide-co-glycolide) (PLGA) devices. *Biomaterials* **2000,** *21* (23), 2475-90.
12. Hamoudeh, M.; Diab, R.; Fessi, H.; Dumontet, C.; Cuchet, D., Paclitaxel-loaded microparticles for intratumoral administration via the TMT technique: preparation, characterization, and preliminary antitumoral evaluation. *Drug Dev Ind Pharm* **2008,** *34* (7), 698-707.
13. Wang, X.; Yang, L.; Zhang, H.; Tian, B.; Li, R.; Hou, X.; Wei, F., Fluorescent magnetic PEI-PLGA nanoparticles loaded with paclitaxel for concurrent cell imaging, enhanced apoptosis and autophagy in human brain cancer. *Colloids Surf B Biointerfaces* **2018,** *172*, 708-717.
14. Yang, C.; Plackett, D.; Needham, D.; Burt, H. M., PLGA and PHBV microsphere formulations and solid-state characterization: possible implications for local delivery of fusidic acid for the treatment and prevention of orthopaedic infections. *Pharmaceutical research* **2009,** *26* (7), 1644-56.
15. Zaghloul, A. A.; Mustafa, F.; Siddiqu, A.; Khan, M., Biodegradable microparticulates of beta-estradiol: preparation and in vitro characterization. *Drug Dev Ind Pharm* **2005,** *31* (8), 803-11.

16. Thote, A. J.; Chappell, J. T., Jr.; Gupta, R. B.; Kumar, R., Reduction in the initial-burst release by surface crosslinking of PLGA microparticles containing hydrophilic or hydrophobic drugs. *Drug Dev Ind Pharm* **2005,** *31* (1), 43-57.
17. Park, C. W.; Lee, H. J.; Oh, D. W.; Kang, J. H.; Han, C. S.; Kim, D. W., Preparation and in vitro/in vivo evaluation of PLGA microspheres containing norquetiapine for long-acting injection. *Drug design, development and therapy* **2018,** *12*, 711-719.
18. Ayoub, M. M.; Elantouny, N. G.; El-Nahas, H. M.; Ghazy, F. E. S., Injectable PLGA Adefovir microspheres; the way for long term therapy of chronic hepatitis-B. *Eur J Pharm Sci* **2018,** *118*, 24-31.
19. Xie, X.; Lin, W.; Xing, C.; Yang, Y.; Chi, Q.; Zhang, H.; Li, Y.; Li, Z.; Yang, Y.; Yang, Z.; Li, M., In Vitro and In Vivo Evaluations of PLGA Microspheres Containing Nalmefene. *PLoS One* **2015,** *10* (5), e0125953.
20. Gomez, C.; Blanco, M. D.; Bernardo, M. V.; Olmo, R.; Muniz, E.; Teijon, J. M., Cytarabine release from comatrices of albumin microspheres in a poly(lactide-co-glycolide) film: in vitro and in vivo studies. *Eur J Pharm Biopharm* **2004,** *57* (2), 225-33.
21. Han, F. Y.; Thurecht, K. J.; Whittaker, A. K.; Smith, M. T., Bioerodable PLGA-Based Microparticles for Producing Sustained-Release Drug Formulations and Strategies for Improving Drug Loading. *Frontiers in Pharmacology* **2016,** *7* (185).
22. Park, K.; Skidmore, S.; Hadar, J.; Garner, J.; Park, H.; Otte, A.; Soh, B. K.; Yoon, G.; Yu, D.; Yun, Y.; Lee, B. K.; Jiang, X.; Wang, Y., Injectable, long-acting PLGA formulations: Analyzing PLGA and understanding microparticle formation. *J. Control. Release* **2019,** *304*, 125-134.
23. Jaraswekin, S.; Prakongpan, S.; Bodmeier, R., Effect of poly(lactide-co-glycolide) molecular weight on the release of dexamethasone sodium phosphate from microparticles. *Journal of Microencapsulation* **2007,** *24* (2), 117-128.
24. Sun, F.; Sui, C.; Teng, L.; Liu, X.; Teng, L.; Meng, Q.; Li, Y., Studies on the preparation, characterization and pharmacological evaluation of tolterodine PLGA microspheres. *Int J Pharm* **2010,** *397* (1-2), 44-9.
25. Parumasivam, T.; Leung, S. S.; Quan, D. H.; Triccas, J. A.; Britton, W. J.; Chan, H. K., Rifapentine-loaded PLGA microparticles for tuberculosis inhaled therapy: Preparation and in vitro aerosol characterization. *Eur J Pharm Sci* **2016,** *88*, 1-11.
26. Yang, Q.; Owusu-Ababio, G., Biodegradable progesterone microsphere delivery system for osteoporosis therapy. *Drug Dev Ind Pharm* **2000,** *26* (1), 61-70.
27. Ramazani, F.; Chen, W.; van Nostrum, C. F.; Storm, G.; Kiessling, F.; Lammers, T.; Hennink, W. E.; Kok, R. J., Strategies for encapsulation of small hydrophilic and amphiphilic drugs in PLGA microspheres: State-of-the-art and challenges. *International Journal of Pharmaceutics* **2016,** *499* (1), 358-367.
28. Ashton, S.; Song, Y. H.; Nolan, J.; Cadogan, E.; Murray, J.; Odedra, R.; Foster, J.; Hall, P. A.; Low, S.; Taylor, P.; Ellston, R.; Polanska, U. M.; Wilson, J.; Howes, C.; Smith, A.; Goodwin, R. J.; Swales, J. G.; Strittmatter, N.; Takats, Z.; Nilsson, A.; Andren, P.; Trueman, D.; Walker, M.; Reimer, C. L.; Troiano, G.; Parsons, D.; De Witt, D.; Ashford, M.; Hrkach, J.; Zale, S.; Jewsbury, P. J.; Barry, S. T., Aurora kinase inhibitor nanoparticles target tumors with favorable therapeutic index in vivo. *Sci Transl Med* **2016,** *8* (325), 325ra17.
29. Zhang, Z.; Wang, X.; Li, B.; Hou, Y.; Cai, Z.; Yang, J.; Li, Y., Paclitaxel-loaded PLGA microspheres with a novel morphology to facilitate drug delivery and antitumor efficiency. *RSC Advances* **2018,** *8* (6), 3274-3285.

30. Qutachi, O.; Vetsch, J. R.; Gill, D.; Cox, H.; Scurr, D. J.; Hofmann, S.; Muller, R.; Quirk, R. A.; Shakesheff, K. M.; Rahman, C. V., Injectable and porous PLGA microspheres that form highly porous scaffolds at body temperature. *Acta Biomater* **2014,** *10* (12), 5090-5098.
31. Arpagaus, C., PLA/PLGA nanoparticles prepared by nano spray drying. *Journal of Pharmaceutical Investigation* **2019,** *49* (4), 405-426.
32. Yu, L., Amorphous pharmaceutical solids: Preparation, characterization and stabilization. *Advanced Drug Delivery Reviews* **2001,** *48* (1), 27-42.
33. Nežić, I.; Sander, A.; Meštrović, E.; Čavužić, D., Production of stable amorphous form by means of spray drying. *Particulate Science and Technology* **2019,** *37* (5), 628-638.
34. Dannenfelser, R. M.; Yalkowsky, S. H., Data base of aqueous solubility for organic non-electrolytes. *Science of the Total Environment, The* **1991,** *109-110* (C), 625-628.

CHAPTER V

SUMMARY AND PERSPECTIVES

Summary and Perspectives

Within the scope of this work, novel nano- and microparticulate formulations for industrial preclinical research were developed and successfully tested. The overall goal was to improve the pharmacokinetics, biodistribution and pharmacodynamics for a variety of BI research compounds, utilizing biocompatible drug delivery systems. Special emphasis was placed on the challenges relevant to preclinical formulation development in pharmaceutical industry.

The main part of this thesis consisted in the development of novel nanoparticulate formulations for tumor targeted delivery of an immuno-oncologic STING agonist. Microfluidic mixing was utilized to manufacture cyclic dinucleotide (CDN) loaded chitosan-based complexes with suitable properties for intratumoral treatment. In order to facilitate a targeted delivery of nanoparticles into tumor tissue upon i.v. administration, this precursor formulation was further modified with PLGA-PEG. In a subsequent *in vivo* PK/PD study in tumor-bearing mice, an increased accumulation of the API in the tumor tissue and tumor-only biomarker response was detected. Therefore, it can be reasonably assumed, that the CDN, entrapped in the chitosan/PLGA-PEG nanoparticles, is released only upon delivery into the tumor tissue minimizing the systemic exposure. Hereby, the side effects of this highly potent immune-oncologic API can be reduced, allowing for an i.v. administration, as to broaden the indication spectrum. These findings strongly suggest superiority of the developed formulation compared to the currently available formulations.

Based on the successful outcome of this first study, nanoparticles targeting hepatic tissue for NASH treatment were developed in a similar fashion. Here, two structurally different compounds, namely Fatty acid synthase inhibitors (FASi) and acetyl-CoA carboxylase inhibitors (ACCi), were successfully encapsulated into PLGA-based nanoparticles, confirming general applicability of the established manufacturing method and characterization screening. Additionally, an *in vivo* PK proof of concept study demonstrated accumulation of the API in the hepatic tissue, suggesting targeted delivery of the nanoparticles into the liver. Hereby, adverse reaction of the NASH treatment upon systemic administration may be reduced, enhancing efficacy of the drug.

Despite the promising results of the developed nanoparticulate formulations, additional *in vivo* efficacy studies are yet to be conducted, in order to provide further evidence of the therapeutic effect. A decrease in tumor growth rate or even apoptosis must be demonstrated for the tumor targeted delivery of the STING agonist. Efficacy for a potential NASH treatment with ACCi or FASi loaded nanoparticles is to be evidenced by inhibition of lipogenesis in hepatic tissue only. Furthermore, a procedure for manufacturing larger amounts of nanoparticles is proposed, by utilizing the unique scale-up possibilities of the microfluidic mixing technology. Hereby, within the scope of preclinical research, *in vivo* studies in non-rodent species such as minipig, dog or cynomolgus monkey are feasible. Ultimately, by using microfluidic systems compliant with GMP requirements, even clinical trials are foreseen to be possible at a later stage.

A successful translation from small benchtop manufacturing to large scale production was demonstrated in the last chapter of this work. Here, different model compounds were encapsulated into PLGA microparticles in order to obtain an optimized, tailor-made PK profile for preclinical *in vivo* proof of concept studies. Based on initial trials on a small scale, the described formulation platform was established and transferred to additional internal compounds, verifying the general applicability of the platform. Following the development work described, all PLGA-based extended release formulations for preclinical studies at Boehringer Ingelheim are currently manufactured based on the said formulation platform.

CHAPTER VI

APPENDIX

1 List of Abbreviations

API	Active pharmaceutical ingredient
BI	Boehringer Ingelheim
BI X	STING agonist (BI compound)
BI Y	Stereoisomer of BI X
c-di-AMP	Cyclic-di-adenosine monophosphate
CDN	Cyclic dinucleotide
CS	Chitosan
DD	Deacetylation degree
DI water	Deionized water
DL	Drug load
DLS	Dynamic light scattering
DNA	Deoxyribonucleic acid
DSC	Differential scanning calorimetry
EDTA	Ethylenediaminetetraacetic acid
EPR	Enhanced permeability and retention
EtOH	Ethanol
FASi	Fatty acid synthase inhibitors
H_2O	Water
HPLC	High-performance liquid chromatography
i.v.	Intravenous
IFN	Interferon
IFN-β	Interferon beta
kDa	Kilodalton

LA	Lauric acid
MRT	Mean residence time
mV	Millivolt
MW	Molecular weight
N/P ratio	Nitrogen/phosphate ratio
NaCl	Sodium chloride
NAFLD	Nonalcoholic fatty liver disease
NASH	Non-alcoholic steatohepatitis
nm	Nanometer
PD	Pharmacodynamics
PDI	Polydispersity index
PDI	polydispersity index
PEG	Polyethylenglycol
PEI	Polyethylenimine
PK	Pharmacokinetics
PLGA	Poly lactic-co-glycolic acid
PVA	Polyvinyl alcohol
SD	Standard deviation
SEM	Scanning electron microscope
siRNA	Small interfering ribonucleic acid
STING	Stimulator of interferon genes
TEM	Transmission electron microscopy
TFR	Total flow rate
TPP	Tripolyphosphate

2 Publications

2.1 Original Articles

Strack, P., Külzer, R., Sommer, F., Bretschneider, T., Merkel, O. M., & Grube, A. (2020).

A smart approach to enable preclinical studies in pharmaceutical industry: PLGA-based extended release formulation platform for subcutaneous applications

Drug Development and Industrial Pharmacy, 46(4), 635-645

Strack, P., Scheuerer, S., Baader, M., Budzinski, R., Merkel, O. M., & Grube, A.

Developing a nanoparticulate formulation for NASH treatment: Manufacturing, characterization, optimization and in vivo proof of concept

Manuscript in preparation.

2.2 Meetings and poster presentations

Strack, P., Merkel, O. M., & Grube, A.

Nano-particulate formulations for targeted delivery of cyclic dinucleotides

International M+AS meeting, Boehringer Ingelheim, Ridgefield (USA), 20. June 2019

Strack, P., Merkel, O. M., & Grube, A.

Development of nano particulate formulations for hepatic drug delivery

3rd European Conference on Pharmaceutics, Bologna (Italy), 25. – 26. March 2019

Strack, P., Merkel, O. M., & Grube, A.

Development of new nano-particulate formulations for targeted drug delivery

Boehringer Ingelheim Science Day, Biberach an der Riss (Germany) 23. July 2018